ARCHIVES OF ACOUSTICS
6, 2, 89-110 (1981)

A MODEL OF PISTON IMPACT AND VIBRATION FOR INTERNAL COMBUSTION ENGINE NOISE REDUCTION

A. F. SEYBERT

Department of Mechanical Engineering, University of Kentucky
(Lexington, Kentucky 40506, USA)

J. F. HAMILTON, P. A. HAYES

Department of Mechanical Engineering, Purdue University
(W. Lafayette, Indiana 47907, USA)

In this paper a mathematical model is developed to study piston impact and cylinder liner vibration in internal combustion engines. The aim of this study is to assess the effect on cylinder liner response (and, therefore on piston-impact induced noise) of certain design modifications such as cylinder liner stiffness, piston mass, and piston/cylinder liner running clearance. A single-mode representation of cylinder liner vibration is developed using the assumed modes method, where the cylinder liner is modeled as a thin cylindrical shell with fixed-free boundary conditions. Expressions for the kinetic and potential energy of the system, and for the generalized mass and stiffness of the system are developed. Lagrange's equation of motion is used to derive a differential equation of cylinder liner motion. The equation of motion for the piston is derived by assuming that the piston motion is pure translation. The initial conditions for cylinder liner response are developed from the conservation of momentum of the piston and the cylinder liner at impact. Experimental cylinder liner vibration data from a diesel engine are used to verify the accuracy of the piston impact model. Agreement between the experimental data and the cylinder liner response predicted by the mathematical model is generally good, but some discrepancies do exist. A computer simulation of the model is used to study the effect of parameter changes.

List of symbols

a' – radius of cylinder liner
A – area of the top surface of the piston

E — elastic modulus of cylinder liner material
F — horizontal force applied to the piston
h' — thickness of cylinder liner
k_{11} — generalized stiffness of the cylinder liner
L — length of cylinder liner
m_{11} — generalized mass of the cylinder liner
M — mass of the piston
M_p — generalized mass of the piston
n — circumferential mode number
P — cylinder pressure
q_i — generalized coordinates of the cylinder liner
Q — generalized force on the cylinder liner
R — distance from crankshaft axis to the top of the cylinder liner
R_1 — radius of crankshaft
R_2 — length of connecting rod
t — time
T — kinetic energy
V — potential energy
x — longitudinal coordinate of the cylinder liner
x_1 — longitudinal position of piston pin
y — normal displacement of the cylinder liner
α — angular coordinate of the cylinder liner
ζ — damping ratio
η — displacement of the piston
θ — angular rotation of the crankshaft
μ — Poisson's ratio for cylinder liner material
ϱ — density of cylinder liner material
Φ_i — normalized mode shapes of cylinder liner
Φ_x — mode shape of cylinder liner in the x direction
Φ — mode shape of cylinder liner in the α direction
ω_a — angular velocity of the crankshaft
ω_n — natural frequency of cylindrical shell

1. Introduction

Vehicle noise, particularly noise from trucks and buses, is a major source of annoyance to people living in industrialized urban areas in this country, as well as England, Japan, and most industrialized European countries. The United States and several other countries regulate the amount of noise emitted by heavy trucks and other types of vehicles. In the United States, for example, the Environmental Protection Agency [1] has established noise limit regulations for new medium and heavy trucks stating that the noise level shall not exceed 83 dB(A) (measured at 15.2 m from the side of the truck during a pass-by test) beginning in January 1978. Another set of regulations [2] applies to users of medium and heavy trucks.

Most heavy trucks are powered by diesel engines. Because of increased power requirements and energy considerations, the percentage of medium trucks using diesel engines is increasing. Diesel engines are noisier than spark ignition engines of similar horsepower rating because of a high peak cylinder pressure and a short cylinder pressure rise-time during ignition.

Extensive studies have been conducted to define the sources of noise of diesel engines [3]. Combustion excitation is the main source of noise for naturally-aspirated engines, while piston impact and other mechanical noise sources are of secondary importance. However, for turbo-charged engines, piston-impact generated noise is more important than combustion and other mechanical noise sources [4]. In a turbo-charged diesel engine the peak cylinder pressure, and, therefore, the forces that accelerate the piston, is higher than the peak cylinder pressure in a naturally-aspirated diesel engine. On the whole, however, turbo-charged diesel engines are quieter than their naturally-aspirated counterparts because turbo-charging smooths the combustion process, thereby reducing the combustion noise.

Fig. 1 shows two one-third octave spectra of the noise of a 350 hp turbo-charged diesel engine commonly used in heavy trucks. The upper spectrum is the noise of the engine fitted with standard pistons; the lower spectrum is the

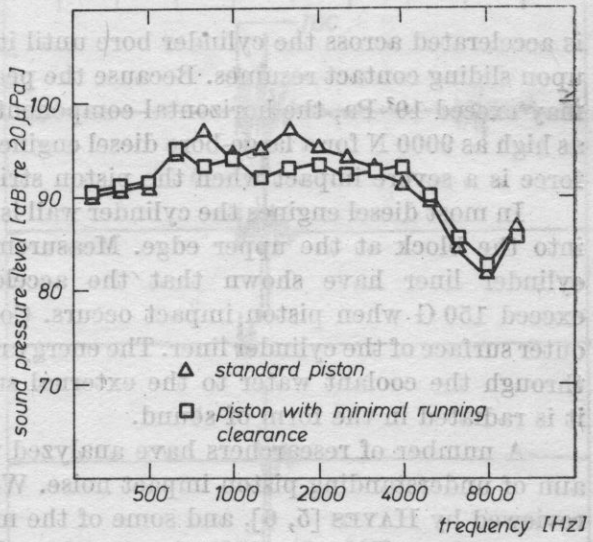

Fig. 1. Diesel engine noise spectra showing the importance of piston impact

noise of the same engine fitted with oversize pistons to minimize piston impact. A reduction of the overall noise by about 3-4 dB(A) was observed by this modification, indicating that piston impact accounts for at least fifty percent of the sound power of this engine.

The mechanisms of the piston impact phenomenon can be seen in simplified fashion in Fig. 2. During the compression phase of an engine cycle the piston is held in sliding contact with one side of the cylinder bore by the horizontal component of the force applied to the piston pin by the connecting rod. This force component reverses direction at top-dead-center (TDC); and the piston

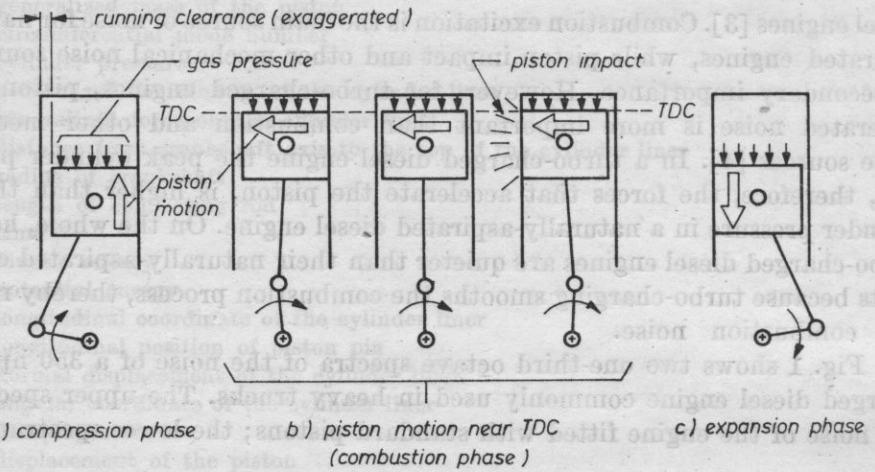

Fig. 2. Sequence of events showing piston-impact phenomenon

is accelerated across the cylinder bore until it impacts the opposite side, whereupon sliding contact resumes. Because the peak pressure in the cylinder at TDC may exceed 10^7 Pa, the horizontal component of the force on the piston can be as high as 9000 N for a large-bore diesel engine. The result of this large horizontal force is a severe impact when the piston strikes the cylinder wall.

In most diesel engines the cylinder wall is actually a cylindrical shell pressed into the block at the upper edge. Measurements on the outer surface of the cylinder liner have shown that the acceleration of the cylinder liner can exceed 150 G when piston impact occurs. Coolant water circulates around the outer surface of the cylinder liner. The energy released upon impact is transmitted through the coolant water to the external surfaces of the engine block where it is radiated in the form of sound.

A number of researchers have analyzed the motion of the piston with the aim of understanding piston impact noise. Work in this field has recently been reviewed by HAYES [5, 6], and some of the more comprehensive studies will be discussed here. FIELDING [7, 8] developed an elaborate set of equations describing the behavior of the piston as it travels across the cylinder bore. He used the final velocity of the piston to calculate the impact energy (kinetic energy on impact) of the piston on the cylinder liner. This parameter was used to estimate what effect certain design changes would have on piston-impact induced noise. FUJIMOTO, et al., [9-11] have studied the effect of oil-film cushioning and ring-groove

friction on piston motion. They used a reciprocating compressor to avoid the complications of combustion, and obtained some photographs showing piston contact area by using a transparent cylinder liner.

Neither of the above studies considered the behavior of the cylinder liner after impact. HADDAD and FORTESCUE [12] and HADDAD [13] have used an analog computer simulation to study the vibration of the cylinder liner. They used a two-mode expansion to represent the cylinder liner.

The remainder of this paper discusses a mathematical model for piston impact and cylinder liner vibration. Of particular importance in this study was the response of the cylinder liner to piston impact. Another aspect of this study [6] was concerned with developing a coherence model to predict piston impact noise. The cylinder liner vibration is used as an input parameter in the model.

2. Experimental observations

As a preliminary to the mathematical model, several experiments were conducted to determine the characteristics of piston impact and vibration. Accelerometers were mounted inside the coolant passage on the external surface

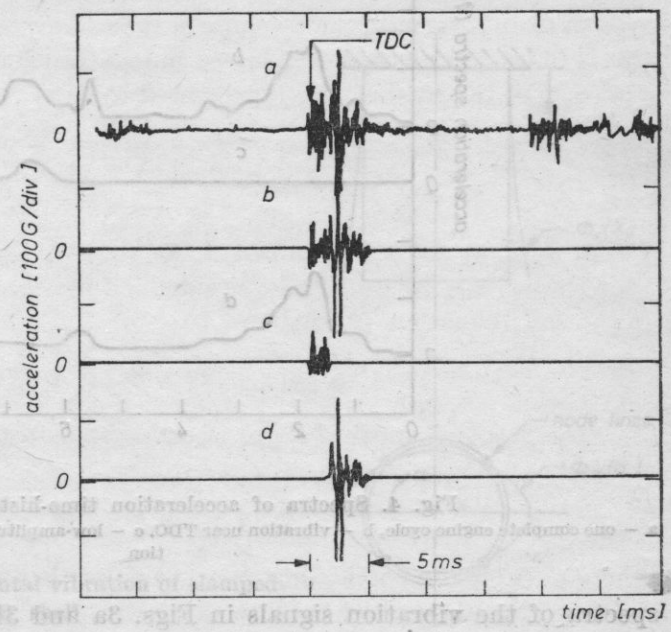

Fig. 3. Typical cylinder liner acceleration time-histories
a – one complete engine cycle (720° of crankshaft rotation), b – major vibration near TDC, c – low-amplitude vibration, d – high amplitude vibration due to piston impact

of the cylinder liners of the diesel engine described with reference to Fig. 1. These accelerometers were mounted at a point on the cylinder liners corresponding to the midpoint of the piston at impact. Fig. 3 shows a typical acceleration

time history, for approximately 720° of crankshaft rotation, with the engine operating at rated horsepower. As can be seen from Fig. 3a, the most significant region of vibration (typically 125 G maximum acceleration) begins slightly prior to TDC (between the compression and expansion strokes) and has a duration of about 5 ms. Figure 3a also reveals vibration due to five other lesser piston impacts that may occur during the intake, compression, expansion, and exhaust cycles of the engine, as well as vibration due to other mechanical forces. The piston impact near TDC is almost always the most important of the six piston impacts that may occur for each 720° of crankshaft rotation [11, 12]. All the vibration except the major vibration near TDC was edited from the data, Fig. 3b. The effect of this can be seen in Figs. 4a and 4b which show the

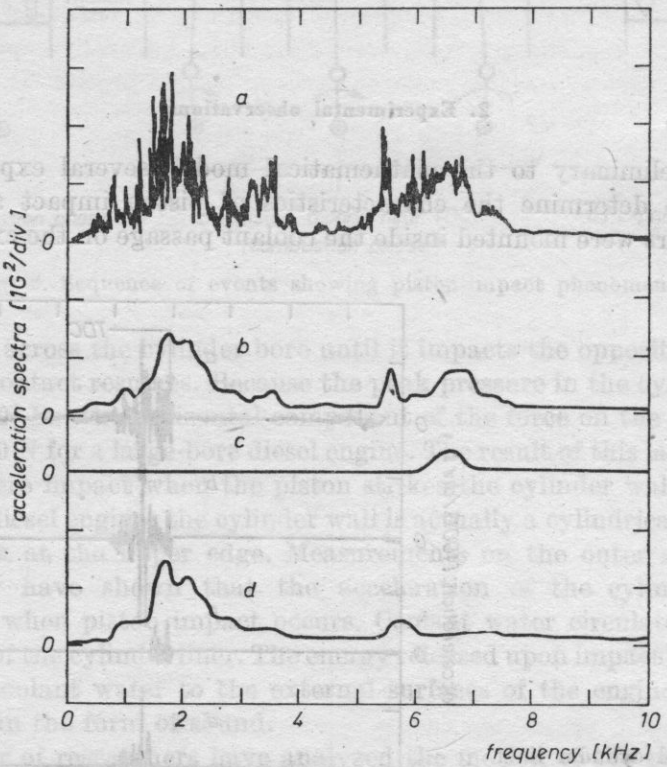

Fig. 4. Spectra of acceleration time-histories in Fig. 3
a – one complete engine cycle, b – vibration near TDC, c – low-amplitude vibration, d – high-amplitude vibration

spectra of the vibration signals in Figs. 3a and 3b, respectively. This editing procedure was used to make interpretation of the spectra easier, as seen by comparing Figs. 4a and 4b. There was not a sufficient number of data cycles available to smooth the spectrum in Fig. 4a using traditional ensemble-averaging techniques. The vibration time-history was further edited when it was noticed

that the vibration near TDC consisted of two parts: a low-amplitude vibration beginning just prior to TDC and lasting about 2 ms, followed by a high-amplitude vibration lasting approximately 3 ms. It was observed that the low-amplitude vibration was very high frequency and random in nature, and it did not repeat well from engine cycle to cycle. On the other hand, the high-amplitude vibration (due to piston impact) was quite repeatable from cycle to cycle. The spectra of the vibration time histories in Figs. 3c and 3d are shown in Figs. 4c and 4d, respectively.

From Figs. 3 and 4 it can be seen that piston impact causes the cylinder liner to vibrate over a broad range of frequencies between 1000 and 3000 Hz, with a maximum vibration around 1900 Hz. The data in Fig. 1 seem to support this conclusion as well. The natural frequencies ω_n of a circular cylinder of uniform thickness, clamped at one end and free at the other, are given by [14]:

$$\omega_n = \frac{1}{a'}\sqrt{\left(\frac{0.595\pi}{n}\right)^4\left(\frac{a'}{L}\right)+\frac{n^4}{12(1-\mu^2)}\left(\frac{h'}{a'}\right)^2}\sqrt{\frac{E}{\varrho}}, \qquad (1)$$

where a', h' and L are the shell radius, thickness, and length, respectively, and where E, ϱ, and μ are the Young's modulus, density, and Poisson's ratio, respectively, of the shell material. The natural frequencies given by equation (1) are for modes with no circumferential node lines and $2n$ longitudinal node lines.

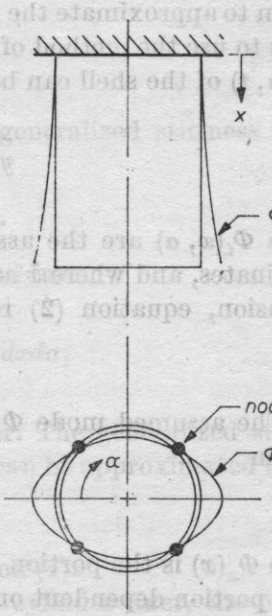

Fig. 5. Mode shape for fundamental vibration of clamped-free cylindrical shell

The lowest natural frequency for such a shell is when $n = 2$ [14], i.e., the shell cross-section deforms into the shape of an ellipse, see Fig. 5. For the steel cylinder liner in the diesel engine used in this study: $L = 277$ mm, $a' = 74.7$ mm, and

$h' = 8.26$ mm which yields a natural frequency of 1600 Hz using equation (1). In reality, the cylinder liner is restrained slightly at the lower end by a viscoelastic gasket. This would cause the actual natural frequency to be somewhat higher than equation (1) predicts.

Mechanical impedance tests were carried out to measure the natural frequency and mode shape of the cylinder liner. This was accomplished by removing the piston from one of the cylinders and attaching a small vibration exciter at the point on the cylinder liner where piston impact occurs. This test revealed the existence of the elliptical mode at approximately 1800 Hz.

The preliminary tests described above indicated that the cylinder liner was responding to piston impacts at its fundamental resonant frequency, and that higher modes were not important. Note, however, that Fig. 4 shows some vibration response near 6 kHz that may be the result of higher modes. But, from the practical viewpoint of noise reduction, only noise in the 500-3500 Hz region is important (see Fig. 1).

3. Piston impact model

When a single vibration mode dominates the overall response of a complex dynamic system, it is convenient to define an equivalent single-degree-of-freedom system to approximate the response of the real system. One way of accomplishing this is to use the method of assumed modes. In general, the normal displacement $y(x, a, t)$ of the shell can be represented by [15]

$$y(x, a, t) = \sum_{i=1}^{m} \Phi_i(x, a) q_i(t), \tag{2}$$

where $\Phi_i(x, a)$ are the assumed mode shapes, where $q_i(t)$ are the generalized coordinates, and where x and a are defined in Fig. 5. For a single mode ($m = 1$) expansion, equation (2) reduces to:

$$y(x, a, t) = \Phi_1(x, a) q_1(t). \tag{3}$$

The assumed mode $\Phi(x, a)$ is orthogonal in terms of x and a and can be written

$$\Phi_1(x, a) = \Phi_x(x) \Phi_a(a), \tag{4}$$

where $\Phi_x(x)$ is the portion of the assumed mode dependent only on x and $\Phi_a(a)$ is the portion dependent only on a (see Fig. 5).

The assumed mode shape was chosen such that the deflection $\Phi_x(x)$ along the length of the cylinder was the static deflection due to a uniformly distributed force. The deflection $\Phi_a(a)$ along the cylinder circumference was chosen to have four node lines.

Thus:

$$\Phi_x(x) = 2\left(\frac{x}{L}\right)^2 - \frac{4}{3}\left(\frac{x}{L}\right)^3 + \frac{1}{3}\left(\frac{x}{L}\right)^4, \qquad \Phi_\alpha(\alpha) = \cos 2\alpha,$$

and

$$\Phi_1(x, \alpha) = \left\{2\left(\frac{x}{L}\right)^2 - \frac{4}{3}\left(\frac{x}{L}\right)^3 + \frac{1}{3}\left(\frac{x}{L}\right)^4\right\}\cos 2\alpha. \tag{5}$$

Regarding external forces as nonconservative, Lagrange's equation of motion has the form

$$\frac{d}{dt}\left(\frac{\partial T}{\partial \dot{q}_1}\right) - \frac{\partial T}{\partial q_1} + \frac{\partial V}{\partial q_1} = Q(t), \tag{6}$$

where $Q(t)$ is the generalized force, and where T and V are the kinetic and potential energies, respectively, of the system. The kinetic energy can be found from

$$T(t) = \frac{1}{2} m_{11} \dot{q}_1^2(t) \tag{7}$$

and the potential energy can be found from

$$V(t) = \frac{1}{2} k_{11} q_1^2(t), \tag{8}$$

where m_{11} is the generalized mass and k_{11} is the generalized stiffness of the system. Using (7) and (8), equation (6) becomes:

$$m_{11}\ddot{q}_1(t) + k_{11} q_1(t) = Q(t). \tag{9}$$

The generalized mass of the cylinder can be found from

$$m_{11} = a' \int_0^{2\pi} \int_0^L m(x, \alpha) \Phi_1^2(x, \alpha)\, dx\, d\alpha, \tag{10}$$

where $m(x, \theta)$ is the surface density of the cylinder. The generalized stiffness of the cylinder cannot be calculated as easily, but it can be approximated by

$$k_{11} \approx \omega_n^2 m_{11}, \tag{11}$$

where ω_n is the natural frequency found from equation (1).

When the piston is in sliding contact with the cylinder liner, the mass of the piston will modify the equivalent mass of the system. This effect can be included by calculating the generalized mass of the piston a point at a distance x_1 from the top of the cylinder liner. (Note: This approach assumes that the piston remains in contact with the cylinder liner after impact. The consequences

of this assumption will be discussed later in this paper.) The generalized mass of the piston M_p is

$$M_p = M\Phi_1^2(x_1, 0), \tag{12}$$

where M is the mass of the piston. M also includes the mass of the piston pin and the mass of that portion of the connecting rod assumed to be lumped at the piston.

The distance x_1 corresponds to the piston pin location and is found from the kinematics of the slider crank mechanism

$$x_1(t) = R + R_1\cos\theta - R_2[1 - (R_1/R_2)^2\sin^2\theta]^{1/2}, \tag{13}$$

where R is the distance from the crankshaft axis to the top of the cylinder liner, R_1 is the radius of the crankshaft, R_2 is the length of the connecting rod, and $\theta = \omega t$ is the angle of rotation of the crankshaft rotating with angular velocity ω; $\theta = 0$ is at the bottom-dead-center position of the piston.

The horizontal component of the force at the piston pin helps to hold the piston in contact with the liner after impact has occurred. Because this force is a time-varying one, it will excite the cylinder liner. Assuming that this force is applied at a point at a distance x_1 from the top of the cylinder liner, the generalized force is

$$Q(t) = F(t)\Phi_1(x_1, 0), \tag{14}$$

where x_1 is given by equation (13) and where $F(t)$ is the horizontal component of the force applied to the piston at the piston pin. This force can be found from [5]:

$$F(t) = \frac{R_1}{R_2}\left\{AP(\theta)\sin\theta - M\omega^2\left[\frac{R_1}{2}\sin 2\theta + \frac{R_1^2}{R_2}\sin 3\theta\right]\right\}, \tag{15}$$

where A is the area of the top surface of the piston and $P(\theta)$ is the cylinde pressure.

It can be seen from Fig. 3d that the cylinder liner vibration is underdamped, but it is difficult to calculate the damping in the system. Several damping mechanisms occur during piston impact. These include: structural damping of the cylinder liner and piston, damping due to oil-film cushioning and ring-groove friction [9], and damping due to the radiation of sound from the external surfaces of the cylinder liner. When such complex damping mechanisms occur in a system, it is common to estimate an equivalent viscous damping ratio from experimental data. Defining the equivalent damping ratio ζ, the generalized damping force is $2\zeta\omega_n(M_{11} + M_p)\dot{q}_1(t)$.

Using equations (9) and (11), as well as the above mentioned results for equivalent viscous damping, an equation representing an equivalent single-

degree-of-freedom system describing the vibration of the cylinder liner after impact is

$$\ddot{q}_1(t)+2\zeta\omega_n\dot{q}_1(t)+\left[\frac{\omega_n^2}{1+M_p/m_{11}}\right]q_1(t)=\frac{Q(t)}{m_{11}+M_p}. \tag{16}$$

This model is represented schematically in Fig. 6. Fig. 6a shows the model while the piston undergoes free-travel just prior to impact, while Fig. 6b represents the model after impact. During piston free-travel, equation (16) with $Q(t)$

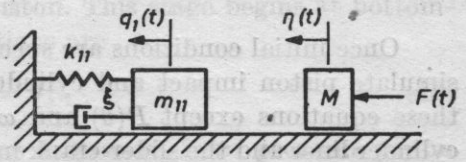

a)

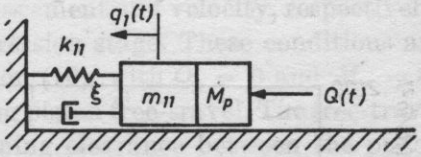

b)

Fig. 6. Models for piston impact and cylinder liner vibration
a – model during piston free-travel, b – model after impact

and M_p set equal to zero represents the motion of the cylinder liner. The motion of the piston during free-travel is governed by

$$F(t)=M\ddot{\eta}, \tag{17}$$

where $\eta(t)$ is the displacement of the piston; $\eta=0$ corresponds to the piston in contact with the non-impact side of the cylinder liner.

Some comments are in order concerning the shortcomings of the model represented by equations (16) and (17). A detailed model of damping has intentionally been avoided by the use of an equivalent viscous damping ratio determined from experimental data. The use of an experimentally determined damping ratio facilitates the description of the model, but provides very little insight into the actual damping mechanisms responsible for dissipation of the mechanical energy of the cylinder liner. This is a very challenging topic of research which was beyond the scope of the present study.

Equation (17) assumes that the piston motion during free-travel is pure translation. This is a highly ideal situation, and results in a very simple formula-

tion for the piston momentum just before impact. In practice, however, there exist unbalanced moments, due to friction and the fact that the piston pin does not usually coincide with the center-of-gravity of the piston, which impart angular momentum to the piston. These effects alter the piston-impact process by producing more than a single impact that results from equation (17). An example of a model that includes rotation is given in [7].

4. Initial conditions

Once initial conditions are specified, equations (16) and (17) can be used to simulate piston impact and cylinder liner vibration. All of the parameters in these equations except $P(\theta)$ and ω can be found from the dimensions of the cylinder liner and the slider-crank mechanism. $P(\theta)$ and ω describe the operating conditions of the engine and must be specified before simulation can take place. This information is usually known by engine designers from theoretical models or prototype engines. For this study the cylinder pressure was measured at rated horsepower and speed ($\omega = 220$ s^{-1},) with a piezoelectric pressure transducer mounted in the cylinder head above one of the cylinders. Fig. 7a shows the measured cylinder pressure (as a function of crankshaft angle), and

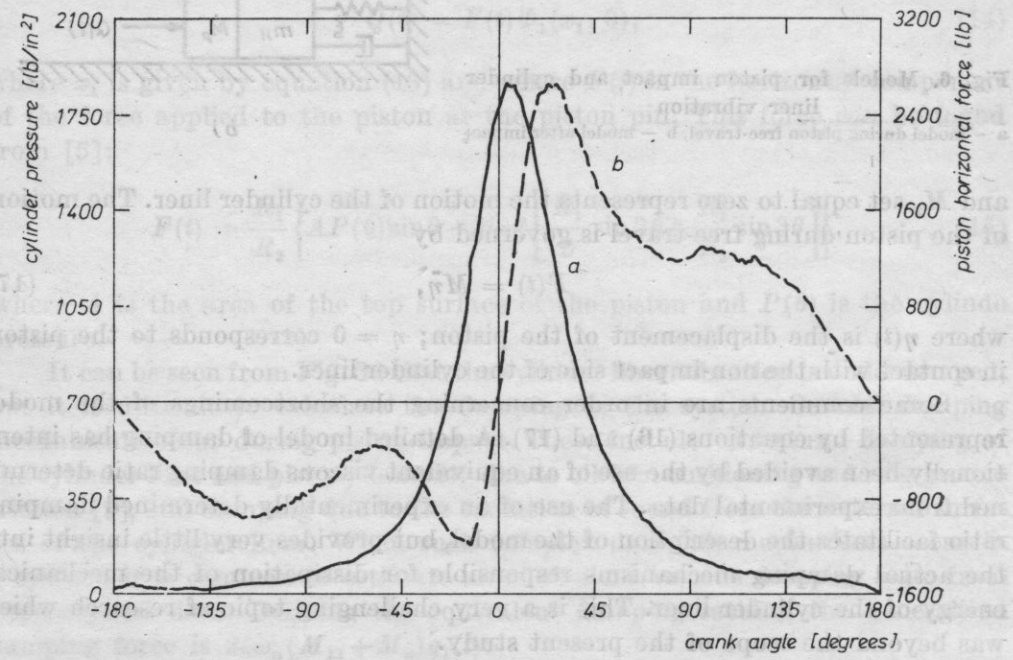

Fig. 7. a — cylinder pressure at rated horsepower as a function of crankshaft angle, b — horizontal component as piston force computed from Fig. 7a using equation (15)

Fig. 7b shows the horizontal component of the piston force computed from the data in Fig. 7a with the aid of equation (15).

The simulation is broken into three stages: the compression stage, in which the piston is in sliding contact with the nonimpact side of the cylinder liner; the free-travel stage, in which the piston traverses the cylinder bore; and the expansion stage, in which the piston is in sliding contact with the impact side of the cylinder liner. These stages are discussed below:

1. Compression stage ($0 \leqslant t \leqslant t_1$): During this stage equation (16) describes the behavior of the cylinder liner and the piston. This stage begins at bottom-dead-center ($\theta, t = 0$), and the initial conditions are

$$q(0) = \dot{q}(0) = 0, \tag{18}$$

i.e., it is assumed that no residual vibration is present from previous piston impacts. This stage terminates when $\theta = \pi$; at this point define $t = t_1$.

2. Free-travel stage ($t_1 < t \leqslant t_2$): During this stage equation (17) governs the piston motion, and the initial conditions are

$$\eta(t_1) = q_1(t_1), \quad \dot{\eta}(t_1) = \dot{q}_1(t_1), \tag{19}$$

where $q_1(t_1)$ and $\dot{q}_1(t_1)$ are the generalized displacement and velocity, respectively, of the cylinder liner at the end of the compression stage. These conditions are also used as initial conditions to solve equation (16), with $Q_p = 0$ and $M_p = 0$, to find the vibration of the cylinder liner during piston free-travel. The free-travel stage ends when $\eta = \delta$, where δ is the running clearance between the piston and the cylinder liner; at this point define $t = t_2$.

3. Expansion stage ($t_2 < t \leqslant t_3$): During this stage impact takes place and the piston is once more in sliding contact with the cylinder liner. Equation (16) governs the vibration of the cylinder liner. The initial displacement of the cylinder liner is $q_1(t_2^+) = q_1(t_2)$, but the initial condition of the generalized velocity must be determined from conservation of momentum. Just before impact the momentum of the piston is $M\dot{\eta}(t_2)$, and the generalized momentum of the liner is $M_{11}\dot{q}_1(t_2)$. The momentum of the piston/cylinder liner just after impact is $(M_p + m_{11})\dot{q}(t_2^+)$, and the initial generalized velocity for this stage is, therefore:

$$\dot{q}_1(t_2^+) = \frac{M\dot{\eta}(t_2) + m_{11}\dot{q}_1(t_2)}{M + m_{11}}. \tag{20}$$

Equation (20) assumes that the piston impact is inelastic (i.e., no piston rebound). This same assumption was made by FIELDING [7] in his work. Other experimental results indicate that rebound is very small [12] or nonexistent [11]. A careful study of the liner vibration (Fig. 3) with an expanded time scale did not reveal any evidence of multiple impacts. If rebound is found to occur, then equation (20) may be modified by including a coefficient of restitution [12].

5. Results and discussion

Using the data in Fig. 7a, along with the dimensions of the diesel engine used in this study [5], a simulation of the mathematical model was made using a digital computer. Fig. 8a shows the results of the computer simulation (solid line) and the measured cylinder liner acceleration time-history (dashed line) for the diesel engine operating at rated horsepower and speed.

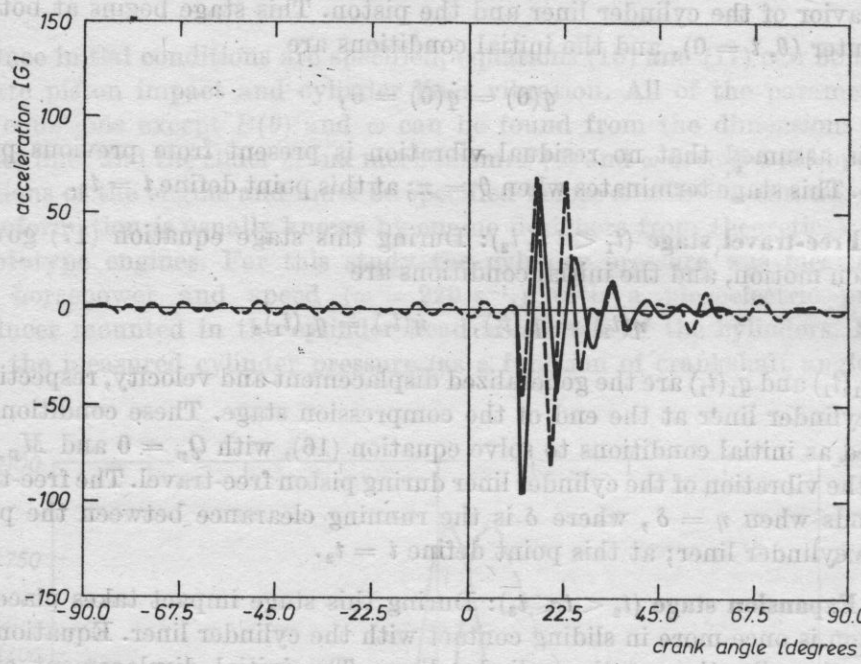

Fig. 8a. Measured (dashed line) and predicted (solid line) cylinder liner acceleration time-histories

The experimental data in Fig. 8a is the same data in Fig. 3a, but a low-pass filter (4000 Hz break frequency) was used to remove the high-frequency vibration that corrupted the original acceleration signal. Note, also, that the accelerations in Fig. 3 are inverted.

The actual cylinder liner and piston running clearance was not precisely known, but the manufacturer believed that it was in the range of 0.13 to 0.20 mm. A clearance of 0.18 mm accurately predicts the point of impact (approximately 12° after TDC) (see Fig. 8a). The damping ratio ζ used in the computer simulation was 0.13. This value of ζ was selected because it made the settling times of the experimental and computer simulation data approximately equal. The high value of damping cannot be accounted for solely by structural damping mecha-

nisms; other damping mechanisms, such as ring-groove friction and oil-film cushioning, are probably more important [11].

The simulation data in Fig. 8a show that cylinder liner vibration is negligible prior to piston impact, and that the vibration after impact is approximately zero for crankshaft angles exceeding 90°. For this example at least, the simulation could be simplified by omitting the compression stage portion of the mathematical model.

From Fig. 8a it can be seen that there is a difference in the overall form of the two acceleration time-histories. The results of the computer simulation show a very large acceleration immediately following impact; this acceleration decays exponentially, as expected for a single-degree-of-freedom system. In comparison, the initial measured acceleration is not nearly so large, but the acceleration during the second cycle of oscillation is very large. This behavior is perhaps due to oil-film cushioning and/or the presence of higher-order vibration modes.

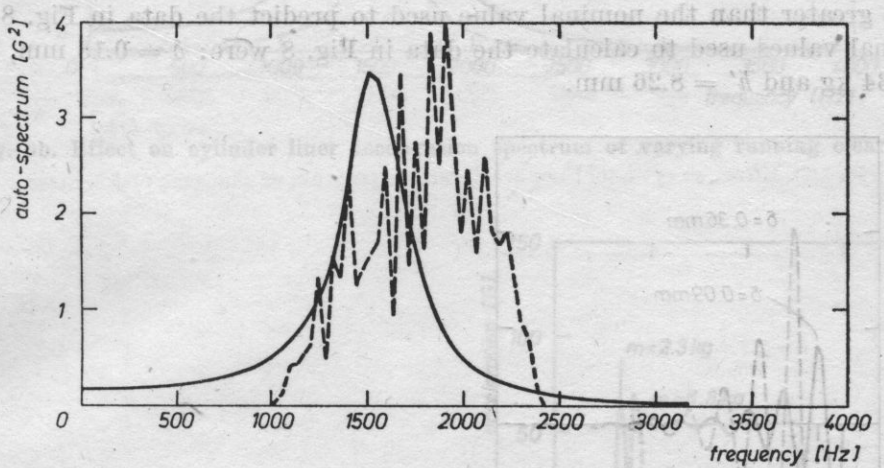

Fig. 8b. Measured (dashed line) and predicted (solid line) cylinder liner acceleration spectra (computed from Fig. 8a)

Fig. 8b shows a comparison between the acceleration spectra of the two signals in Fig. 8a. The frequency resolution of these data is 17.5 Hz, corresponding to the reciprocal of the period of one complete engine cycle (720° of crankshaft rotation). While these spectra agree in form, there are some discrepancies in magnitude and frequency. In Fig. 8b it can be seen that the spectrum of the experimental acceleration time-history has a considerable amount of random error superimposed upon the true spectrum. This random error could be reduced if more data had been used to compute a smooth spectrum by using ensemble-averaging methods.

6. Parameter study

The importance of the mathematical simulation described in this paper lies in its ability to assess the effect of design changes involving critical parameters such as running clearance and piston mass. The results in Fig. 8 show that the mathematical model is not sophisticated enough to accurately predict absolute values of cylinder liner vibration. However, the model does provide an estimate of the general trends in the experimental data. From the standpoint of engineering design, the model may be used to evaluate the effect of relative changes in design parameters. However, one must be careful not to vary the design parameters over a range that violates the assumptions used in formulating the mathematical model. For example, in evaluating the effect of cylinder liner thickness, one would not want to violate the condition $h' \ll a'$ which is an assumption used in the derivation of equation (1).

In this paper only three parameters — running clearance, piston mass, and cylinder liner thickness — are varied; a more complete parameter study is given in [5]. Each parameter is varied twice, one value less than and the other value greater than the nominal value used to predict the data in Fig. 8. The nominal values used to calculate the data in Fig. 8 were: $\delta = 0.18$ mm, $M = 5.34$ kg and $h' = 8.26$ mm.

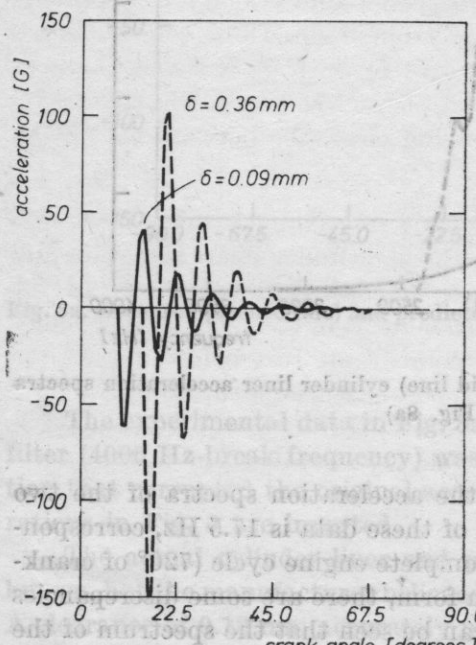

Fig. 9a. Effect on cylinder liner vibration time-history of varying running clearance

Fig. 9 shows the effect on cylinder liner vibration of varying the piston/cylinder liner running clearance δ. Fig. 9a compares the acceleration time-histories for δ equal to 0.090 mm and 0.36 mm. With the larger running clearance, piston

impact is delayed approximately 5°, and the peak acceleration is increased about 2 1/2 times. Fig. 9b shows the accelaration spectra computed from the time-histories in Fig. 9a. Fig. 9b shows that, near 1500 Hz, increasing the running clearance

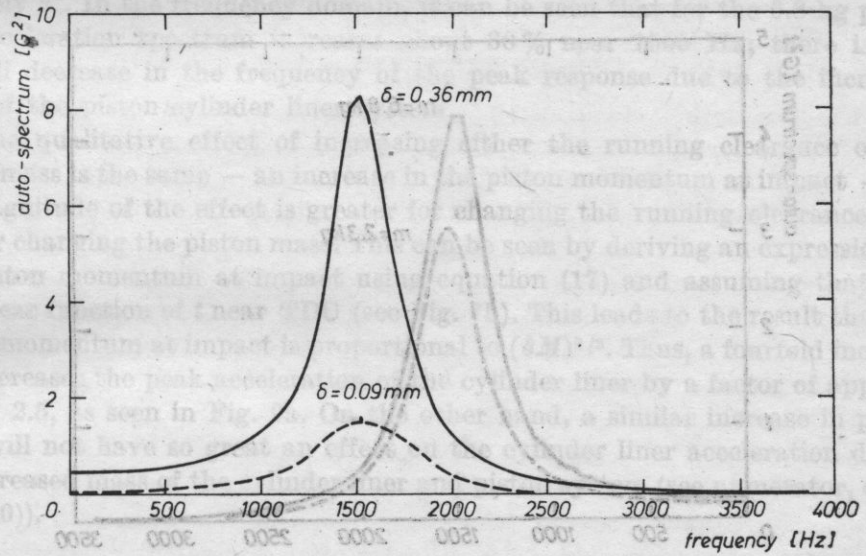

Fig. 9b. Effect on cylinder liner acceleration spectrum of varying running clearance

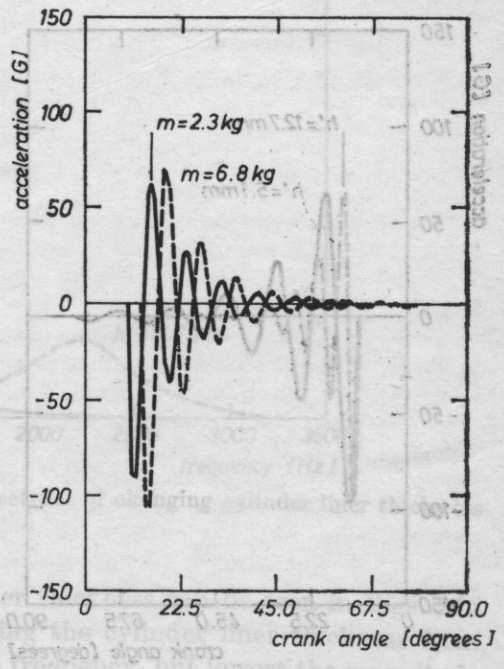

Fig. 10a. Effect on cylinder liner vibration of changing piston mass

has an effect more pronounced than is expected from the data in Fig. 9a. It can be seen from Fig. 9b that the peak response is increased by a factor of six due to a fourfold increase in δ.

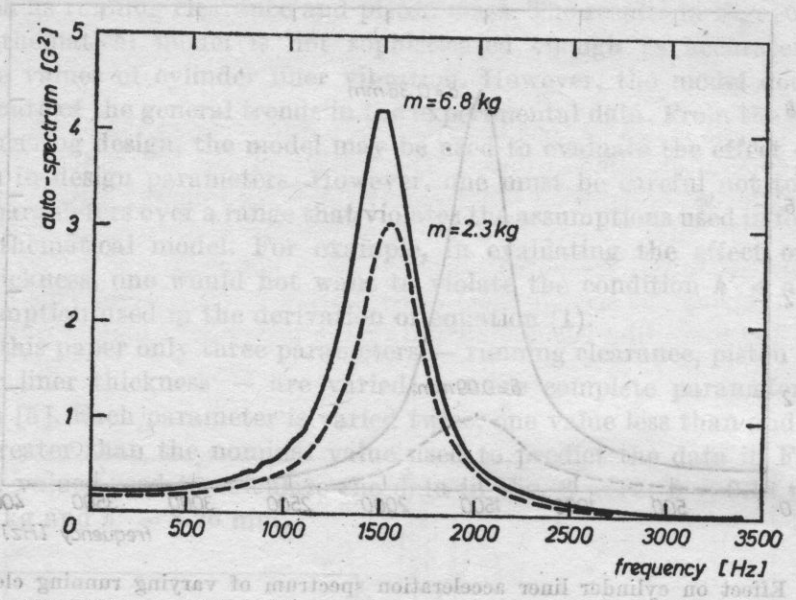

Fig. 10b. Effect on cylinder liner acceleration spectrum of changing piston mass

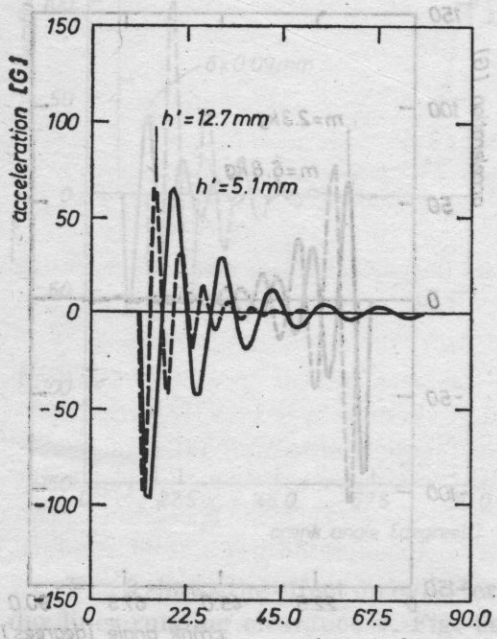

Fig. 11a. Effect on cylinder liner vibration of changing cylinder liner thickness

The effect of changes in piston mass can be seen in Figs. 10a and 10b. In the time domain, Fig. 10a, increasing the piston mass from 2.3 kg to 6.8 kg has only a small effect on the peak acceleration; the impact is delayed approximately 5°. In the frequency domain, it can be seen that for the 6.8 kg piston the acceleration spectrum increases about 30 % near 1500 Hz; there is also a small decrease in the frequency of the peak response due to the increased mass of the piston/cylinder liner system.

The qualitative effect of increasing either the running clearance or the piston mass is the same — an increase in the piston momentum at impact — but the magnitude of the effect is greater for changing the running clearance than it is for changing the piston mass. This can be seen by deriving an expression for the piston momentum at impact using equation (17) and assuming that $F(t)$ is a linear function of t near TDC (see Fig. 7b). This leads to the result that the piston momentum at impact is proportional to $(\delta M)^{2/3}$. Thus, a fourfold increase in δ increases the peak acceleration of the cylinder liner by a factor of approximately 2.5, as seen in Fig. 9a. On the other hand, a similar increase in piston mass will not have so great an effect on the cylinder liner acceleration due to the increased mass of the cylinder liner and piston system (see numerator, equation (20)).

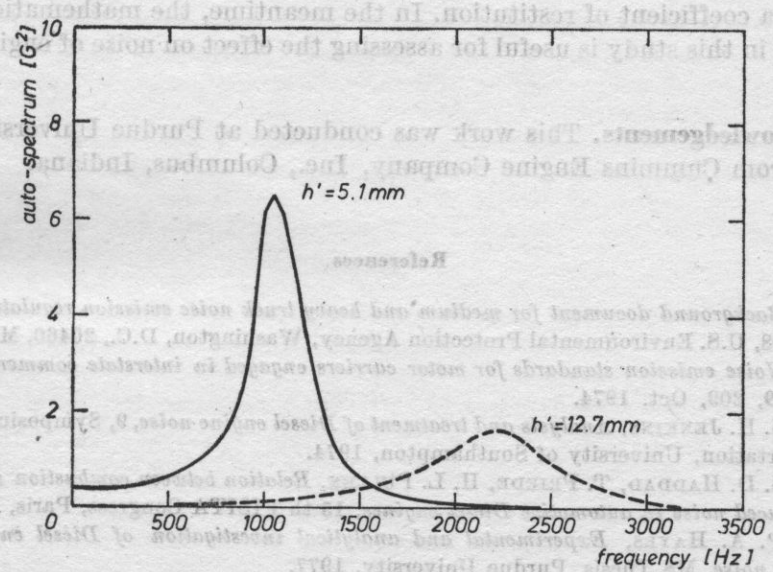

Fig. 11b. Effect on cylinder liner acceleration spectrum of changing cylinder liner thickness

The effect of altering the cylinder liner thickness can be seen in Figs. 11a and 11b. These figures show that increasing the cylinder liner thickness from 5.1 to 12.7 mm increases the peak-response frequency, but lowers the magnitude

of the peak response, Fig. 11b. Both of these effects can be explained by noting that increasing the cylinder liner thickness increases the stiffness and the natural frequency of the cylinder liner, equation (1).

7. Summary and conclusions

A simple mathematical model has been developed to study piston impact and cylinder liner vibration in internal combustion engines. The results of this model agree reasonably well with experimental data, although the model uses several simplifying assumptions. The cylinder liner was modeled as a thin cylindrical shell with fixed-free boundary conditions; only the fundamental mode of vibration of the shell was considered. The experimental data seem to support the use of a single-mode cylinder liner model, at least in the 500-3000 Hz frequency range where piston impact noise is important. During free-travel, the piston was assumed to move in pure translation only. Other piston models (e.g., [7]) include rotational effects; but in view of the results in this study perhaps rotation is of secondary importance.

The model could be refined when more information on piston impact is available. For example, a study of energy dissipation and momentum transfer mechanisms at impact would yield estimates of an equivalent viscous damping ratio and a coefficient of restitution. In the meantime, the mathematical model developed in this study is useful for assessing the effect on noise of engine design changes.

Acknowledgements. This work was conducted at Purdue University under support from Cummins Engine Company, Inc., Columbus, Indiana.

References

[1] *Background document for medium and heavy truck noise emission regulations*, EPA 550/9-76-008, U.S. Environmental Protection Agency, Washington, D.C., 20460, March, 1976

[2] *Noise emission standards for motor carriers engaged in interstate commerce*, Federal Register, **39**, 209, Oct. 1974.

[3] S. H. Jenkins, *Analysis and treatment of Diesel engine noise*, 9, Symposium on Noise in Transportation, University of Southampton, 1974.

[4] S. D. Haddad, T. Priede, H. L. Pullen, *Relation between combustion and mechanically induced noise in automotive Diesel engines*, 15 th FISITA Congress, Paris, 1974.

[5] P. A. Hayes, *Experimental and analytical investigation of Diesel engine piston impact and noise*, MS Thesis, Purdue University, 1977.

[6] P. A. Hayes, A. F. Seybert, J. F. Hamilton, *A coherence model for piston-impact generated noise*, SAE Engine Noise Conference, P-80, 125-132, 1980.

[7] B. J. Fielding, *Identification of mechanical sources of noise in a Diesel engine*, Ph. D. Thesis, University of Manchester, England, 1968.

[8] B. J. Fielding, J. Skorecki, *Identification of mechanical sources of noise in a Diesel engine: sound originating from piston slap*, Proceedings, Institution of Mechanical Engineers, **184**, 857-873 (1969-70).

[9] Y. FUJIMOTO, et al., *Experimental studies on piston slap in reciprocating machinery* (in Japanese), preprint of JSME, March 1976.

[10] T. SUZUKI, et al., *Studies on piston slap in reciprocating machinery* (in Japanese), preprint of JSME, March 1976.

[11] Y. FUJIMOTO, T. SUZUKI, Y. OCHIAI, *On piston slap in reciprocating machinery*, Vibration in Rotating Machinery, Institution of Mechanical Engineers, c215/76 (1976).

[12] S. D. HADDAD, P. W. FORTESCUE, *Simulating piston slap by an analog computer*, Journal of Sound and Vibration, **52**, 1, 79-93 (1977).

[13] S. D. HADDAD, *Origins of noise and vibration in vee form Diesel engines with emphasis on piston slap*, Ph. D. Thesis, University of Southampton, 1974.

[14] H. KRAUS, *Thin elastic shells*, 132, John Wiley and Sons, Inc., 1967.

[15] L. MEIROVITCH, *Elements of vibration analysis*, section 7.4, McGraw Hill, 1975.

Received on January 18, 1980

ARCHIVES OF ACOUSTICS
6, 2, 111-122 (1981)

NOISE PREDICTION ON SHIPS

EDWARD SZCZERBICKI

Ship Research Institute, Technical University of Gdańsk
(80-952 Gdańsk, ul. Majakowskiego 11/13)

ANDRZEJ SZUWARZYŃSKI

Technical and Research Department, Maritime Institute
(80-307 Gdańsk, ul. Abrahama 1)

This paper presents the results of the first stage of investigations aimed at the development of an effective method for predicting noise on ships. The results of measurements taken on Polish ships by the Technical and Research Department of the Maritime Institute under the departmental problems 103 and 104 were used. A statistical method of multiple linear regression was used for data processing. Calculated and measured results were compared. It has been shown that statistical methods are valid for predicting noise in the accomodation in the superstructure of a ship. The direction of further research, intended to improve the method presented, is defined.

1. Introduction

Noise control is particularly important on a ship where the crew not only work but also rest. The people on board a ship are exposed to much higher noise levels than are found in the conditions on land. It is most important to secure low noise levels in accomodations so as to assure good rest after work.

The permissible noise levels on sea-going merchant ships were established in Poland by the regulation of the Minister of Navigation on October 28, 1978. According to this regulation the noise level in accomodation on a ship should not exceed 60 dB(A). In practice this value is very often exceeded. The results of measurements of noise levels taken in 1360 accomodations on 45 ships of different types are shown in Fig. 1. It follows from this figure that the permissible noise level is exceeded in almost 30 percent of the accomodation.

It is difficult to solve the problem of excessive noise on a ship which is already operational. The possible effects achieved by improving the existing structures are usually incomparably small compared to the expense involved. Constructing a "silent" ship requires efforts towards noise reduction at the preliminary design stages. Noise level prediction in accomodation in the superstructure of a ship is difficult because of the complexity of the problem resulting from the existence of a large number of noise sources of differing characteristics and from a complex steel structure which is the propagation path of the sound

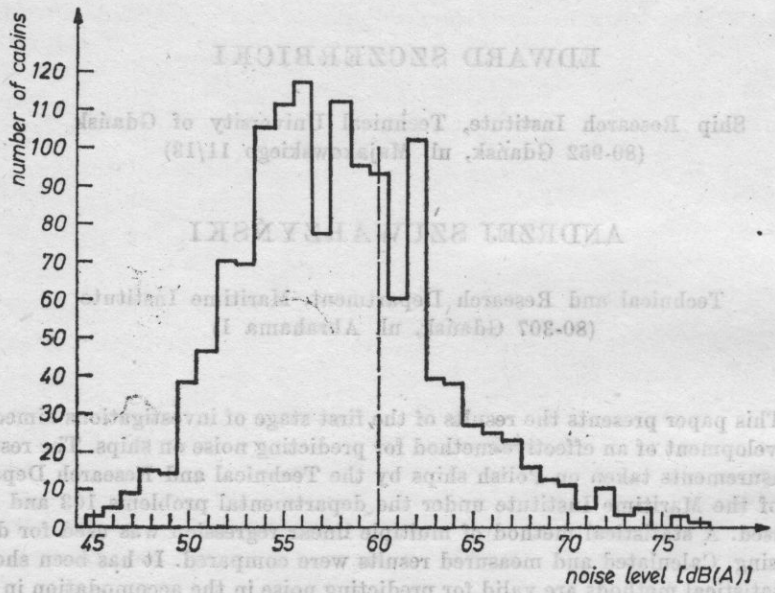

Fig. 1. The distribution of noise levels in accomodations in the ships of PLO and PŻM

The sources that determine noise in accomodation in the superstructure include: the main engine, the auxiliary engines, the gearbox and the screw propeller [1, 5]. There are a number of other sources such as ventilation systems, pumps, loading winches etc., but these are only important locally. The sound generated by the noise sources mentioned above is transmitted to accomodation in the superstructure, mainly by the structure of the ship in the form of longitudinal, torsional, transverse and flexural waves [6]. These wave motions are coupled, which makes it difficult to analyze them theoretically. Thus the methods for noise prediction given in the literature [1, 2, 5, 6, 7, 10] are based on a simplified model of sound propagation in the structure of a ship. It is generally assumed that one wave motion dominates and determines the flux of energy propagated [6]. A block diagram of the analysis of sound propagation in the structure of a ship, which is similar in all the known methods, consists of four stages [5]: determination of source strength, definition of propagation paths in the steel structure, determination of coupling between the steel structure and

the cabin lining, and coupling between the cabin lining and the ambient air. Each stage is repeated for all the main noise sources (cf. [2, 10]). The total noise level in a given accomodation is obtained by summing the contribution of the individual sources.

The input data in the first stage, i.e. the levels of structureborne sound at the foundations of the machinery, are obtained, in the present methods, from measurements. These measurements are taken at experimental posts in a shipyard or onboard ships. There are also empirical formulae which permit the calculation of these values (e.g. in [1, 10]). The second stage requires information about the paths of sound propagation and the damping properties of the structure. These properties are usually determined by model investigations [5, 6] or exciter investigations on real objects [10]. For the third and fourth stages, the necessary data on the characteristics of the lining system can be obtained by laboratory investigations or from calculations.

The methods currently used for noise prediction cannot be regarded as methods for the calculation of the real noise levels in an accomodation; they can, however, be a source of valuable suggestions for the designer. As in all engineering calculations, noise prediction has a limited accuracy. The noise prediction programme developed by Det Norske Veritas assures an accuracy of 3-5 dB [6, 7]. Comparison of calculated results, obtained from an algorithm proposed by BUITEN and AARTSEN [1], with measured values showed that in 46 percent of the cases the difference in the levels of the estimated and the measured noise did not exceed 3 dB (A). The standard deviation of the difference between the measured and the calculated values did not exceed 4 dB (A).

The methods presented — of necessity only briefly — for noise level prediction are based on a simplified analytical model involving a number of empirical coefficients. Application of these methods at the stage of planining or preliminary designing can be very difficult in view of the lack of sufficient data, e.g. designs of: the steel structure, the arrangement of the machinery in the engine room, the linings, etc.. It is therefore necessary to develop a method based on simple parameters which permits noise level prediction. It is also possible to use statistical methods for this purpose, an example of which is the prediction [9], at an early design stage of the vibration characteristics of a ship.

2. Multiple regression model

The present model, on the basis of which the calculations were made, is known as a standard linear model of multiple regression [3, 4, 8]. This model assumes that the values observed for a dependent variable are realizations of the n-element random vector $\boldsymbol{Y}$, which can be written as $\boldsymbol{X}\beta+\varepsilon$, where $\boldsymbol{X}$ is the $(n \times K)$ - dimensional matrix of observations of order K, consisting of values taken by K explanatory variables, β is a column vector of K unknown

parameters, ε is an n-element vector of random components, whose vector of conditional expected value and conditional matrix of covariance are, for a given X, equal to $E(\varepsilon|X) = 0$ and $V(\varepsilon|X) = \sigma^2 I$, respectively, where σ^2 is an unknown positive parameter, while I is a unit matrix of the n-th degree. Since the assumptions are conditionally made with respect to X, nothing is lost when the matrix X is considered to be a matrix with nonstochastic elements equal exactly to the values observed for the explanatory variables.

The parameters of the present model are estimated by the method of least squares, i.e. by minimizing the sum of the squared deviations (remainders) from the hyperplane of regression. This leads to a solution [3, 8], where the vector b obtained by test from the formula

$$b = (X^T X)^{-1} X^T Y, \tag{1}$$

is an unweighted estimator of the regression coefficients. According to the Gauss-Markov theorem this is the best unweighted linear estimator.

The quantity R, calculated experimentally from the formula

$$R = \sqrt{1 - \frac{Y^T Y - b^T X^T Y}{Y^T Y - \frac{1}{n}(1^T - Y)^2}}, \tag{2}$$

where 1^T is an n-dimensional line vector of unity, is the estimate of the correlation coefficient, which measures the degree of correlation of variable Y with all the independent variables.

Statistical conclusions about the regression coefficients, i.e. the construction of confidence intervals and significance testing, are drawn on the basis of the t distribution for n-K degrees of freedom for an assumed confidence level.

It is interesting to note here the importance of the significance testing of the regression coefficients. The results of the test which give coefficients insignificantly different from zero permit gradual elimination from the model of explanatory variables, of those with no influence (or very small influence) on the value of the dependent variable.

The classical method of least squares loses its optimum character when a significant autocorrelation of random errors occurs. The von Neumann test can be used to check this significance, by approximating the distribution of the relevant statistics (the so called von Neumann quotient) by the normal distribution with a mean $2\,n/(n-1)$ and the variance $4/n$. When the test shows a high value of the autocorrelation coefficient P, then it should be estimated and subsequently all the observations should be transformed accordingly [3]. Using the transformed vector of dependent variables, Y^*, and the transformed matrix of independent variables, X^*, the method of least squares serves again to give the final estimated parameters of the model.

The linear regression function is a convenient prediction tool, and it should also be noted that the technique of prediction based on the regression model is considered to be one of the best. In order to implement practically the calculation process related to this technique, the programme whose block diagram is shown in Fig. 2 was written in Algol 1900 and introduced into an Odra 1325 computer.

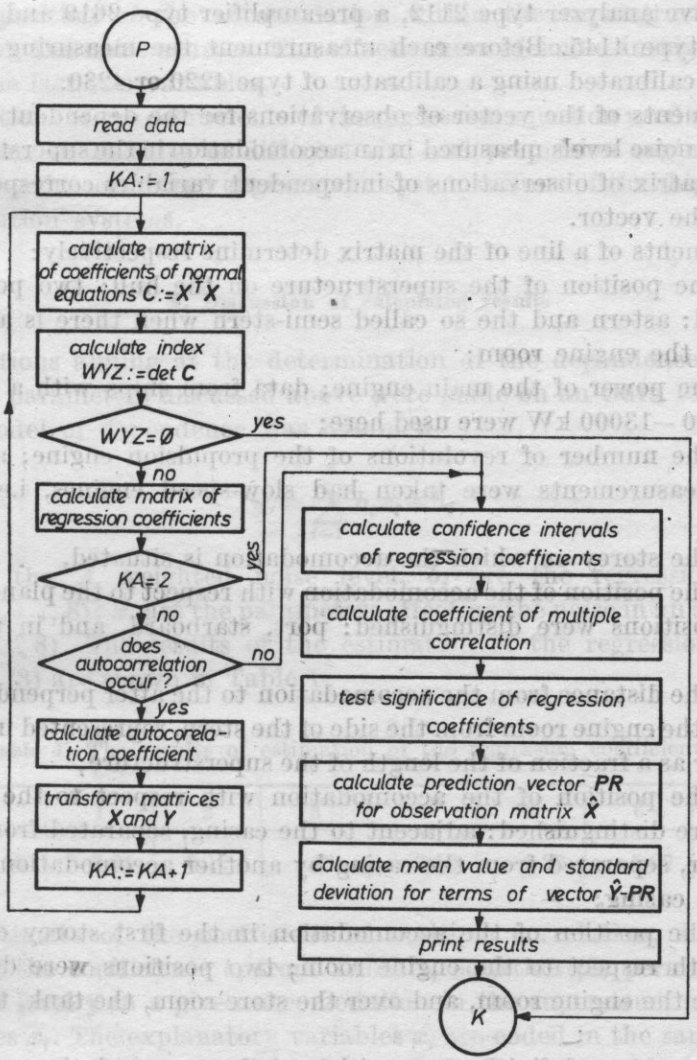

Fig. 2. A block diagram of the estimation of the parameters of the model of linear and multiple regression

KA – auxiliary variable, *X*, *Y* – given matrices whose elements are used for estimation of the parameters of the model, $\hat{X}$, $\hat{Y}$ – given matrices whose elements are not included in estimation of the parameters of the model

3. Data for calculations

The calculations used the results of measurements of noise levels taken by the Maritime Institute on Polish ships. In each case these measurements were taken on a ship with a typical load, at a sea state below 3, with revolutions of the propeller screw being no less than 95 percent of rated revolutions. The measurements used Brüel and Kjaer instrumentation in the following systems: a precision sound level meter type 2204 and a condenser microphone type 4145 or a 1/3 octave analyzer type 2112, a pre-amplifier type 2619 and a condenser microphone type 4145. Before each measurement the measuring system was checked and calibrated using a calibrator of type 4220 or 4230.

The elements of the vector of observations for the dependent variable are values of the noise levels measured in an accomodation in the superstructure. One line of the matrix of observations of independent variables corresponds to each element of the vector.

The elements of a line of the matrix determine respectively:

x_{i1} — the position of the superstructure on the hull; two positions were distinguished: astern and the so called semi-stern when there is an additional hold behind the engine room;

x_{i2} — the power of the main engine; data from ships with a main engine power of 3000 –13000 kW were used here;

x_{i3} — the number of revolutions of the propulsion engine; all the ships on which measurements were taken had slow-speed engines, i.e. below 250 revs./min.;

x_{i4} — the storey on which the accomodation is situated,

x_{i5} — the position of the accomodation with respect to the plane of symmetry; three positions were distinguished: port, starboard, and in the plane of symmetry;

x_{i6} — the distance from the accomodation to the after perpendicular or the bulkhead of the engine room from the side of the stern, represented in a dimensionless manner as a fraction of the length of the superstructure;

x_{i7} — the position of the accomodation with respect to the casing, four positions were distinguished: adjacent to the casing, separated from the casing by a corridor, separated from the casing by another accomodation, outside the area of the casing;

x_{i8} — the position of the accomodation in the first storey of the superstructure with respect to the engine room; two positions were distinguished: directly over the engine room, and over the store-room, the tank, the workshop etc.

The parameters defining the position of the accomodation were coded in such a manner that they could be used in the regression model. The position of the superstructure astern was given the value of 1, while that on the semi-stern was assigned 2. The same coding principle was assumed for the variables x_{i5},

x_{i7} and x_{i8}. E.g. the four possible positions connected with the variable x_{i7} were given the values of 1, 2, 3 and 4, respectively. If an independent variable takes more than two values, then the principle should be maintained that these must be in direct proportion to the corresponding values of the dependent variable.

The selection of explanatory variables took into consideration the significance of their contribution to the noise in the accomodation and the ease of determinating them in the preliminary design stage. The first three variables describe the influence of propulsion system. The variables x_{i4}, x_{i5} and x_{i6} define the position of the accomodation within the superstructure and the distance from the noise sources. The effectiveness of sound insulation is determined by the last two variables.

Calculations of the coefficients of the regression equation used data from 300 accomodations on 15 ships of different size and propulsion engine power, but with similar architecture and engine room systems. None of the ships had special sound insulation systems.

4. Discussion of calculated results

Calculations aiming at the determination of the dependence of the noise level on the parameters discussed above were made on an Odra 1325 computer. A linear model of dependence was assumed

$$y = \sum_{i=1}^{8} b_i x_i + b_0, \tag{3}$$

where y is the A weighted noise level, b_i are the regression coefficients ($i = 0, 1, 2, \ldots, 8$), x_i are the parameters affecting the noise in an accomodation ($i = 1, 2, \ldots, 8$). The results of the estimation of the regression coefficients of equation (3) are shown in Table 1.

Table 1. The results of estimation of the regression coefficients

i	0	1	2	3	4	5	6	7	8
b_i	62.46	−3.05	0.17	1.21	−0.16	−0.28	−5.07	−0.37	3.25

The estimate of the coefficient of multiple correlation, $R = 0.8$. After insertion of the coefficients b_i from Table 1, equation (3) permits calculation of the noise level y in a given accomodation in the superstructure, defined by the variables x_i. The explanatory variables x_i are coded in the same way as the relevant elements of the matrix of observations X used to calculate the coefficients of equation (3). The high coefficient of multiple correlation and the results of significance testing of regression coefficients indicate the validity of the linear model assumed.

In order to check practically the usefulness of the formula derived, noise levels were predicted for a matrix of observations $\hat{X}$ (independent variables) which was not included in the establishment of the model. The vector of point predictions PR (calculated from formula (3)) obtained was compared with the corresponding results of measurements of the noise level $\hat{Y}$. By calculating the mean and the standard deviation of the elements of the vector $W = \hat{Y} - PR$, additional quantities were obtained, which may serve to evaluate the quality of the prediction, and at the same time to evaluate the relation of the model to

Table 2. Comparison of predicted and measured levels of noise

	Ship data	Noise level [dB(A)] predicted PR	Noise level [dB(A)] measured $\hat{Y}$	Differences in noise levels $W = \hat{Y} - PR$ [dB(A)]	Parameters characterizing the distribution of values of W
1	2	3	4	5	6
		63.2	65	1.8	
		63.0	65	2.0	
		61.0	62	1.0	
		63.2	62	−1.2	
		61.3	60	−1.3	the mean value
	bulk carrier, superstructure	60.8	60	−0.8	
	astern, power 5888 kW, re-	56.6	57	0.4	$\overline{w} = -0.37$
	volutions 145 per min	55.3	55	−0.3	the standard
A		55,0	55	0.0	deviation
		56.1	57	0.9	$\sigma = 1.44$
		55.1	53	−2.1	
		54.8	53	−1.8	
		57.6	55	−2.6	
		55.2	54	−1.2	
		63.6	64	0.4	
		60.6	62	1.4	
		60.0	60	0.0	
		59.2	58	−1.2	
		57.7	56	−1.7	the mean value
		60.3	61	0.7	
	bulk carrier, superstructure	59.5	61	1.5	$\overline{w} = -0.89$
	astern, power 5300 kW,	53.9	54	0.1	the standard
B	revolutions 130 per min	54.0	55	1.0	deviation
		55.9	60	4.1	$\sigma = 1.45$
		56.0	57	1.0	
		54.1	55	0.9	
		55.3	58	2.7	
		53.8	54	0.2	
		53.7	56	2.3	

cd. Table 2.

1	2	3	4	5	6
		60.0	62	2.0	
		59.5	62	2.5	
		58.5	59	0.5	
		57.0	56	−1.0	
		55.1	55	−0.1	
		60.1	61	0.9	
		59.6	60	0.4	
		58.3	61	2.7	
		60.0	62	2.0	
		59.5	61	1.5	
		54.0	54	0.0	
		53.6	52	−1.6	
		53.0	51	−2.0	the mean value
	semi-containership, superstructure on the semi-stern,	52.0	52	0.0	
		51.8	53	1.2	$\overline{w} = -0.77$
C	power 17075 kW, revolutions	51.8	52	0.2	the standard
	120 per min	52.0	52	0.0	deviation
		54.4	54	−0.4	$\sigma = 2.11$
		53.4	54	0.6	
		52.4	48	−4.4	
		51.9	51	−0.9	
		51.6	47	−4.6	
		51.6	49	−2.6	
		53.2	51	−2.2	
		52.4	50	−2.4	
		51.4	49	−2.4	
		51.6	47	−4.7	
		51.6	49	−2.6	
		52.6	51	−1.6	

reality. The results for 59 accomodations on 3 ships are shown in Table 2. By considering all the values of the difference w (column 5, Table 2), their mean and the standard deviations were calculated, thus obtaining $\overline{w} = -0.25$ and $\sigma = 1.92$. The mean value close to zero (at the significance level 0.05 there is no justification for rejecting the hypothesis $H_0 : \overline{w} = 0$) indicates that the method presented has no constant trend. The standard deviation can, however, be regarded as the mean difference between the estimated and measured values.

The distribution parameters calculated for the individual ships, shown in column 6, Table 2, permit the statement that the prediction for ships *A* and *B* is in better agreement with the empirical values than for ship *C*. This is also indicated by the results obtained for the individual accomodations (column 5, Table 2). This results from the fact that the parameters of ships *A* and *B* lie in the variability intervals of the corresponding parameters of the input test. The parameters of ship *C* exceed, however, these intervals. This indicates that extrapolation causes a decrease in accuracy.

5. Remarks and conclusions

1. The harmful effect of noise on the human organism and the scope of this phenomenon should generate an interest in these problems from the owners of ships and shipbuilders. The research towards the prevention of excessive noise levels gives only sufficient effect when it is introduced at a sufficiently early stage of the ship design.

2. Prevention should be based on the prediction of noise levels in accomodations of the superstructure. The results obtained and their comparison with the measured data indicate the validity of the model assumed and permit the statement that the application of the method of multiple regression in noise prediction on ships gives good results.

3. The present model, because it is based on a statistical method, considers one of the very important factors that sometimes determine the noise level, i.e. the technology and workmanship used in ship building.

4. The present method of noise prediction, due to its simplicity, can be used at a very early stage of the design.

5. The range of application of the correlation and the regression methods is in each case defined by the two following principles:

(a) If there is a causal relation between the phenomena investigated, then the power of this relation can be determined by the correlation calculus. If the power is large enough (i.e. when $R^2 > 0.5$) it is worthwhile to seek the equation of the hyperplane of regression, and to use it subsequently as a prediction tool.

(b) If there is an assumption that a causal relation exists between the phenomena investigated, then the presence of a distinct correlation in sufficient numerical material strengthens, to a large extent, the hypothesis that the causal relationship exists.

The first of the principles mentioned above was followed in the selection of the explanatory independent variables. That there is a causal relation between the values of these variables and the noise level at a point defined by these variables seems evident.

Further investigations should be performed in the two directions:

(a) expansion of the set of independent variables according to the second of the principles mentioned above;

(b) adoption of the present method to prediction of octave spectra.

References

[1] J. Buiten, H. Aartsen, *Simplified method for predicting sound level A in accomodation spaces aboard sea-going motorships*, Proceedings Inter-Noise 79, ed. S. Czarnecki, IPPT PAN Warszawa 1979, 585-589.

[2] G. L. Fox, *Noise and vibration control techniques for the U. S. Navy 3000-LT Surface-effect ship*, Marine Technology, **17**, 1, 16-28 (1980).

[3] J. GREŃ, *Mathematical statistics* (in Polish), PWN, Warszawa 1978, 200-235.

[4] Z. HELLWIG, *Linear regression and its application in economics* (in Polish), PWE, Warszawa 1963.

[5] T. KIHLMAN, J. PLUNT, *Prediction of noise levels in ships*, Proceedings of International Symposium on Shipboard Acoustics, ed. J. H. JANSSEN, Elsevier Scientific Publishing Company, Amsterdam 1977, 297-315.

[6] A. C. NILSSON, *Noise prediction and prevention*, Technical Report No. 78-030, Det Norske Veritas Research Division, 1978.

[7] *Noise and vibration control onboard ships*, Det Norske Veritas Maritime Advisory Services, 1978.

[8] H. THEIL, *Principles of econometrics* (in Polish), PWN, Warszawa 1979.

[9] K. UMEZAKI, H. MIZUNO, Y. SHIMODA, *Study for application of the statistical method to the predicting of ship vibration characteristics*, Naval Architecture, **16**, 168-178 (1978).

[10] G. WARD, A. HOYLAND, *Ship design and noise levels*, North East Coast Institution of Engineers Shipbuilders, **95**, 4, 177-196 (1979).

Received on April 28, 1980

ARCHIVES OF ACOUSTICS
6, 2, 123-134 (1981)

ON THE INFLUENCE OF THE NOZZLE EXTERNAL CONFIGURATION ON THE RADIATED SCREECH AND THE DECAY OF SUPERSONIC JETS*

GIOVANNI MARIA CARLOMAGNO

Institute of Aerodynamics

CARMINE IANNIELLO, PAOLO VIGO

Institute of Applied Physics, Faculty of Engineering,
University of Naples, 80125 Naples, Italy

The behaviour of screeching jets exhausting from an axisymmetric convergent-divergent nozzle was studied. The nozzle had a 2.9 mm throat diameter and a 1.95 theoretical exit Mach number. Compressed nitrogen was used to obtain nozzle stagnation pressures from 0.15 to 1.4 MPa (absolute), i.e. conditions of overexpanded, correctly expanded and underexpanded streams at the nozzle exit section. The jet exhausted into a free field room and tests were performed for several nozzle external configurations. Measurements were made in terms of noise level emitted by the jet and impact pressure downstream. It was found that in the weakly overexpanded and in the underexpanded regimes the nozzle external configuration influences markedly the screech intensity while it does not affect substantially its frequency. The latter generally decreases as the stagnation pressure increases; in particular in the weakly overexpanded regime two screeching frequencies are present for a given stagnation pressure. High intensity screech jets have down-stream impact pressures lower than low intensity ones and therefore higher decay rates. Even for correctly expanded jets, screech levels and impact pressures are configuration influenced. In the strongly overexpanded regime, several harmonically related spectral peaks are present whose frequencies increase for increasing stagnation pressure; they appear not to be substantially influenced by the nozzle configuration but correspond, rather, to pure shock noise.

* Work sponsored by National Research Council of Italy (C.N.R.).

1. Introduction

It is well established that the noise emitted by jets strongly depends on the fluid dynamic field associated with them. LIGHTHILL [12] gave an analytical theory, describing the generation of aerodynamic noise in subsonic jets, which predicts that the overall sound power is proportional to the eighth power of the jet speed. This theory, however, is not applicable to the theoretical prediction of the noise emitted by choked jets having a shock cellular structure, which show a peculiar behaviour.

The complex interaction between the jet shock structure and the turbulent mixing flow, the oscillation of the shock itself, and the interaction of the radiated noise field with the fluid dynamic field and the ambient configuration (near the origin of the jet), make the whole problem rather cumbersome so that a satisfactory descriptive model is still far off. Much of the knowledge rests on experimental results from which some insight into the noise generation mechanisms has been gained. For jets having a shock structure these mechanisms may be roughly divided into three classes:

1) turbulence noise due to fluctuations of momentum flux;

2) shock noise associated with instability of the shock, arising when the convected turbulent eddies pass through it;

3) screech, a particular narrowband shock noise enhanced by a type of regenerative amplification.

The latter is of primary interest within the present context.

POWELL [17] first gave a model for the screech phenomenon which was later confirmed in more detail by DAVIES and OLDFIELD [5]. Briefly, the mechanism can be described in the following manner. Sound waves, arising when a flow disturbance convected downstream interacts with the shock cell pattern of the jet, propagate themselves upstream toward the nozzle exit section where they slightly affect the nozzle pressure ratio. This event results in a disturbance of the flow, growing up like a vortex, which is convected downstream along the jet boundaries. The vortex, in turn, excites the emission of sound waves. When the right conditions exist, the feedback loop is selfsustained by tuning itself at certain discrete frequencies: the screech tones.

The general interest in the problem is connected with three different areas:

1. noise "per se", since the screech tones, if they lie in the audible frequency range, may be by far the loudest component of the noise;

2. structural damage, since the hypothesis that the screech severely fatigues aircraft structures has been put forward [10, 18];

3. jet decay process, since the screech affects the spreading of the jet itself [1-4, 7].

Much work has been published [11, 13-15, 20] describing, phenomenologically, the screech and the characteristics of the jets from which it originates.

More or less empirical relationships have been given which predict the screech frequency for the tested conditions, although the screech intensity remains essentially unpredictable. All the papers on the problem are generally related to underexpanded jets issuing from two-dimensional plane and axisymmetric convergent nozzles (choked jets). With regard to the frequency of the screech tones, changes in the upstream stagnation pressure result in quite different behaviour for the two types of jets. Two-dimensional plane jets show a continuously decreasing screech frequency with increasing stagnation pressure, while axisymmetric jets, still retaining this general trend, also exhibit remarkable jumps in the screech frequency in certain stagnation pressure ranges. This discontinuous behaviour is closely related to sharp changes in the cell pattern [5].

Referring to the screech intensity and to the jet decay characteristics, several papers [5, 7-9, 17, 19] show the influence on the radiated noise and/or on the jet decay, of both sound absorbing and sound reflecting surfaces placed near the nozzle orifice. The very solid annular zone surrounding the exit section of the nozzle itself can modify both the noise and the decay of the jet [1-4, 16].

In fact the ambient configuration near the origin of the jet interacts with the sound waves propagating upstream and therefore a peculiar feedback system is set up. One may conclude that modifications of the ambient configuration can be used, in a sense, to distinguish pure shock noise from shock noise that can be tuned into by the feedback system and which turns out as screech. This is indeed implicitly done in the study of pure shock noise where screech is suppressed with sound absorbing layers or small projections on the nozzle lip [9]. It has to be pointed out that this practice is not correct if the turbulent noise component of a particular jet is to be studied. In fact, since the jet decay is highly influenced by the screech tones, a different decay can in turn influence the broadband noise. To authors' knowledge, at the present time little screech data has been published for jets issuing from convergent-divergent nozzles, i.e. jets which start supersonically. In the present context, these nozzles have mainly been considered as means to suppress screech noise [6, 21], in the sense that a correctly expanded jet, having a practically shockless structure, will lack any screech.

The aim of this work has been to investigate experimentally those screeching jets which emit supersonically (i.e. issuing from a convergent-divergent nozzle), to determine their behaviour above and below the theoretically correct nozzle pressure ratio. The main motivation is that a cellular shock pattern exists both for underexpanded streams (as for choked jets) and for overexpanded streams.

2. Experimental procedures

The measurements were performed in a free field room. The tested nozzle shown in Fig. 1, has a 2.9 mm throat diameter, a conical divergent with 1 : 20 taper ratio, and a 1.95 theoretical exit Mach number. Compressed pure nitrogen

at nearly room temperature was sent to the nozzle through a pressure regulating valve and a settling chamber. The stagnation pressure was varied from 0.15 up to 1.4 MPa (absolute). Both the settling chamber, that was placed in the free field room, and its supporting structures were lined with sound absorbing acoustic foam in order to reduce the influence of reflected waves on the jet noise field. A 1.5 mm OD externally chamfered pitot tube was placed on the jet axis at 300 mm from the nozzle exit section. Schlieren visualizations, not reported herein, were performed at various pressure ranges.

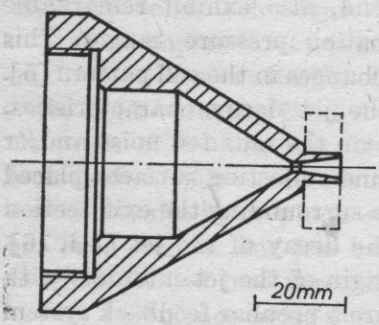

Fig. 1. Configurations of the tested nozzle; the broken line indicates the 26 mm OD brass flange

The noise was measured, at 150° to the downstream oriented jet axis [3] and at 1 m from the center of the nozzle exit section, with a B and K type 4133 ½" microphone and recorded on a Nagra IV-SJ tape recorder which had a frequency response ±1.0 dB from 25 Hz to 35 kHz and a −3 dB point at 40 kHz The recorded noise was subsequently analysed with a B and K system consisting of a 2120 noise frequency analyser and a 2305 graphic level recorder. Frequency spectra were obtained, for both 3% and 1% constant percentage bands, swept over the range 6.3-50 kHz. Due to the tape recorder characteristics the pressure level spectra presented are slightly understimated in the range 35-40 kHz and greatly underestimated in the range 40-50 kHz. Peak frequency values in the range 35-50 kHz have been detected with a 1% bandwidth. Since the noise analyser allowed frequency analysis up to 20 kHz, during the play mode the tape was slowed down by a 1:10 speed ratio in order to accomodate the recorder frequency band in the 3Hz-20 kHz analyser band available.

Most of the tests were performed with both of the external configurations represented in Fig. 1 where the broken line indicates a 26 mm OD brass flange. In the tests without the flange the thickness of the annular zone surrounding the nozzle exit section was about 0.8 mm. Some tests were also performed with two different (13 and 49 mm OD) brass flanges and with a 26 mm OD sound absorbing flange.

3. Results and discussion

The diagrams of Fig. 2 show the 3% bandwidth sound pressure level spectra of the noise emitted by the jet for the two nozzle external configurations represented in Fig. 1, i.e. the nozzle without a flange, and the nozzle with the

26 mm OD brass flange. Each line corresponds to a particular value of the stagnation pressure, p_0, which varies from one corresponding to almost correct nozzle expansion (theoretically located at $p_0 = 0.73$ MPa), to values that involve an underexpanded stream at the nozzle exit section. On the basis of the diagrams of Fig. 2 and of other tests performed, the following conclusions can be drawn:

– Each spectrum shows a marked peak at a given frequency. The 1% bandwidth analysis has shown that these peaks are narrowband in nature. In accordance with previous results [17], especially at the high pressures and for the "with flange" tests, a second peak has been found at twice the frequency of the first one. The amplitude of the signal in the range 40-50 kHz, and in particular for the harmonic peaks, is underestimated since the tape recorder attenuated the signal (see previous section).

– The peak frequency seems substantially independent of the nozzle external configuration. This behaviour has been confirmed by the tests performed with different OD brass flanges, and with the sound absorbing flange.

– The difference between the peak pressure levels for the two configurations of Fig. 1 is irrelevant at the stagnation pressure $p_0 = 0.7$ MPa which

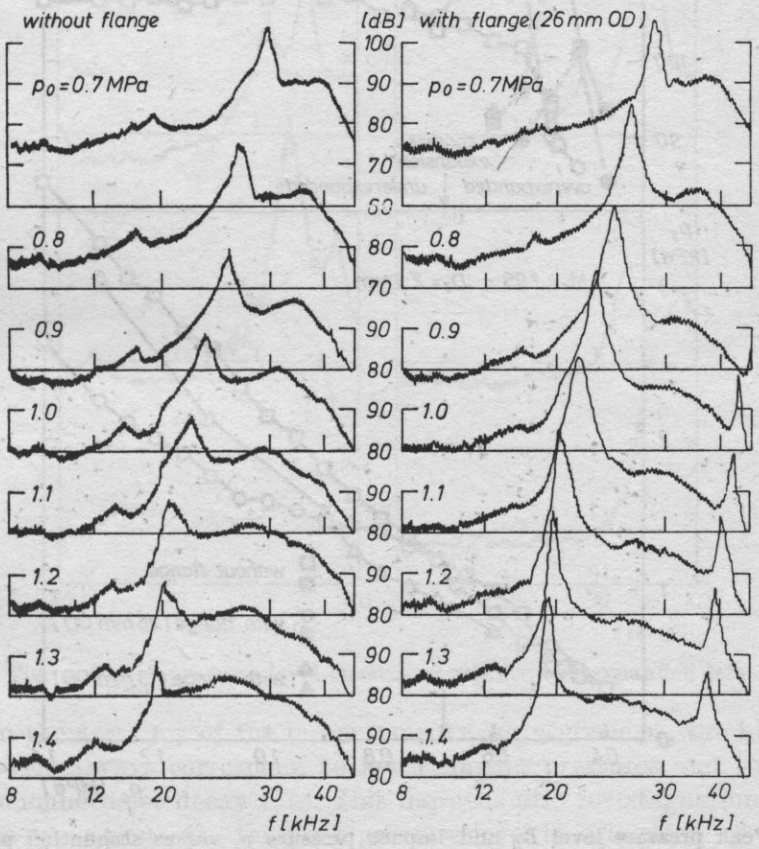

Fig. 2. Sound pressure level spectra of almost correctly expanded, and underexpanded jets

corresponds to almost correct nozzle expansion (a similar result has also been found at $p_0 = 0.75$ MPa), but it increases with increasing stagnation pressure. At $p_0 = 1.3$ MPa the peak pressure level of the noise emitted by the jet issuing from the nozzle with a flange is about 18 dB higher than that from the nozzle without a flange. Some tests performed with the other brass flanges have shown peak pressure levels which are generally intermediate between those related to the two different configurations of Fig. 1. A completely different behaviour has, however, been found in tests performed at $p_0 = 0.7$ MPa, with both the 13 mm and the 49 mm OD brass flanges, which showed peak pressure levels about 10 dB higher than those corresponding to the two configurations of Fig. 1. Tests

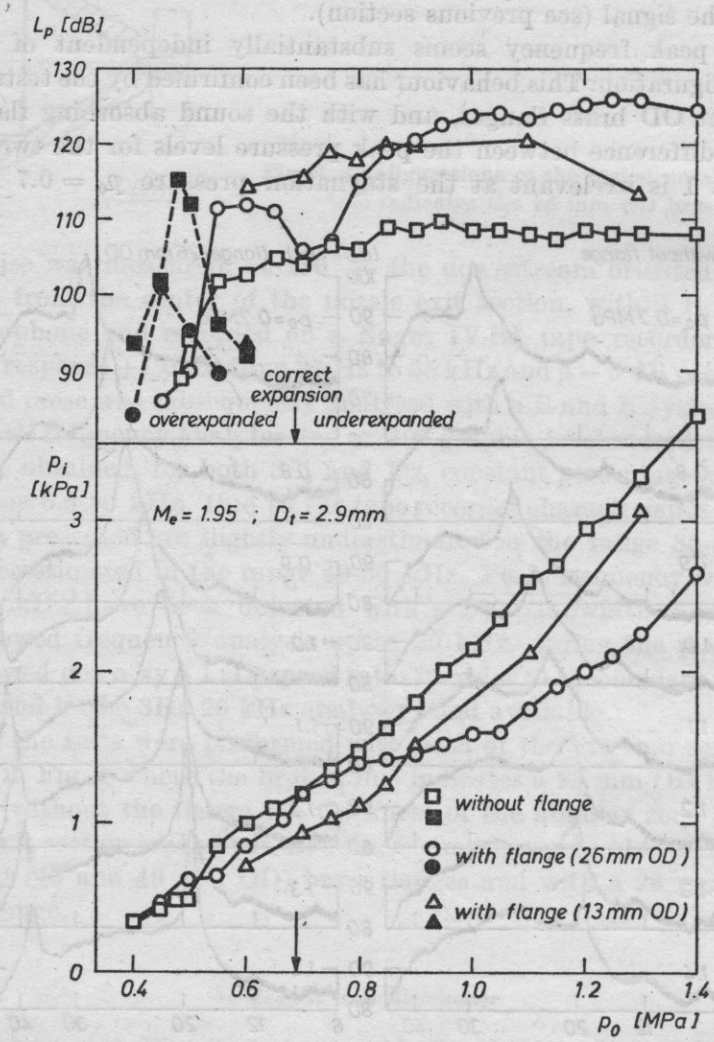

Fig. 3. Peak pressure level L_p and impact pressure p_i versus stagnation pressure p_0

performed with the sound absorbing flange have indicated peak pressure levels which are about 3 dB lower than those corresponding to tests without a flange.

— The peak frequency decreases with increasing stagnation pressure.

The peak pressure level values, L_p (for the nozzle external configurations: without a flange, with 26 mm and with 13 mm OD brass flanges) have been compared in Fig. 3 with the measured impact pressures p_i for a wider range of the stagnation pressure p_0.

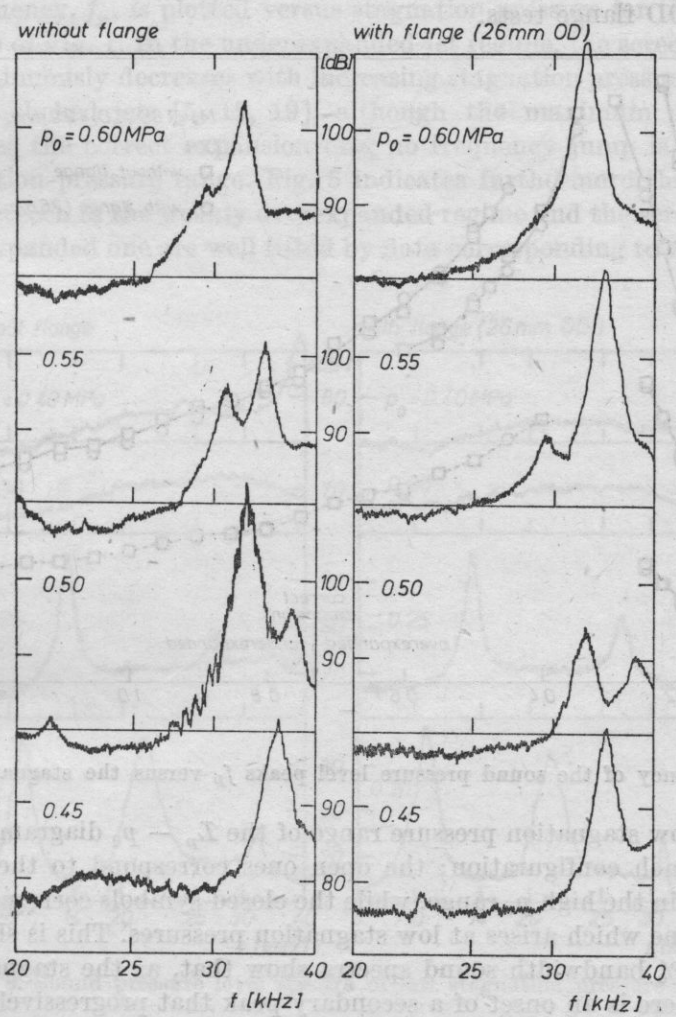

Fig. 4. Sound pressure level spectra of weakly overexpanded jets

Within the accuracy of the measurements, for a given p_0, the higher peak pressure levels always correspond to lower impact pressures and therefore to a more pronounced jet decay rate. This happens also for stagnation pressures close to the correct one, i.e. the peak pressure level is influenced by the nozzle

configuration and so is the impact pressure. It has to be pointed out, however, that in this range the smaller flange (13 mm OD) shows high peak levels, while the larger one (26 mm OD) influences neither L_p nor p_i. These results are in accordance with the results previously reported by the present authors [2, 3]. Schlieren visualizations showed that the higher the peak pressure level of the jet, the lower was the number of its apparent cells; e.g. at $p_0 = 1.1$ MPa eleven cells were visible for runs without a flange, while only eight were seen during the 26 mm OD flange tests.

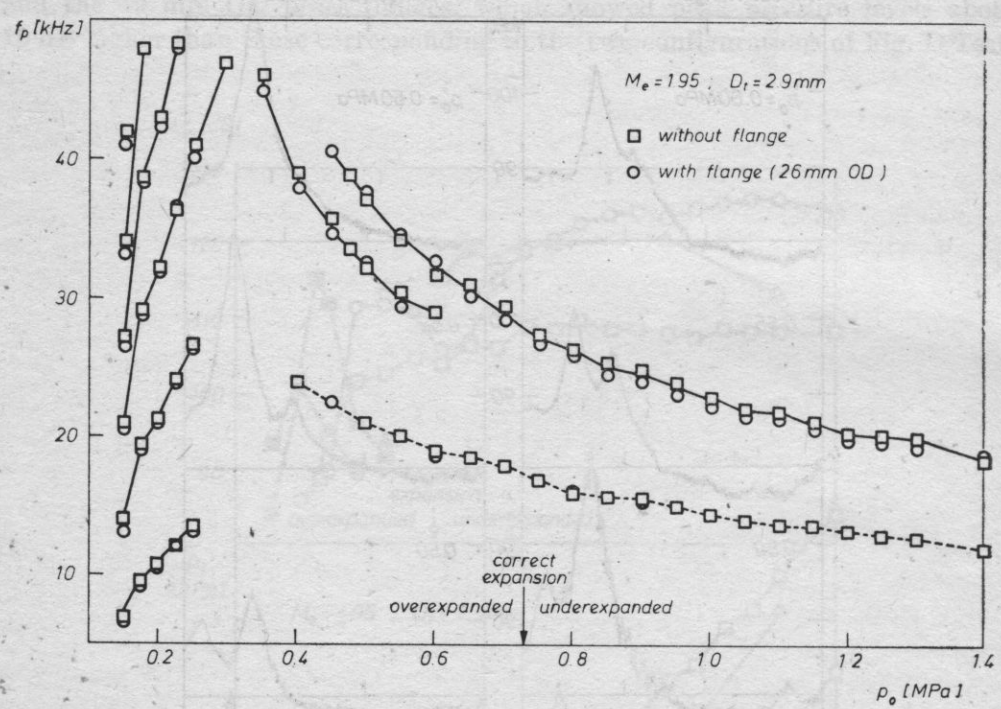

Fig. 5. Frequency of the sound pressure level peaks f_p versus the stagnation pressure p_0

In the low stagnation pressure range of the $L_p - p_0$ diagram, two symbols appear for each configuration; the open ones correspond to the tone already encountered in the high p_0 range, while the closed symbols correspond to a lower frequency tone which arises at low stagnation pressures. This is shown in Fig. 4 where the 3 % bandwidth sound spectra show that, as the stagnation pressure decreases, there is an onset of a secondary peak that progressively replaces the previous one which eventually vanishes. Both peaks occur at frequencies that decrease with increasing stagnation pressure. The behaviour described seems to be "delayed" in the "with flange" tests.

For very low stagnation pressures (see Fig. 3) this secondary peak also tends to decrease its intensity, and its effect on the impact pressure. The sound spectra of Fig. 4 suggest the simultaneous presence of two relatively high intensi-

ty screeching tones for a significant range of stagnation pressures. However, it has to be pointed out that, since the analyser integrates signals in time, the two peaks found could possibly be due to continuous jumping of the feedback loop between two almost stable configurations to which the two different screech tones correspond. Also in this pressure range, Schlieren visualizations showed essentially the same behaviour as was described for the underexpanded jets.

The overlapping range of the two screech tones is also evident from Fig. 5 where the peak frequency, f_p, is plotted versus stagnation pressure for the two nozzle configurations of Fig. 1. In the underexpanded jet regime, the screech frequency (full line) continuously decreases with increasing stagnation pressure. Unlike the behaviour for choked jets [5, 15, 19], although the maximum pressure ratio is almost twice the correct expansion one, no frequency jump is found in the tested stagnation pressure range. Fig. 5 indicates furthermore that the higher tones of the screech in the weakly overexpanded regime and the screeching tones of the underexpanded one are well fitted by data corresponding to nearly correct expansion.

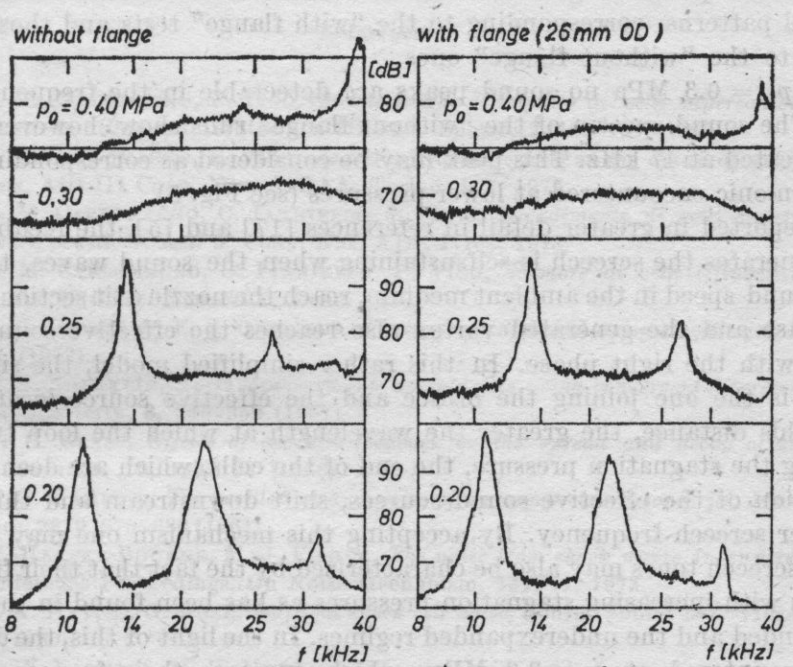

Fig. 6. Sound pressure level spectra of low stagnation pressure jets

Beside the dominant tone, the sound spectra, especially for the "without flange" tests, show a secondary peak (dashed line in Fig. 5), at a lower frequency, which also decreases in amplitude with increasing p_0 without showing any shift of frequency. This peak, of much lower pressure level, is evident in some of the spectra of Figs. 2 and 4. It behaves like a screeching tone and starts to appear in the weakly overexpanded jet region at $p_0 = 0.4$ MPa (Fig. 6).

The data in Fig. 5 also shows the frequencies of the sound pressure level peaks which are present in the strongly overexpanded jet regime. These peaks, which are harmonically related, are evident, at low stagnation pressure values, in the 3 % bandwidth sound spectra of Fig. 6 obtained for the two different nozzle configurations of Fig. 1. Whereas in the weakly overexpanded and the underexpanded regimes, the peak frequencies decrease with increasing stagnation pressure, in the strongly overexpanded regime, the peak frequencies increase. The two sets of spectra look very similar except at high frequencies where the spectra of the tests with a flange show generally lower sound pressure levels. This may be due to the fact that, since for low stagnation pressures the shock cell pattern shortens, the 26 mm OD flange has a masking effect on the jet noise propagation toward the microphone. Sound spectra obtained in tests with the other brass flange look very similar to those of Fig. 6. Within the accuracy of the measurements no impact pressure difference was detected below 0.3 MPa for the various nozzle external configurations. Schlieren visualizations in the strongly overexpanded regime did not show substantial differences between the shock cell patterns corresponding to the "with flange" tests and those corresponding to the "without flange" ones.

For $p_0 = 0.3$ MPa no sound peaks are detectable in the frequency range shown. The sound spectra of the "without flange" runs show, however, a peak that is located at 47 kHz. This peak may be considered as corresponding to the third harmonic encountered at lower pressures (see Fig. 5).

As reported in greater detail in references [17] and [5], the feedback loop which generates the screech is selfsustaining when the sound waves, travelling at the sound speed in the ambient medium, reach the nozzle exit section with the right phase and the generated vortex also reaches the effective sound source location with the right phase. In this rather simplified model, the significant distance is the one joining the orifice and the effective source location: the greater this distance, the greater the wavelength at which the loop tunes. By increasing the stagnation pressure, the end of the cells, which are deemed to be the location of the effective sound sources, shift downstream and this results in a lower screech frequency. By accepting this mechanism one may conclude that the screech tones may also be characterized by the fact that their frequency decreases with increasing stagnation pressures as has been found in the weakly overexpanded and the underexpanded regimes. In the light of this, the dominant tones encountered at $p_0 < 0.3$ MPa, which increase their frequencies with increasing p_0, may be considered as pure shock noise. The other tones which, instead, decrease their frequencies with increasing p_0, can all be considered as screech tones and are therefore configuration influenced.

The present results present a phenomenology which is wider than the one usually encountered in experiments with choked jets. The cellular shock pattern, still present in the overexpanded regime and in the correctly expanded one (especially for conical divergent nozzles, as shown by Schlieren visualizations),

is able to generate screeching tones which, if correctly tuned by the feedback mechanism (depending on the nozzle external configuration), again influence the emitted noise and the jet decay rate. This event is of particular importance for correctly expanded jets. In fact, it has been suggested [6] that, in order to suppress the screech noise of a jet operating at a high pressure ratio, there is a definite advantage in using a convergent-divergent nozzle designed for that pressure ratio instead of a simple convergent one. The present results show, however, that while this may be true for a specific configuration (cf. tests with the 26 mm OD brass flange), it is not in general true for different configurations as is indicated by the data at $p_0 = 0.7$ MPa for both the 13 mm and 49 mm OD brass flanges.

In any case, since convergent-divergent nozzles, especially in propulsion, are seldom operated at a fixed pressure ratio, the acoustic behaviour of the jet issuing from them is of great importance in practical applications.

References

[1] G. M. Carlomagno, P. Vigo, *Caratteristiche di impatto di getti supersonici*, in presenza di acustiche riflesse, l'Aerotecnica Missili e Spazio, **2**, 101-104 (1975).

[2] G. M. Carlomagno, P. Vigo, *Acoustic feedback effects on the decay of axisymmetric supersonic jets*, Atti III Cong. Naz. AIDAA, Torino, 1-7, 1975.

[3] G. M. Carlomagno, C. Ianniello, P. Vigo, *Decadimento di getti supersonici in presenza di onde acustiche*, Atti 6° Conv. Naz. AIA, Ivrea, 1978.

[4] G. M. Carlomagno, C. Ianniello, P. Vigo, *Rumore di getti effluenti da ugelli supersonici*, Atti 7° Conv. Naz. AIA, Siena. 1979.

[5] M. G. Davies, D. E. S. Oldfield, *Tones from a choked axisymmetric jet*, Acustica, **12**, 257-277 (1962).

[6] R. E. Franklin, *Noise measurements on cold jets using convergent-divergent nozzles*, Aeronautical Quarterly, **8**, 346-359 (1957).

[7] D. R. Glass, *Effects of acoustic feedback on the spread and decay of supersonic jets*, AIAA Journ., **6**, 10, 1890-97 (1968).

[8] A. G. Hammitt, *The oscillation and noise of an overpressure sonic jet*, Journ. Aerospace Sciences, **28**, 9, 673-680 (1961).

[9] M. Harper-Bourne, M. J. Fisher, *The noise from shock waves in supersonic jets*, AGARD Conference Proceedings, On Noise Mechanism, **131**, 11, 1973.

[10] J. A. Hay, E. G. Rose, *In flight shock cell noise*, Journ. Sound and Vibration, **11**, 4, 411-420 (1970).

[11] L. W. Lassiter, H. H. Hubbard, *The near noise field of static jets and some model studies of devices for noise reduction*, NACA Rept. 1261, 1956.

[12] M. J. Lighthill, *On sound generated aerodynamically*, Proc. Roy. Soc., **A211**, 564-587 (1952).

[13] D. L. Martlew, *Noise associated with shock waves in supersonic jets*, NATO AGARD Conference Proceedings, Aircraft Engine Noise and Sonic Boom, **42**, 7 (1969).

[14] M. Merle, *Ondes sonores emises par un jet d'air*, Comptes Rendus, **240**, 2055-2057 (1955).

[15] M. Merle, *Sur la frequence des ondes sonores emises par un jet d'air a grande vitesse*, Comptes Rendus, **243**, 490-493 (1956).

[16] M. MERLE, *Influence d'un baffle sur l'emission acoustique d'un jet d'air sonique*, Comptes Rendus, **248**, 2534-2536 (1963).

[17] A. POWELL, *On the noise emanating from a two-dimensional jet above the critical pressure*, Aeronautical Quarterly, **4**, 103-122 (1953).

[18] E. J. RICHARDS, D. J. MEAD, *Noise and acoustic fatigue in aeronautics*, J. Wiley, New York 1968.

[19] P. M. SHERMAN, D. R. GLASS, K. C. DULEEP, *Jet flow field during screech*, Appl. Sc. Res., **32**, 8, 283-303 (1976).

[20] R. WESTLEY, J. H. WOOLLEY, *The near field sound pressures of a choked jet during a screech cycle*, NATO AGARD Conference Proceedings, Aircraft Engine Noise and Sonic Boom, **42**, 23 (1969).

[21] J. C. YU, D. S. DOSANJH, *Noise field of a supersonic Mach 1.5 cold model jet*, The Journal of the Acoustical Society of America, **51**, 5, 1400-1410 (1972).

Received on December 29, 1979; revised version on October 31, 1980

ARCHIVES OF ACOUSTICS
6, 2, 135-146 (1981)

THE BLURRED CUT-OFF FREQUENCY OF ACOUSTIC HORNS

TOMASZ ZAMORSKI

Institute of Physics of Higher Pedagogical School, Rzeszów
(35-310 Rzeszów, ul. Rejtana 16A)

On the basis of discussion of the Webster equation the conditions and possibilities of a blurred cut-off frequency for horns of arbitrary geometry were analyzed. The transmission properties of horns in the blurred region were discussed. Subsequently the blurred cut-off frequency was considered for hyperbolic horns of annular cross-section.

1. Introduction

The notion of the cut-off frequency of a horn occurs in the theory of acoustic horns in a discussion of the so-called Webster equation [7, 8]. This equation describes the wave motion in the horn with the simplifying assumptions that the propagating wave is plane, harmonic, of infinitely small amplitude, and propagates without energy losses. In the case when the geometrical axis of the horn coincides with the axis of the abscissa, the Webster equation written in the reduced form is the following [8]

$$\frac{d^2F}{da^2}+\left(\mu^2-\frac{1}{\varrho}\frac{d^2\varrho}{da^2}\right)F=0, \tag{1}$$

where F is the wave function [1] related to the sound pressure p and the area of cross section of the horn S by the formula

$$p=\frac{F}{\sqrt{S}}, \tag{2}$$

a is the dimensionless abscissa determined by the formula

$$a=\frac{x}{x_0}, \tag{3}$$

with x_0 being the coefficient of divergence of the walls of the horn; μ is dimensionless frequency

$$\mu = \frac{f}{f_0}, \tag{4}$$

where f is the absolute frequency and f_0 is a constant with the dimensions of frequency defined by the relation

$$f_0 = \frac{c}{2\pi x_0}, \tag{5}$$

with c being adiabatic velocity of the acoustic wave; ϱ is the dimensionless radius of the cross-section of the horn defined by the formula

$$\varrho = \sqrt{\frac{S}{S_0}}, \tag{6}$$

with S_0 being the area of the horn inlet.

The form of the solution of the wave equation (1) depends on the sign of the expression in the brackets by the function F. If this expression is larger than zero, which occurs when $\mu^2 < \varrho^{-1} d^2\varrho/da^2$, then the function F becomes periodic. However, in the case where the term in the brackets is less than zero, F is an aperiodic function. This occurs when $\mu^2 < \varrho^{-1} d^2\varrho/da^2$. The function F is connected with the acoustic pressure by formula (2) and describes the wave motion in the horn; it should, therefore, be a periodic function. It should be stated, therefore, that for the frequencies which satisfy the condition $\mu^2 > \varrho^{-1} d^2\varrho/da^2$ the wave motion occurs in the horn, while for the frequencies for which $\mu^2 < \varrho^{-1} d^2\varrho/da^2$ this motion does not occur and the horn does not guide acoustic waves. The boundary between these two frequency ranges can be obtained by equating the above mentioned expression, which occurs in formula (1), to zero. Then one obtains the cut-off frequency of the horn, μ_{gr}, which was mentioned in the introduction and below which the wave motion in the horn will decay

$$\mu_{gr} = \sqrt{\frac{1}{\varrho}\frac{d^2\varrho}{da^2}}. \tag{7}$$

It can be seen from formulae (6) and (7) that the cut-off frequency μ_{gr} depends on the geometry of the horn. For the horns discussed so far in the literature the expression under the square root sign in formula (7) took a constant value, which implied a constant value for μ_{gr}. For example, in the case most frequently described and used practically, Salmon's horn, this expression is equal to unity [5, 6, 8],

$$\frac{1}{\varrho}\frac{d^2\varrho}{da^2} = 1. \tag{8}$$

Thus the dimensionless cut-off frequency μ_{gr} is also equal to unity, and from (4) it can be seen that in this particular case the absolute cut-off frequency is equal to the constant f_0.

Generally, however, the expression under the square root sign in formula (7) must be a function of the position on the axis of the horn. This function will be subsequently denoted by $V_{(a)}$ in this paper,

$$V_{(a)} = \frac{1}{\varrho} \frac{d^2 \varrho}{da^2}. \tag{9}$$

In this case the frequency μ_{gr} also becomes a function of position and extends over a certain frequency range for a horn of a given length. This is the so called blurred cut-off frequency. Analysis of this phenomenon is the subject of the present paper.

2. Analysis of the transmission properties of a horn in the blurred cut-off frequency region

Let us assume that $V_{(a)}$ is a continuous function. Moreover, we shall assume that the function is monotonic* and consider the case where $V_{(a)}$ decreases. This case is illustrated by Fig. 1 for a horn of length a_l, whose inlet was placed at the origin of the coordinate system.

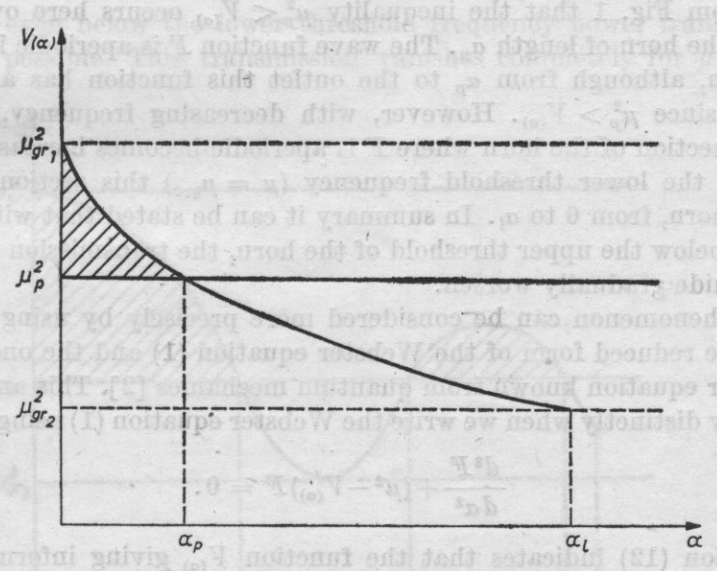

Fig. 1. The monotonically decreasing function $V_{(a)}$ as a "geometric barrier" of the horn for waves at frequencies $\mu < \mu_{gr1}$

* assumption of monotonicity of the function $V_{(a)}$ corresponds to horns used in practice.

Fig. 1 shows that for frequencies higher than μ_{gr_1} over the whole length of the horn $\mu^2 > V_{(a)}$. According to what has been said in section 1, this signifies that wave motion occurs in the horn for $\mu > \mu_{gr1}$. Below the frequency μ_{gr2} over the whole length of the horn the relation $\mu^2 < V_{(a)}$ is satisfied, which is a lack of periodicity in the wave function F and a decay of wave motion. However, at frequencies in the interval from μ_{gr2} to μ_{gr1} the function F is periodic only over some sections of the horn: this is the interval of the blurred cut-off frequency of the horn. Accordingly, it is proposed that the quantities μ_{gr2} and μ_{gr1}, which are the limits of this interval, should be called the lower and upper threshold frequencies of the horn. In the present case μ_{gr1} and μ_{gr2} can be determined from formula (7) by insertion into it of the dimensionless value of the abscissa of the inlet ($a = 0$) and the outlet ($a = a_1$) of the horn

$$\mu_{gr1} = \sqrt{\frac{1}{\varrho_{(0)}}\varrho''_{(0)}}, \tag{10}$$

$$\mu_{gr2} = \sqrt{\frac{1}{\varrho_{(a_l)}}\varrho''_{(a_l)}}, \tag{11}$$

where the dashes denote differentiation with respect to the dimensionless abscissa a.

In order to consider more closely the phenomena occurring in the frequency interval $[\mu_{gr2}, \mu_{gr1}]$ one can consider a frequency μ_p within this interval. It can be seen from Fig. 1 that the inequality $\mu_p^2 < V_{(a)}$ occurs here over the inlet section of the horn of length a_p. The wave function F is aperiodic in this region of the horn, although from a_p to the outlet this function has an oscillatory character, since $\mu_p^2 > V_{(a)}$. However, with decreasing frequency, for $\mu < \mu_p$, the outlet section of the horn where F is aperiodic becomes increasingly longer. Finally, at the lower threshold frequency ($\mu = \mu_{gr2}$) this section expands to the whole horn, from 0 to a_l. In summary it can be stated that with increasing frequency below the upper threshold of the horn, the transmission properties of the waveguide gradually worsen.

This phenomenon can be considered more precisely by using the analogy between the reduced form of the Webster equation (1) and the onedimensional Schrödinger equation known from quantum mechanics [2]. This analogy occurs particularly distinctly when we write the Webster equation (1) using equation (9)

$$\frac{d^2F}{da^2} + (\mu^2 - V_{(a)})F = 0. \tag{12}$$

Equation (12) indicates that the function $V_{(a)}$ giving information about the geometry of the horn is an analogue of the potential energy function in quantum theory. Thus, the problem of the transmission properties of the horn in the interval $[\mu_{gr2}, \mu_{gr1}]$ is analogous to the problem of the penetration of particles through the potential barrier in quantum mechanics. Since, as in quan-

tum mechanics, one can speak of an energy barrier (potential barrier) for elementary particles, one can now speak of a "geometric" barrier formed by the horn for a wave of a given wavelength. The dashed region in Fig. 1 can, therefore, be considered to be a measure of the size of the barrier for a wave of a given frequency $\mu = \mu_p$.

Using the WKB approximation known from quantum mechanics [2, 3] one can, taking into consideration the analogy mentioned above, use the formula that is employed in the WKB method for the coefficient, D_t, of transmission through the potential barrier. In the present case it will be the coefficient of power transmission by the horn. For example, when $\mu = \mu_p$ and μ_p^2 lies below the peak of the barrier the formula for D_t has the form

$$D_t = \exp\left[-2\int_0^{a_p} \sqrt{V_{(a)} - \mu_p^2}\, da\right]. \tag{13}$$

It can be seen from Fig. 1 that the size of the barrier increases with decreasing frequency, since the barrier becomes increasingly higher and wider. This is accompanied by an increase in the integral in formula (13) and accordingly a decrease in the transmission, coefficient D_t. Below the lower threshold frequency, the barrier no longer changes its width which is a_l, but its height continues to increase with decreasing μ. This causes a further increase in the value of the integral in formula (13) and decrease in the transmission coefficient D_t. It should be noted that this coefficient is, in this case, different from zero, which means that even below the lower threshold frequency power transmission by the horn is possible. This transmission vanishes completely for $\mu < \mu_{gr2}$ only

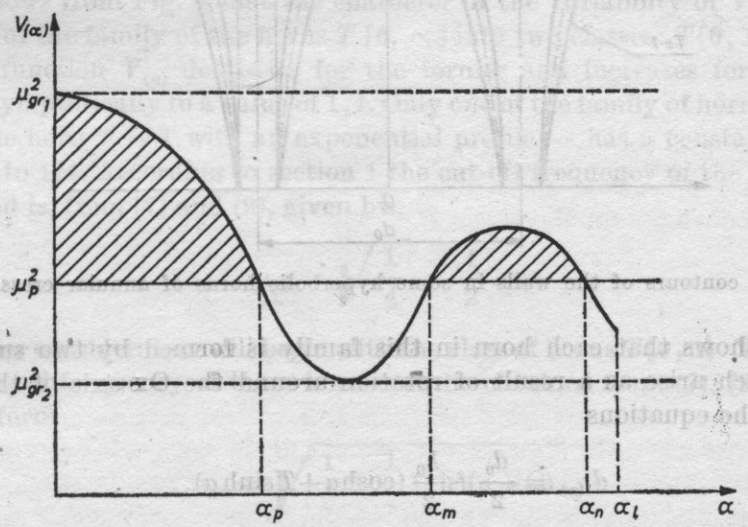

Fig. 2. The "geometric barrier" of the horn for waves at frequencies $\mu < \mu_{gr1}$ when $V_{(a)}$ is not a monotonic function

when the horn is a waveguide of infinite length, since in this case a_l tends to infinity and the value of the integral in formula (13) also becomes infinitely large, resulting in the coefficient D_l taking a value of zero.

In the case where $V_{(a)}$ is an increasing function, analogous considerations can be made. The more general version, where $V_{(a)}$ is a continuous function, but is not monotonic, does not contribute any new elements to the problem under consideration and only requires more development in terms of calculation. Thus, for example, for the function $V_{(a)}$ shown in Fig. 2 it has to be considered in evaluating formula (13) that the "geometric" barrier of the horn for a wave of frequency μ_p occurs not only in the interval $[0, a_p]$, but also in the interval $[a_m, a_n]$.

3. Blurred cut-off frequency of hyperbolic horns of annular cross section

In order to illustrate the general considerations in section 2 one can discuss the phenomenon of the blurred cut-off frequency for the family of hyperbolic horns of annular cross section.

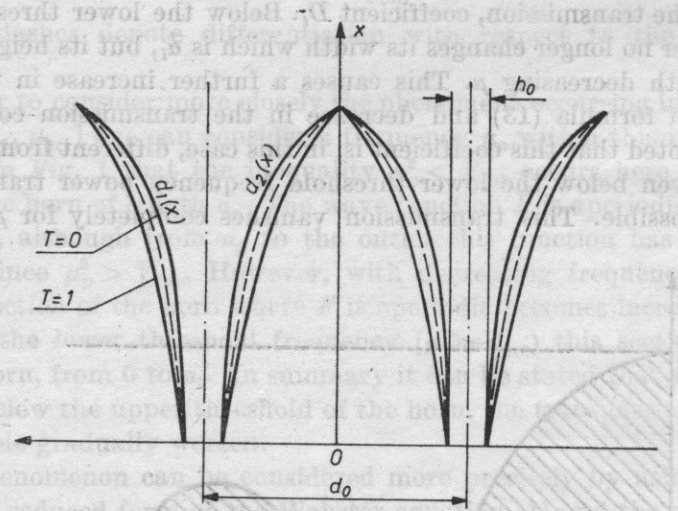

Fig. 3. The contours of the walls in some hyperbolic horns of annular cross section

Fig. 3 shows that each horn in this family is formed by two surfaces of rotation which arise as a result of rotation around the Ox axis of the curves defined by the equations

$$d_{1(x)} = \frac{d_0}{2} + \frac{h_0}{2}(\cosh a + T \sinh a), \tag{14}$$

$$d_{2(x)} = \frac{d_0}{2} - \frac{h_0}{2}(\cosh a + T \sinh a), \tag{15}$$

where d_0 is the central diameter of the annular channel of the horn, and h_0 is the width of the channel of the horn at the inlet. The constant T defines the shape of the profile of the walls of the horn. For the family of waveguides considered here this constant lies in the interval $[0, \infty)$. For $T = 0$ the horn has a catenoidal profile, and an exponential one for $T = 1$. The profile of the horn takes other shapes for other values of T, one of which is shown as an example by the dashed line in Fig. 3.

It follows from geometrical considerations that the area of the cross section S of the family of waveguides under discussion is defined by the formula

$$S = S_0(\cosh\alpha + T\sinh\alpha), \tag{16}$$

where

$$S_0 = \pi d_0 h_0 \tag{17}$$

is the area of the inlet of the horn.

The horns of the form (16) have not been discussed to date in the literature, although they have been used in practice, e.g. in axial dynamic flow generators [4].

The expression for the function $V_{(\alpha)}$ can be obtained from formulae (6), (16) and (9)

$$V_{(\alpha)} = \frac{1}{2} - \frac{1}{4}\left(\frac{\sinh\alpha + T\cosh\alpha}{\cosh\alpha + T\sinh\alpha}\right)^2. \tag{18}$$

The behaviour of the function $V_{(\alpha)}$ for different values of the parameter T is shown in Fig. 4.

It follows from Fig. 4 that the character of the variability of $V_{(\alpha)}$ suggests a division of the family of the horns $T\,[0, \infty]$ into two classes: $T[0, 1)$ and $T(1, \infty)$. The function $V_{(\alpha)}$ decreases for the former and increases for the latter tending asymptotically to a value of 1/4. Only one of the family of horns discussed here — the horn $T = 1$ with an exponential profile — has a constant value of $V_{(\alpha)}$ equal to 1/4. According to section 1 the cut-off frequency of the horn is not blurred and is, from (7) and (9), given by

$$\mu_{gr} = \sqrt{\frac{1}{4}} = \frac{1}{2}. \tag{19}$$

Further consideration will begin with the class of horns $T[0, 1)$. The formula for the cut-off frequency of these horns can be obtained from (7), (9) and (18). It has the form

$$\mu_{gr} = \sqrt{\frac{1}{2} - \frac{1}{4}\operatorname{tgh}^2(\alpha + \Omega)}, \tag{20}$$

where Ω is an abbreviation for

$$\Omega = \operatorname{artgh} T. \tag{21}$$

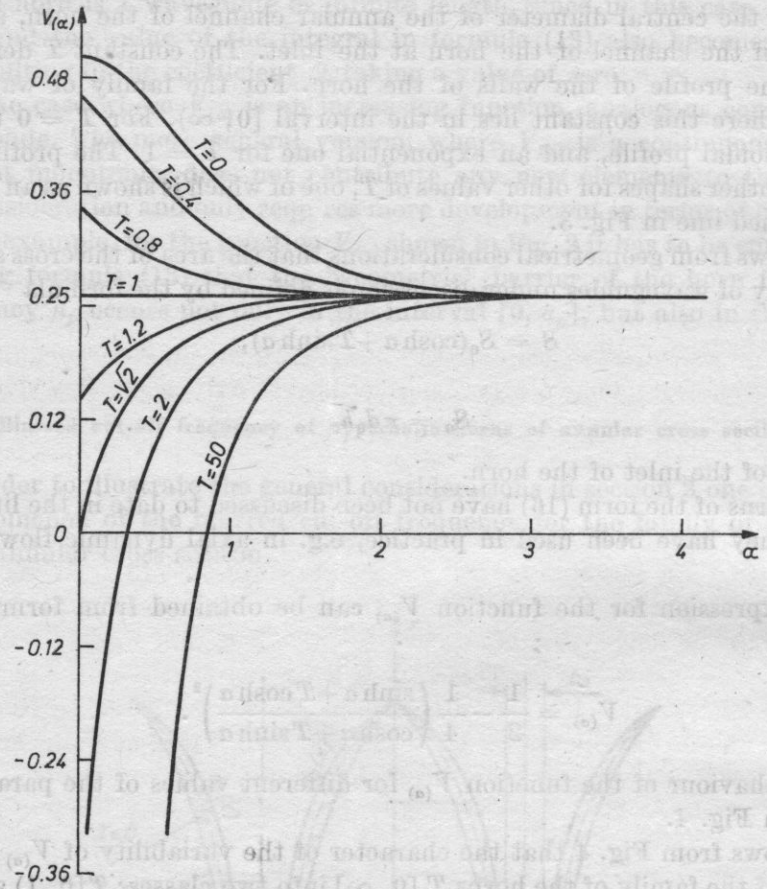

Fig. 4. The behaviour of the function $V_{(\alpha)}$ for the family of hyperbolic horns with a cross sectional shape in the form of a circular ring

Insertion into (20) of the dimensionless abscissa of the inlet ($\alpha = 0$) and the outlet ($\alpha = \alpha_l$) of horn gives, according to (10) and (11), the upper and lower threshold frequencies for the horns T [0, 1),

$$\mu_{gr1} = \sqrt{\frac{1}{2} - \frac{T^2}{4}}, \tag{22}$$

$$\mu_{gr2} = \sqrt{\frac{1}{2} - \frac{1}{4}\operatorname{tgh}^2(\alpha_l + \Omega)}. \tag{23}$$

In the case when the dimensionless length of the horn α_l is so large that the hyperbolic tangent in formula (23) can, to a good approximation, be taken as equal to unity, formula (23) can be written in the simpler form

$$\mu_{gr2} \cong \sqrt{\frac{1}{4}} = \frac{1}{2}. \tag{24}$$

The same value is obtained here as in the particular case of the horn $T = 1$ (cf. formula (19)). It should be noted, however, that an equality of the dimensionless frequencies does not signify the equality of their absolute values, since the horns with different profiles most frequently have differing coefficients of the divergence of the walls, x_0, which leads (cf. formula (5)) to differences in the values of the constant f_0. This constant which was introduced when μ was defined (formula (4)) must be considered in the conversion of the dimensionless frequencies into absolute frequencies and vice versa.

Formulae (22) and (23) indicate that the upper and lower dimensionless threshold frequencies are less than unity for the family of the horns $T\,[0, 1)$. Thus it can be seen from (4) that both the absolute upper threshold frequency $f_{gr1} = \mu_{gr1} f_0$, and the absolute lower threshold frequency $f_{gr2} = \mu_{gr2} f_0$ are, for these horns, always lower than f_0. This fact differentiates these horns distinctly from the Salmon family of horns, that are similar to them in terms of geometry, [6], but whose cut-off frequency is not blurred and is equal to the constant f_0. Moreover, it can be seen from formulae (22) and (23) that the width of the blurred interval of the cut-off frequency $[\mu_{gr2}, \mu_{gr1}]$, for a horn of a given length depends on the parameter T which characterizes the shape of the profile of the horn. The horn $T = 0$ has the most blurred cut-off frequency.

In order to investigate the phenomena for values of T higher than unity one needs consider the family of horns $T\,(1, \infty)$. In this case, after consideration of formulae (7), (9), (18) one obtains the formula for the cut-off frequency

$$\mu_{gr} = \sqrt{\frac{1}{2} - \frac{1}{4}\operatorname{ctgh}^2(a + \hat{\Omega})}, \tag{25}$$

where $\hat{\Omega}$ is an abbreviation for

$$\hat{\Omega} = \operatorname{artgh}\left(\frac{1}{T}\right). \tag{26}$$

The threshold frequencies can be found from relation (25) using (10) and (11)

$$\mu_{gr1} = \sqrt{\frac{1}{2} - \frac{1}{4}\operatorname{ctgh}^2\hat{\Omega}}, \tag{27}$$

$$\mu_{gr2} = \sqrt{\frac{1}{2} - \frac{1}{4}\operatorname{ctgh}^2(a_l + \hat{\Omega})}. \tag{28}$$

It can be noted that in the case analyzed here, contrary to the situation for horns of the class $T\,[0, 1)$, μ_{gr1} is lower than μ_{gr2}. Thus the magnitude of μ_{gr1}, which for the horns $T\,[0, 1)$ played the role of the upper threshold frequency, now becomes the lower threshold frequency, while μ_{gr2} changes conversely. Both these quantities decrease with increasing T. It follows from formulae (26) and (27) that for $T = \sqrt{2}$, the lower threshold frequency μ_{gr1} is equal to zero, while the

upper threshold frequency μ_{gr2} is equal to zero for $T = T_l$ which satisfies the equation

$$\operatorname{ctgh}^2\left[\alpha_l + \operatorname{artgh}\left(\frac{1}{T_l}\right)\right] = 2. \tag{29}$$

In order to determine T_l from formula (29) it is necessary to find first the relation of the quantities α_l and T from relation (16). After manipulation one obtains

$$\alpha_l = \frac{l}{x_0} = \operatorname{arsinh}\left(\frac{S_w}{S_0\sqrt{T^2-1}}\right) - \operatorname{artgh}\left(\frac{1}{T}\right), \tag{30}$$

where S_w is the area of the outlet of the horn.

Insertion of (30) into (29) leads to

$$T_l = \sqrt{\left(\frac{S_w}{S_0}\right)^2 + 1}. \tag{31}$$

A negative number is obtained under the square root sign in formula (25) for $T > T_l$, which signifies an imaginary value of μ_{gr}. Since an imaginary value of the cut-off frequency would be physically meaningless, it must therefore be concluded that for $T > T_l$ the horn transmits all the frequencies of the wave.

Finally it is possible to give a numerical example which shows the dependence of the absolute upper and lower threshold frequencies on the parameter T, for a horn of specified dimensions (cf. Fig. 5).

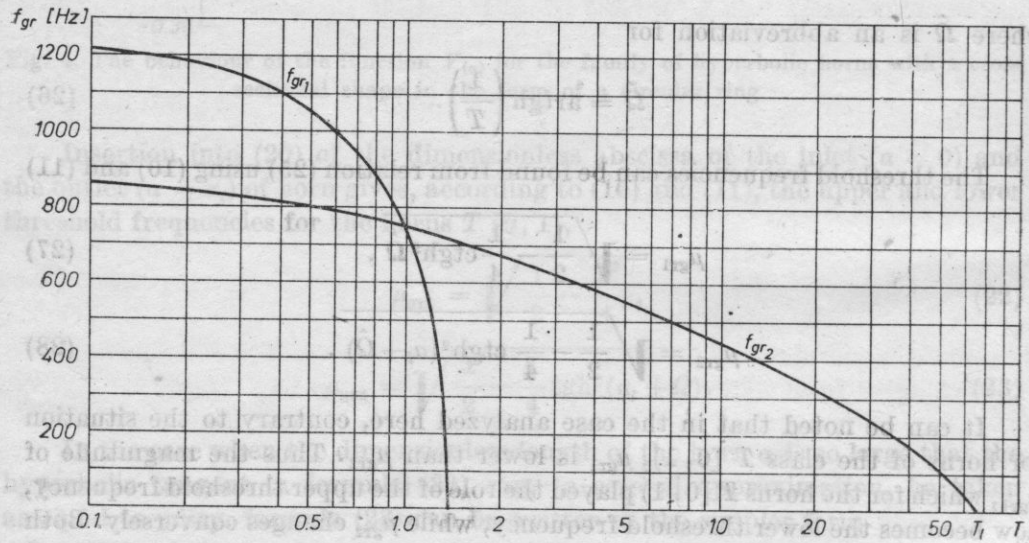

Fig. 5. The dependence of the upper and lower threshold frequency on the value of T for specific diameters of the inlet and the outlet, and a specific length of the horn

It was assumed for the calculations for Fig. 5 that, irrespective of the change in the shape of the profile T, the sizes of the inlet and the outlet of the horn and its length are constant and given by:

- the width of the channel of the horn at the inlet $h_0 = 1.5 \cdot 10^{-3}$ m;
- the central diameter of the annular channel of the horn $d_0 = 10^{-1}$ m;
- the radius of the outlet of the horn $h_l = 10^{-1}$ m;
- the length of the horn $l = 1.5 \cdot 10^{-1}$ m.

Fig. 5 thus shows a special case of the results of the general considerations of this section for the family of hyperbolic horns with annular cross section. It can be seen that with increasing T in the interval $(0, 1)$, the blurred interval of the cut-off frequency becomes narrower and at the same time the upper and lower threshold frequencies decrease. The upper threshold frequency decreases more rapidly and accordingly, for $T = 1, f_{gr1} = f_{gr2}$. For $T > 1$ the threshold frequencies change places: f_{gr1} is now the lower and f_{gr2} the upper threshold frequency. Both f_{gr1} and f_{gr2} tend, in this case, to zero with increasing T. The lower threshold frequency f_{gr1} reaches a value of zero for $T = \sqrt{2}$, while the upper threshold frequency f_{gr2} does so for $T = T_l$, where T_l is defined by formula (31). For $T > T_l$ the horn should transmit all the frequencies of the waves propagating in it.

4. Conclusions

The phenomenon of the blurred cut-off frequency occurs in horns for which the function $V_{(\alpha)}$ in the propagation equation (12) does not take a constant value. These horns are used in practice. For specific dimensions of the horn (the diameter of the inlet and of the outlet, and the length) the blurred cut-off frequency depends on the profile of the walls of the waveguide.

The equation of wave propagation in the horn has an analogous form to a onedimensional Schrödinger equation in quantum mechanics. Because of this formal analogy, the blurred cut-off frequency of the horn and its transmission properties in the blurred interval can be determined only by way of discussion and not by solving the propagation equation.

References

[1] A. H. Benade, E. V. Jansson, *On plane and spherical waves horns with nonuniform flare*, Acustica, **31**, 2, 79-89 (1974).

[2] A. S. Dawydow, *Quantum mechanics* (in Polish), PWN, Warszawa 1967.

[3] S. Flugge, H. Marschall, *Calculation methods of quantum theory* (in Polish), PWN, Warszawa 1958.

[4] A. Puch, *Generalized model of an axial dynamic generator*, Archives of Acoustics, **3**, 1, 17-34 (1978).

[5] V. SALMON, *Generalized plane wave horn theory*, JASA, **17**, 3, 199-211 (1946).

[6] V. SALMON, *A new family of horns*, JASA, **17**, 3, 212-218 (1946).

[7] A. G. WEBSTER, *Acoustical impedance and the theory of horns and of the phonograph*, Proc. Natl. Acad. Sci. V. S., **5**, 275-282 (1919).

[8] R. WYRZYKOWSKI, *Linear theory of acoustic field in gaseous media* (in Polish), RTPN – WSP, Rzeszów 1972.

Received on February 4, 1980

ARCHIVES OF ACOUSTICS
6, 2, 147-162 (1981)

QUANTITATIVE IMAGE INDICES IN ULTRASONIC DIAGNOSTICS OF INHOMOGENEOUS MATERIALS

ROBERT C. CHIVERS

Physics Department, University of Surrey, Guildford, Surrey, U.K.

The use of a commercial image analyser for dimensional analysis of discrete features of ultrasonic images has been described previously. The present paper reports a pilot study on the use of such an analyser for quantitative analysis of the diffuse texture of an ultrasonic image of an inhomogeneous material. Althought such a use may provide valuable arbitrary diagnostic indices, a procedure is outlined by which such indices may be used in conjunction with visual perceptual studies to optimise the display or to investigate the physical mechanisms of image formation.

1. Introduction

The use of an image analyser for obtaining quantitative information on the dimensions of discrete structures in ultrasonic *B*-scan pictures has been described previously [1]. As was indicated in that communication, the use of such an analyser may be extended to the derivation of quantitative information which is related to the visual texture of ultrasonic grey-scale scans of inhomogeneous materials. This paper reports a pilot study of such an application. The discussion is couched in terms which are directly related to the problems of medical diagnostics. This is a reflection both of the fact that the original stimulus to the investigation was a medical problem, and also of the fact that medical diagnostic techniques for inhomogeneous materials have developed rather faster than their counterparts in industrial applications. It should therefore be borne in mind throughout the paper that the discussion could equally well apply to the ultrasonic diagnostics of other inhomogeneous systems such as concrete, sediments, metal inclusions, etc.

The first quantitative approach to the diagnostics of inhomogeneous material appears to be that of DENIER in 1946 [2], who reported on the basis of a one-dimensional *A*-scan, an excess of echoes from cancerous tissue compared

to normal tissue. The first qualitative use of texture in *B*-scans (two dimensional tomograms) appears to be that of HOWRY whose brief atlas of diagnostic ultrasonic results published in 1965 [3], proved a model which has only in relatively recent years been superseded. The technological developments that have made possible the display of a very wide range of echo amplitudes in grey-scale imaging [4, 5] have permitted the textural analysis suggested by Howry to be performed, to some extent, by almost any operator. The technological development of KOSSOFF and his workers was accompanied by the development of quantitative methods of tissue characterization [6-9]. The circumstantial evidence which supported these developments has been previously collated [8-10] while the current status of ultrasonic tissue characterization has been comprehensively reviewed very recently [11], and some of the fundamental difficulties with these approaches outlined [12].

The essential problems of these quantitative methods are the relatively poor current definition of the ultrasonic beam radiated into water, the rudimentary level of understanding of the way in which tissues whose gross acoustical properties are known will affect the beam pattern, and the essential difficulty of relating this information to the in vivo situation, where the content, structure and properties of the tissues lying between the skin and the region which has been selected for analysis are unknown in detail.

One of the methods of tissue characterization which involves these problems only in an indirect way is a simple analysis of the echo patterns actually displayed on the *B*-scan. This paper discusses some of the elements of such analyses. It reports novel measurements in which the area of interest may be sampled by a light pen for subsequent microprocessor analysis and outlines the conditions under which such a method may be used for empirical tissue characterization. Finally a procedure is suggested by which this method may be used to discover the relative importance of different factors in the process of image formation, and two approaches to the optimization of the ultrasonic visualization of inhomogeneous materials, by any of the visualization techniques available at the present time.

2. Methods of analysis

It is implicit in image formation and display that each of stages in the process from the generation of the initial electrical signal to the final display of the image will introduce some limitation on the extent or the significance of the analysis of the image that can be performed. In turn the method of analysis will have its own limitation and, of course, the most restraining limit in the chain is the one that is effectively operative.

Two main methods of analysis are available: analogue (optical) techniques and digital (computational) techniques. The computational techniques devised

primarily for microscopic analysis [13] are impressive both in range and sophistication. They have undoubted advantages in the problems that involve spatial (dimensional) information, including area on a point by point basis. Additionally they offer memory for the storage of results, and a light pen facility for the convenient selection and display of an area of interest.

By comparison, optical techniques must be considered limited, cumbersome and difficult in the area of spatial (dimensional) analysis, but they have particular potential in the analysis of spatial frequency distributions. With relatively simple apparatus, [14], they can rapidly provide a (spatially) continuous transformation of the information in the original picture. In turn this transformation may be masked and retransformed to obtain a spatially filtered version of the original image. Whether or not this is appropriate for the images that exist, or that may exist, as ultrasonic images of inhomogeneous systems, remains to be investigated. The major disadvantages of this approach tend to be the relative inflexibility of the shape of the area that can be selected for analysis, and the fact that the result of the transformation remains, in the first instance, another unquantified image requiring subjective assessment.

The change of image may nevertheless be extremely useful as can be seen from the examples shown in an optical transform atlas [15], and optical image analysis is certainly worthy of investigation, in spite of the photographic problems mentioned in section 4. However, the present author has pursued the computational techniques, both for the potential ease of implementation in a clinical situation, and also because of their importance in the logical development towards optimization of instrumentation (section 5).

3. Experimental material and methods

The pictures upon which the analyses were performed were taken during routine examinations with a commercial compound grey-scale scanner. They were recorded on 70 mm roll film (as negatives) and since the work reported here was not conceived when they were taken, no constraints were placed on the gain, brightness, exposure or development settings to make them particularly suitable for this analysis. Matt prints (on resin coated paper) were made from the negatives using automatic timing and developing systems, and the analyses were performed under identical illumination and magnification of the prints.

The analysis was performed on the commercially available image analyser previously described [1] (Quantimet Model 720*M*, Cambridge Instruments, Royston, Herts, U.K.). A light pen was used to select an area of interest on the television display of the image of the print. The area of the selected region was measured, in terms of the number of picture points (there are 60400 points in the whole 720 line display), and the setting of the scaled "grey-level" control on the analyser gradually reduced. This "grey-level" control effectively changes

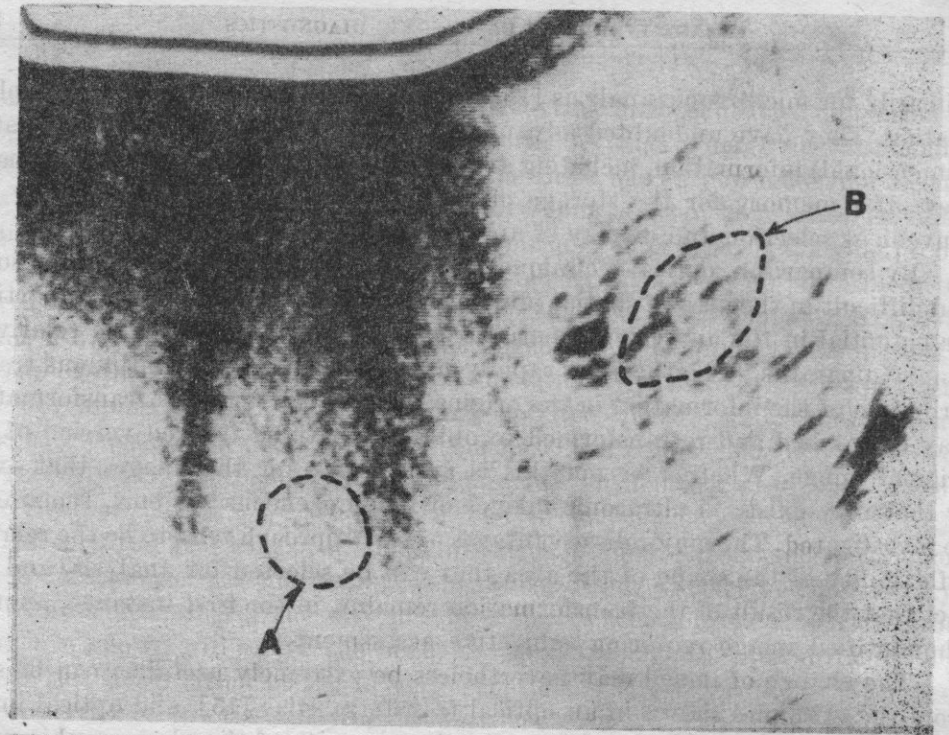

Fig. 1. Ultrasonic *B*-scan, number 1, with the regions *A*, *B*, selected for analysis

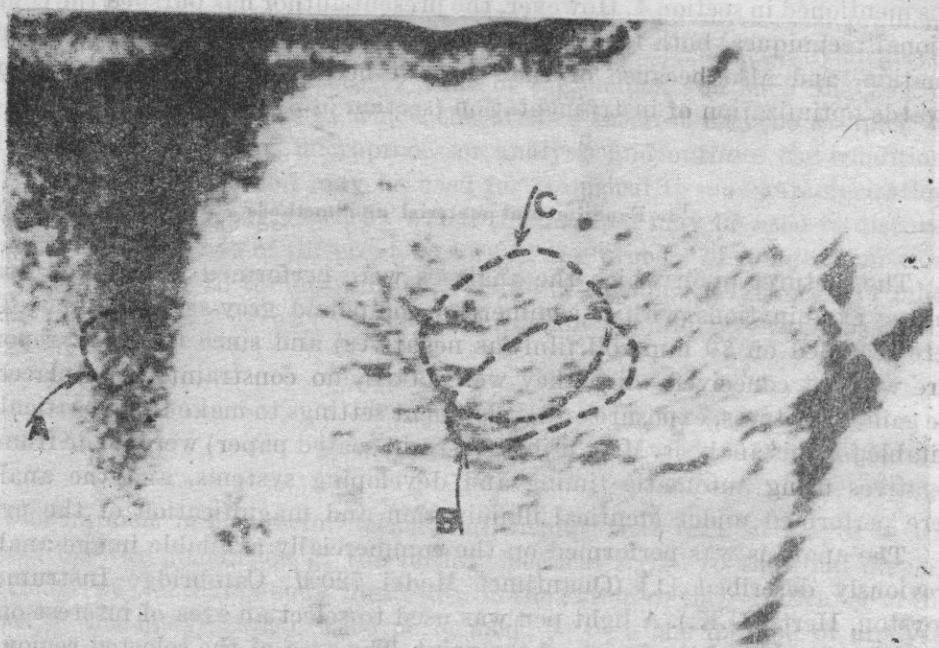

Fig. 2. Ultrasonic *B*-scan, number 2, with the regions *A*, *B*, *C* selected for analysis

the threshold of brightness in the image that is required before a point will register and be displayed on the television monitor. One of the facilities of the analyser is an automatic readout of the area (within the region selected with the light pen). Thus as the setting of the grey-level control is reduced, it is possible to determine the percentage of the area of the selected region which is above a certain brightness. This is the analysis that was performed in this work. The grey level scale is an arbitrary one: a level of 55 corresponds to a threshold at which all the points in the selected region register (i.e. it represents darkness), and while measurable areas remained below a grey level of 10 none of the images had areas below a grey level of 8.

Three original scans which were analysed are shown in Figs. 1-3, the approximate regions selected for analysis being outlined and labelled with letters. The numbers 1-3 are used as original scan indices. Table 1 shows the areas of the selected regions in terms of the number of analyser picture points contained. (The limit of resolution is 4 picture points). The regions were selected for different reasons. Regions $1A$ and $1B$ are clearly different from a visual point of view, as is region $2A$ from regions $2B$ and $2C$. The difference, visually, between regions $2B$ and $2C$ is relatively small, although the latter appears to have rather more white space in it. Similarly $3A$, $3B$ and $3C$ are visually distinct

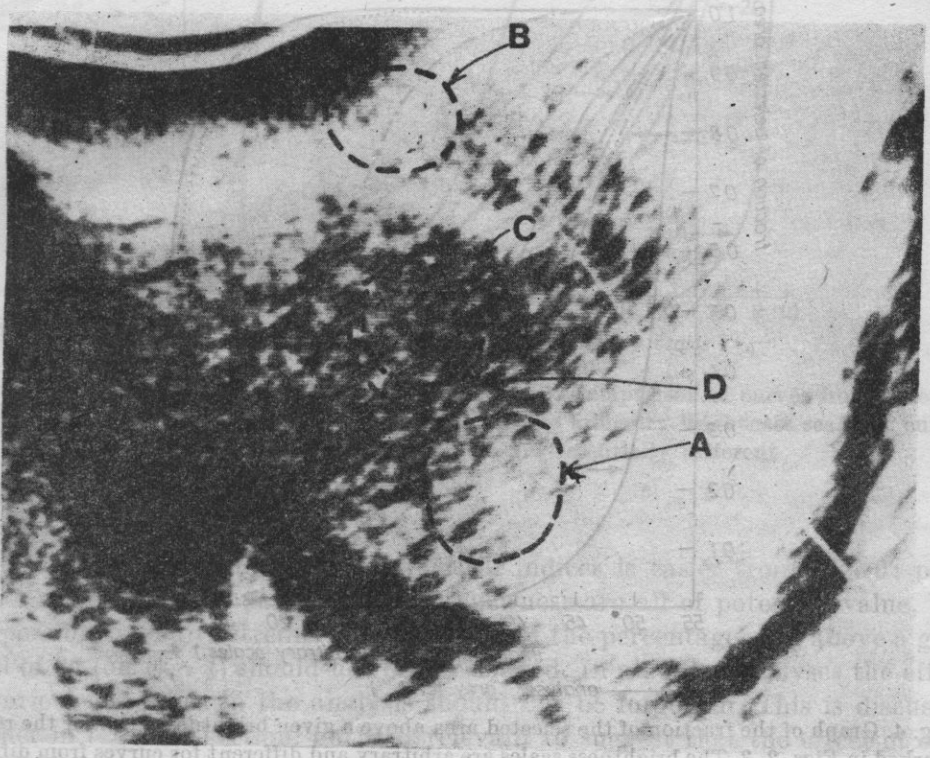

Fig. 3. Ultrasonic B-scan, number 3, with the regions A, B, C, D selected for analysis

from each other and from 1*A*, 1*B*, 2*A*, 2*B* and 2*C* but are closest to the last two. Finally 3*D* was an attempt to assess the reproducibility of 3*C*.

The results of the analyses are shown in Fig. 4 for all these selected regions of three original scans. The lack of control of the photographic and display parameters in obtaining the original scans (Figs. 1-3) implies that the arbitrary brightness scales used for analysing the individual scan pictures differ essentially from each other. It means that these scales for selected regions labelled with different numbers cannot be compared to each other. This must be borne in mind when interpreting Figs. 4-6 in which the curves from all three scans have been superimposed for illustrative purposes. The immediate impression is that the index chosen (i.e. the way in which the regional images have been quantified) is one which accords well with the visual (subjective) analysis. Fig. 5 shows Fig. 4 plotted with a logarithmic grey scale. As may

Table 1. Relative areas of selected regions (in analyser picture points)

Region	Area (picture points)
1*A*	5352
1*B*	9820
2*A*	3204
2*B*	12740
2*C*	16220
3*A*	18234
3*B*	15400
3*C*	18508
3*D*	17164

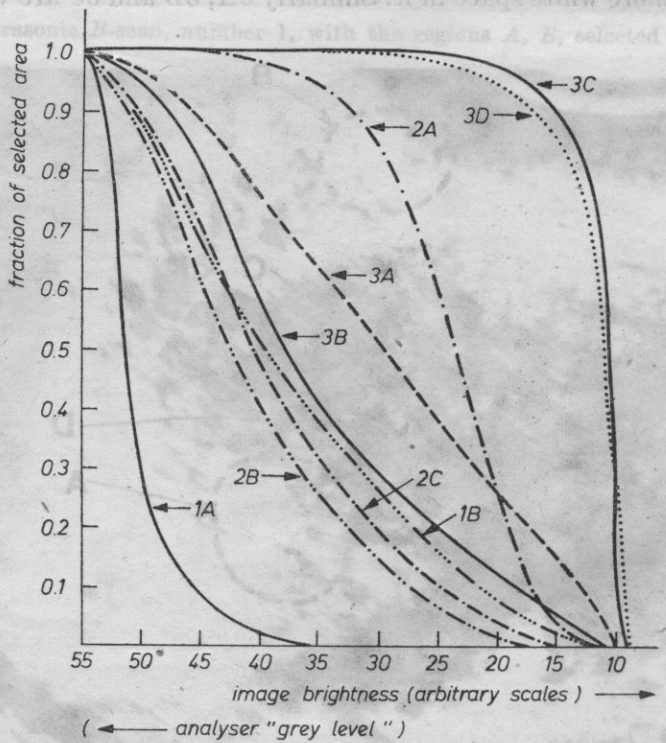

Fig. 4. Graph of the fraction of the selected area above a given brightness level for the regions marked in Figs. 2, 3. The brightness scales are arbitrary and different for curves from different scans (i.e. labelled with different numbers)

be expected the general results are qualitatively similar as far as discrimination is concerned, although Fig. 4 appears to be more reliable. Fig. 6 shows the gradients (first derivatives) of the curves in Fig. 4. These gradients can only be regarded as approximate, since they have been sketched by manual methods (by plotting the gradient of the chord between adjacent data points in Fig. 4 at the mid point of their abscissae). This form of display has obvious advantages for differentiation, although the possibility of points at which curves cross (see Fig. 4, *1B*, *2C*) coinciding with the points of inflexion, and the potential similarity of curves *3B* and *2C*, implies that both types of display (Figs. 4 and 5) should be used in the first instance.

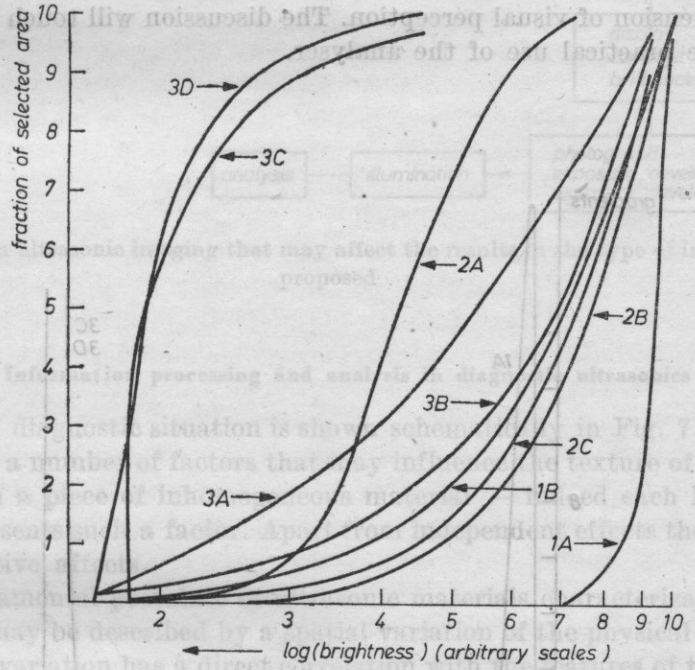

Fig. 5. Fig. 4 with a logarithmic brightness axis. N. B. Comparison of curves from different scans (i.e. Figs. 1-3) can only be illustrative, since the arbitrary brightness scales of curves labelled with different numbers are essentially different

Certainly the extraction of numerical indices is easier from Fig. 6: peak position, peak height, peak width and skewness are all of potential value, but the possibility of an extremely simple index of the percentage area above a grey level of 30 (on Fig. 4) should not be overlooked. In all these analyses the effect of various processes in the analysis should not be forgotten. This is discussed further in the next section, but it is relevant to suggest that the effect of over or under exposure in the photographic processes, or of changing the analyser

illumination, could change curve *2C* into curve *3B* (or vice versa) if the system is linear, or simply to change the shape of the curve if it is not. This would not only affect the simple index of the percentage area above a brightness level of, say, 30 mentioned above, but also shift the peaks of Fig. 6 (or if nonlinearity is present, change their amplitude).

The method of analysis chosen for these experiments was the simplest available, and the range of potential analyses and indices is great. There are severe qualifications on the apparently successful pilot study reported, and the particular procedures used. The remainder of the article is thus devoted to a discussion of the circumstances under which the analyser, with its inflexible numerical regimentation may be more usefully employed than the subtle adaptive comprehension of visual perception. The discussion will touch on the limitations of the practical use of the analyser.

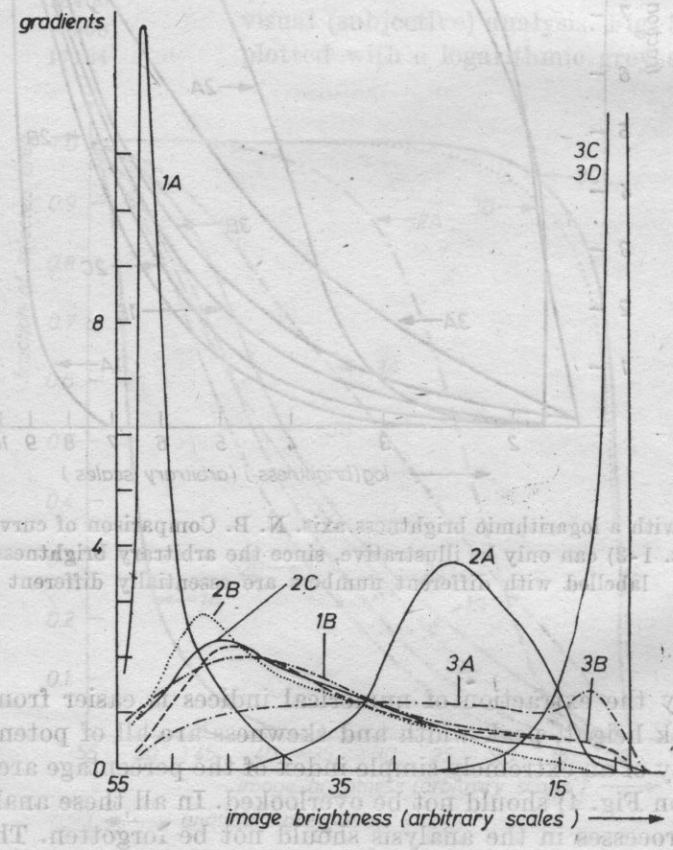

Fig. 6. The gradients (first derivative) of the curves of Fig. 4 plotted against brightness. N. B. See note on Fig. 5

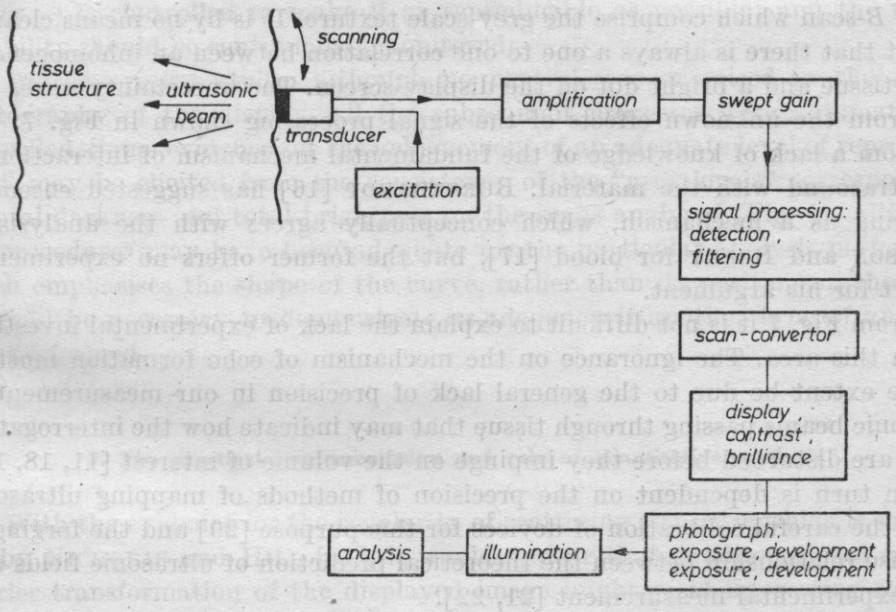

Fig. 7. Factors in ultrasonic imaging that may affect the results in the type of image analysis proposed

4. Information processing and analysis in diagnostic ultrasonics

A typical diagnostic situation is shown schematically in Fig. 7. It is clear that there are a number of factors that may influence the texture of the picture obtained from a piece of inhomogeneous material — indeed each label in the diagram represents such a factor. Apart from independent effects they may also have cooperative affects.

The fundamental postulate of ultrasonic materials characterization is that the material may be described by a spatial variation of the physical parameters and that this variation has a direct correlation with the features of the material that are of interest to the diagnostician, e.g., strength for composite materials; type and condition for human tissues. The parameters that are considered relevant for the propagation of ultrasound are the velocity of propagation, the density, and the bulk modulus (or the elastic constants for a crystalline material). Opinion is divided about the relative significance of these and the linear scale of their variation in human tissue largely, the present author believes [11], because of a shortage of reliable data.

The traditional mechanism suggested for the production of the diffuse echo pattern under discussion is a scattering process [8-11], although the identity of the inhomogeneities that give rise to the scattering is, certainly in tissue, unclear at present. We may refer to "scattering centres" as points from which the scattered waves appear to emanate (sources) to produce the bright dots

on the *B*-scan which comprise the grey-scale texture. It is by no means clear at present that there is always a one to one correlation between an inhomogeneity in the tissue and a bright dot on the display screen. The uncertainty arises not only from the unknown effects of the signal processing shown in Fig. 7, but also from a lack of knowledge of the fundamental mechanism of interaction of the ultrasound with the material. BURCKHARDT [16] has suggested ensemble scattering as a mechanism, which conceptually agrees with the analysis of ATKINSON and BERRY for blood [17], but the former offers no experimental support for his argument.

From Fig. 7 it is not difficult to explain the lack of experimental investigation in this area. The ignorance on the mechanism of echo formation must to a large extent be due to the general lack of precision in our measurement of ultrasonic beams passing through tissue that may indicate how the interrogating waves are disturbed before they impinge on the volume of interest [11, 18, 19]. This in turn is dependent on the precision of methods of mapping ultrasonic fields, the careful calibration of devices for this purpose [20] and the forging of a precise relationship between the theoretical prediction of ultrasonic fields and their experimental measurement [21, 22].

There is almost no doubt that the field emitted by a transducer will, in some way, influence the signals that present themselves for subsequent visualization. To date only GORE and LEEMAN [23], following Atkinson and Berry [17], appear to have included some measure of accommodation for this in their theoretical development. They use a "beam profile" but with no indication as to where or how it may be measured.

The scanning regime is of particular importance. The storage of superimposed (compound) scans may produce degradation of the visual information due to uneven scanning with a hand-held scanner or due to angular scattering effects. Real-time scanners obviously overcome these problems at source, whether mechanically or electronically scanned. However not all of these have a scan convertor attached — which is the only easy way of feeding the image signal directly into the unconventional raster of the analyser avoiding the intermediate photographic processes. More importantly each different scanner would require a careful investigation of the effect of element shape and automatic scanning regime on the angular and spatial scatterer visualization.

The importance of the majority of the electronic system components is discussed in more detail elsewhere [23]. The vital feature of the display device, if photographic methods are used as the intermediary between the scanner display and the analyser, is linearity between the amplitude of the electrical signal input and the optical intensity displayed. This may, alternatively, be assessed as an overall linearity between the amplitude of the electrical signal and the intensity of the light fed to the image analyser, whether analogue or digital (see section 2). If the latter is used, as in this study, considerable care must be taken to ensure that each stage of the process — exposure, development,

fixing – is controlled to make it as reproducible as possible; and the reproducibility should be continuously monitored.

In the present study, although no control was exercised in the initial photography of the display, all the subsequent processes were automatically controlled. Some evidence for the achievement of an adequate level of reproducibility may be elicited from the consistency of the "grey-levels" corresponding to total darkness and total brightness on the scans analysed (Fig. 4). Although the procedures may have been adequate for the particular analysis performed, which emphasises the shape of the curve, rather than its position on the axis, it would be necessary to demonstrate its adequacy if another type of analysis was performed.

5. The practical implementation and role of quantitative analysis

With the evidence for the regularity of scattering structure which is suggested by NICHOLAS and HILL [24], it would appear that twodimensional spatial Fourier transformation of the displayed image might yield interesting results. That this may be achieved by digital techniques is evident, if demanding in terms of computational resources. The main argument in favour of analogue (optical) methods, in spite of photometric problems, is the lack of a major sampling limitation in one direction (for television displays the limitation occurs perpendicular to the scan lines). This argument is reinforced by the immediate simultaneous display of spatial Fourier transforms in all directions. It is worth noting that if a small area is selected for Fourier analysis, the resolution of spatial frequencies will be limited by a relationship identical to that quoted for the equivalent time-domain problem [10].

For all other types of analysis, digital techniques are likely to prove most effective and rapid. For empirical tissue characterization (with all its limitations [11]) it is clear that the optimum approach would be to read from the scan convertor directly into the image analyser. Various types of analysis could be attempted on the material system under test, with a view to producing a purpose-built microprocessor based system for commercial implementation. The main disadvantages of this are, of course, the fundamental ones outlined in section 4, which may limit the successful extent of a particular (apparently appropriate) type of analysis to one diagnostician and his apparatus. Alternatively, individual *A*-scans may be digitized and analysed, but any processing at all (e.g. [25]) that is involved in reducing the amount of data to economic proportions, computationally, will need careful consideration in terms of its influence on the significance of the final image analysis that is performed.

With whatever system is chosen, empirical studies are possible and may lead to significant advances in selected areas. They will nevertheless be without the benefit of scientific understanding, and as RHYNE has pointed out for biological

tissues, they are capable of an infinitude of variation. Instrumental development in these circumstances can only be guided by a popular (subjective) idea of a "better" picture which has no objective grounds or direction. It may be argued that the human eye – particularly that of a skilled practictioner – is more subtle and flexible in its analytical capability than any computational system. Whereas the present author would in no way dispute this, it does appear that it is important to direct investigations in such a way that ultrasonic scanners are optimized in terms of their imaging capability. Whereas scientific procedures for the investigation of inhomogeneous systems are of clear importance, they are also extremely difficult and complex [12], and it is proposed that the type of quantitative analysis described above may be a crucial element in both optimization of visual display, and in the development of our fundamental understanding.

It is generally agreed that the languages for the description of images, their structure and content are not well developed [26], and may need to be confined in their application to specialized fields or particular aspects of a problem. As yet no such specialized vocabulary exists for ultrasonic grey-scale images of inhomogeneous systems, and the development of such terminology is certain to be somewhat hampered by the differences that are produced of one object (or system) with different machine settings, and (more grossly) with different machines. Furthermore there is, at the present time [27], no clear consensus on calibration techniques or test objects or test images for ultrasonic pulse and continuous wave imaging systems. Some of the elements of these problems are discussed in reference [27], although the two papers concerned with ultrasonics avoid many of the crucial problems of detail discussed above.

The author suggests that the analyser discussed in the earlier part of the paper may be used as a bridge, or common point of reference. It may be used to provide a language basis or set of objective physical measures for the displays which on one hand are to be optimised for perceptual discrimination, and on the other hand are to be investigated with regard to the way in which they are affected by such factors as material composition and properties, transducer beam pattern, and signal processing.

A simple example may illustrate the practical importance of this approach. It is not intended to be specific to the analysis which has been employed: the methodology is the prime concern. Consider three typical curves from Fig. 4: *1A*, *3B* and *3C*. It may be possible by perceptual studies to determine a rank order for these (or any other shape of curve) in terms of the perceptual sensitivity to slight changes that they provide. A parallel investigation can be made, using this same arbitrary choice of numerical analysis and data display, of the way in which, with a particular type of material, the shape of the curve is affected by the transducer beam pattern and subsequent signal processing. Forging a compromise between these effects and the perceptual studies will permit the optimum visualization of that material to be performed. In other words it

will permit that choice of the physical parameters of the instrumentation that can be varied which will present a display of the material in which changes in its scattering properties are most susceptible of perception.

The methodology outlined above is not in "closed form", since it depends upon a particular choice of numerical analysis and data display (Fig. 4) which is essentially arbitrary, and other displays (e.g. Figs. 5, 6) or analysis are numerous. Perceptual studies may permit a rank ordering of the benefits of the different analyses but limits to this will arise from the extent of the experiments performed and the conceptual frameworks within which they are conducted. Thus although optimization in an absolute sense may be impossible, in the shorter term the use of objective criteria as a pivot for development, however arbitrary, would appear to be only of benefit.

It has been suggested [12] that for human tissues, a direct link may be made between pathology and display. The extent of potential benefit can more clearly be seen in its application to model systems of known characteristics [27]. In this context it can provide extremely useful information on the extent of variations in acoustical parameters that can be detected, as well as the effect of their shape, spatial extent and distribution, on the image produced. In connection with parameter variation over a scale that is smaller than can be measured remotely by present techniques, the physical aspects of ultrasonic image formation in tissue and their relative importance may be assessed (in terms of arbitrary indices). The language of communication thus established can lead to comparison of results between laboratories and will inevitably lead to the demand for higher standards in the description of the ultrasonic systems used.

6. Conclusion

The pilot study presented, using an expensive commercial image analyser has shown the feasibility of deriving quantitative indices from ultrasonic grey-scale *B*-scans of inhomogeneous systems that reflect the textual discrimination that is visually achieved. The potential of this technique in empirical materials characterization for developing microprocessor-based equipment to give numerical indices of a specific diagnostic problem is clear. Such techniques will still be instrumentation dependent and the main value of the types of analysis presented is in using the indices to optimize the display for visual perception. Further extension to inhomogeneous systems whose microstructure is known will permit the optimization of ultrasonic visualization systems to an extent which is only limited by the arbitrary nature of the visual indices used. The cost of the analyser which has significant flexibility, prohibits the widespread development of these studies, and work is in progress to assess the feasibility of transferring data from different laboratories to one central analyser. The results of these studies will be reported in a future communication.

Acknowledgements. The author is grateful to Dr. B. GOMPELS, Consultant Radiologist at Epsom District Hospital for providing the original scans, to Mr. H.J.W. DUDLEY (Dept. of Microbiology) for his skilled and enthusiastic assistance in the use of the analyser, Professor J.E. SMITH (Dept. of Microbiology) for his interest and encouragement, and to Mrs. Sheila RUDMAN for drawing most of the diagrams.

References

[1] R. C. CHIVERS, H. J. W. DUDLEY, *The use of an image analyser for dimensional quantification in ultrasonic images*, Archives of Acoustics, **5**, 2, 169-180 (1980).

[2] A. DENIER, *Essai de detection de masse tumorale du cerveau par ultrasonoscopie*, Comptes rend. soc. biol., **140**, 763 (1946).

[3] D. H. HOWRY, *A brief atlas of diagnostic ultrasonic radiologic results*, Rad. Clin. N. Am., **3**, 433-440 (1965).

[4] G. KOSSOFF, *Measurements using ultrasonic techniques*, Proc. Roy. Soc. Med., **67**, 135-140 (1974).

[5] R. C. CHIVERS, *B-scanning and holography in ophthalmology*, Ultrasonics, **12**, 209-213 (1974).

[6] J. M. REID, R. A. SIGELMANN, M. G. NASSER, D. W. BAKER, *The scattering of ultrasound by human blood*, Proc. 8th Int. Conf. Med. Biol. Eng., Chicago, 10-7, 1969.

[7] C. R. HILL, R. C. CHIVERS, *Investigations of backscattering in relation to ultrasonic diagnosis*, Ultrasonics in Biology and Medicine (L. Filipczyński. ed.), 119-123, PWN, Warsaw 1972.

[8] R. C. CHIVERS, *The scattering of ultrasound by human tissue* (Ph. D. Thesis), University of London, 1973.

[9] R. C. WAAG, R. M. LERNER, *Tissue macrostructure determination with swept frequency ultrasound*, Proc. 1973 Ultrasonics Symp., Monterey, California, IEEE **CHO 807-8SU**, 73 (1973).

[10] R. C. CHIVERS, C. R. HILL, *A spectral approach to ultrasonic scattering measurements*, Phys. Med. Biol., **20**, 799-815 (1975).

[11] R. C. CHIVERS, *Tissue characterization*, Ultrasound Med. Biol., **7**, 1-20 (1981).

[12] R. C. CHIVERS, *Some scientific and technical aspects of medical ultrasonics*, J. Med. Eng. Tech., **5**, 128-133 (1981).

[13] *Quantimet image analysers — a bibliography*, Cambridge Instruments Ltd., Royston, Herts, U.K.

[14] C. A. TAYLOR, H. LIPSON, *Optical transforms*, G. Bell, London 1964.

[15] G. HARBURN, C. A. TAYLOR, T. R. WELBERRY, *An atlas of optical transforms*, G. Bell, London 1975.

[16] C. P. BURCKHARDT, *Speckle in ultrasound B-mode scans*, IEEE Trans. Sonics and Ultrasonics, **SU-25**, 1-6, (1978).

[17] P. ATKINSON, M. V. BERRY, *Random noise in ultrasonic echoes diffracted by blood*, J. Phys. A., **7**, 1293-1302 (1974).

[18] R. C. CHIVERS, *Phase and amplitude fluctuations in the propagation of acoustic waves in inhomogeneous continua with velocity, density and bulk modulus variations*, Report No. 41/78 IPPT-PAN, Warszawa 1978.

[19] R. C. CHIVERS, *Phase and amplitude fluctuations in the propagation of acoustic waves in inhomogeneous continua with velocity, density and bulk modulus variations — results*, Ultrasound Med. Biol., **4**, 353-361 (1978).

[20] R. C. CHIVERS, P. A. LEWIN, *A comparison of different designs of miniature hydrophone probes*, Proc. Ultrasonics International, Graz, 434-446, Iliffe Press, Guildford 1979.

[21] R. C. CHIVERS, *Some practical considerations in the measurement of the output of medical ultrasonic devices*, J. Med. Eng. Tech., (submitted for publication).

[22] R. C. CHIVERS, L. BOSSELAAR, P. R. FILMORE, *On the effective area for diffraction correction*, JASA, **68**, 80-84 (1980).

[23] R. C. CHIVERS, *On the analysis of ultrasonic images of inhomogeneous materials including human tissue in vivo*, Ultrasonics Report 7902, University of Surrey Guildford U.K., 1979.

[24] D. NICHOLAS, C. R. HILL, *Acoustic Bragg diffraction from human tissue*, Nature, **257**, 305-6; **261**, 330 (1976).

[25] J. MILAN, *An improved ultrasonic scanning system employing a small digital computer*, Brit. J. Radiol., **45**, 911-916 (1973).

[26] J. M. EVANS, R. KIRSCH, R. N. NAGEL, eds., *Workshop on standards for image pattern recognition*, National Bureau of Standards, Special Publication, 500-508, 35-47, 51-81, Washington D.C., USA, 1977.

[27] R. C. CHIVERS, *On the purpose and practice of modelling in medical ultrasonics*, Proc. UBIOMED IV, (P. GREGUSS, ed.), 3-8, Visegrad, Hungary.

Received on March 10, 1980; revised version on October 13, 1980

ARCHIVES OF ACOUSTICS
6, 2, 163-172 (1981)

THE INVESTIGATION OF RELAXATION PROCESSES IN CHOSEN LIQUID CRYSTALS BY ULTRASONIC AND DIELECTRIC METHODS

ADAM DRZYMAŁA

The Technical University of Rzeszów, The Institute of Mathematics and Physics
(35-959 Rzeszów, ul. W. Pola 2)

Relaxation processes have been found to occur in 4-*n*-methoxybenzoated-4-*n*-pentylphenylene and 4-*n*-octyloxyphenylene-4-*n*-pentyloxybenzoate. The findings are based on ultrasonic and dielectric investigations. Both chemical compounds exhibit two regions of relaxation in the range of frequencies investigated. A comparison has been made of the values of the activation energy derived from the dielectric and acoustic investigations.

1. Introduction

In the last few years there has been particular interest in acoustic methods of investigating liquid crystals [1,3-5, 8, 9]. One of the reasons for this is the unique physical properties of liquid crystals which combine the properties of liquids, such as fluidity, with the properties of solid bodies, such as anisotropic physical properties and the possibility of observing a long-range order. Critical phenomena [7] in liquid crystals have also been examined. This paper is devoted to the investigation of the propagation of elastic waves in a frequency range of 2.5-60 MHz in samples of two chosen nematic materials.

2. Materials and apparatus

In the investigations performed, the following organic compounds were used: 4-*n*-methoxybenzoate-4-*n*-pentylphenylene produced in the Institute of

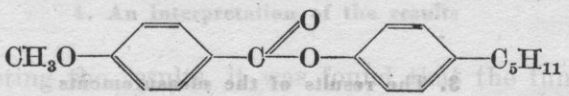

Basic Chemical Sciences of the Medical Academy in Łódź; and 4-*n*-octyloxyphenylene-4-*n*-pentyloxybenzoate received from The Institute of Chemistry of the

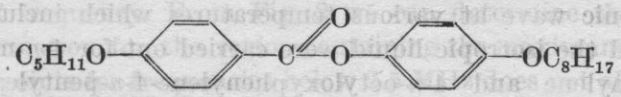

M. Luther University in Halle.

The substances in question reveal, under a microscope, the properties of nematic crystals. Transition phase temperatures obtained by the DSC method for 4-*n*-methoxybenzoate-4-*n*-pentylphenylene are: solid state→29.1 °C nematic phase →41.6 °C isotropic liquid, while for 4-*n*-octyloxyphenylene-4-*n*-pentyloxybenzoate the temperatures are: solid state→51.6 °C nematic phase→83.1 °C isotropic liquid. The measurements of the transition phase temperatures were performed in the University in Halle using a DSC apparatus made by Perkin-Elmer. The measurements of the coefficient of absorption and the velocity of propagation of the ultrasonic waves were performed with an ultrasonic set of high frequency, the US-6, and an ultrasonic interferometer, the UI-15, both made by IPPT of Warsaw (Fig. 1).

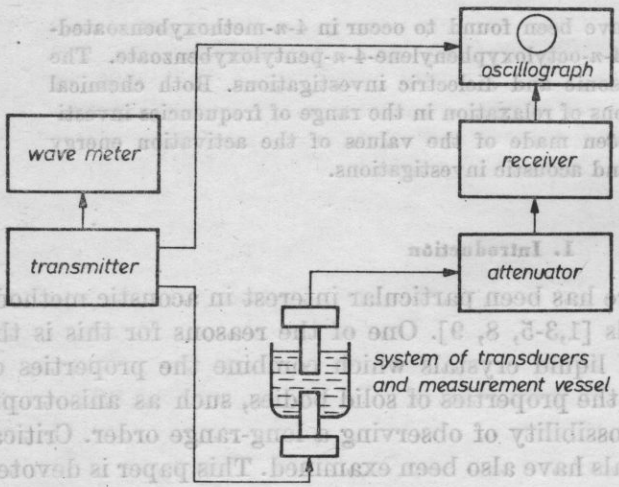

Fig. 1. The block diagram of the measuring set

The relative error in determining the value of the absorption coefficient o the ultrasonic wave was 6 % for $f = 2.5$ MHz reducing to 2 % for $f = 60$ MHz.

Before measurement the sample was thermally stabilized for two hours. The temperature of the liquid crystal was taken with a copper-constantan thermocouple and a digital voltmeter V-534.

3. The results of the measurements

Measurements of the absorption coefficient and the velocity of propagation of the ultrasonic wave at various temperatures which included the nematic mesophase and the isotropic liquid were carried out for 4-*n*-methoxybenzoate-4-*n*-pentylphenylene and 4-*n*-octyloxyphenylene-4-*n*-pentylexybenzoate. The results of the measurements of the absorption coefficient and the velocity at

different frequencies, for given temperatures can be used to establish the experimental dependencies

$$\frac{a}{f^2} = F(f), \qquad a\lambda = F(f),$$

where a denotes the absorption coefficient, f the frequency, $a\lambda$ the absorption coefficient in relation to the length of the wave.

Some of the measurements obtained on 4-*n*-methoxybenzoate-4-*n*-pentylphenylene have been presented previously [2]. For 4-*n*-octyloxyphenylene-4-*n*-pentyloxybenzoate, Table 1 shows, as an example, typical results of the measurements of the absorption coefficient and the velocity of the ultrasonic wave (at a temperature of 58 °C).

Table 1. The measurements and calculations for

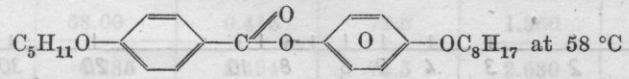

at 58 °C

f [MHz]	a [cm^{-1}]	v [m·s^{-1}]	$a\lambda \cdot 10^2$	$\frac{a}{f^2} \cdot 10^{-14}$ [cm^{-1}·s^2]
2.5	1.03	1405	5.79	16.48
5.0	1.12	1400	3.14	4.48
7.5	1.08	1410	2.04	1.93
9.6	1.84	1402	2.69	1.99
11.0	1.82	1452	2.40	1.50
13.6	2.23	1442	2.36	1.21
15.8	2.40	1422	2.16	0.96
18.8	3.46	1166	2.14	0.98
22.3	5.49	1293	3.18	1.10
27.0	9.34	1350	4.07	1.28
34.4	24.69	1307	9.38	2.09
35.0	25.60	1260	9.22	2.09
37.0	27.65	1295	9.68	2.02
40.0	15.70	1360	5.34	0.98

4. An interpretation of the results

While interpreting the results, it was found that the function $a\lambda = F(f)$ is a complicated one, possibly containing information about more than one relaxation time. Based on the data given in Table 1, Fig. 2 shows the dependence as a function of frequency. From Fig. 2 we can determine the value of the frequency of relaxation for the region containing the maximum, but the lack of experimental points for frequencies below 2.5 MHz does not allow us to state the second frequency of relaxation.

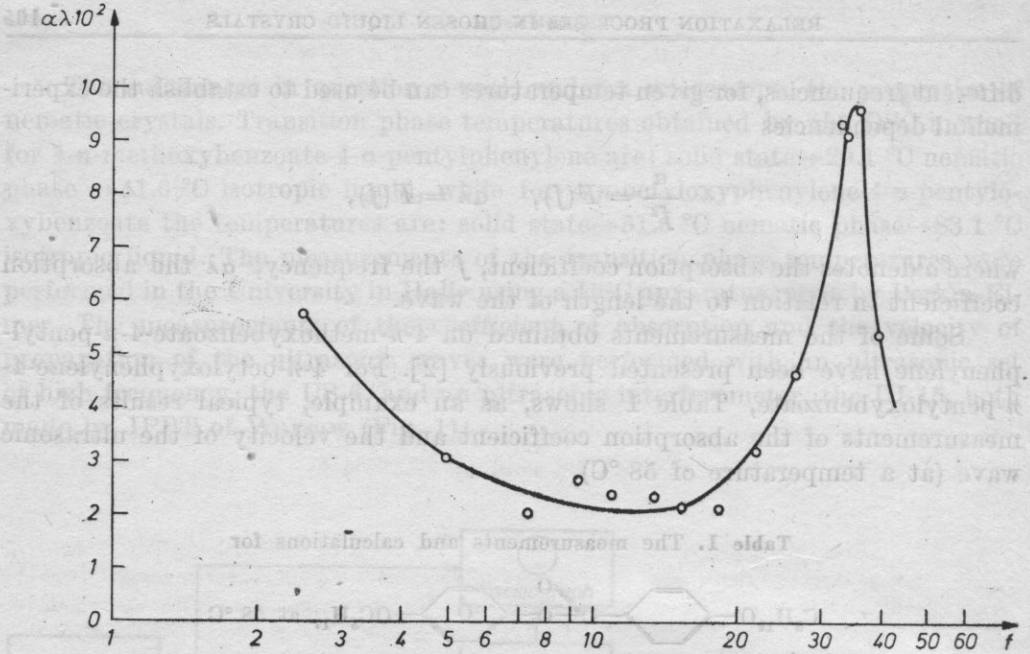

Fig. 2. The dependence of $\alpha\lambda$ on the frequency of 4-*n*-octyloxyphenylene-4-*n*-pentyloxybenzoate at 58 °C

$t = 58.0$ °C, $f_R = 36.2$ MHz

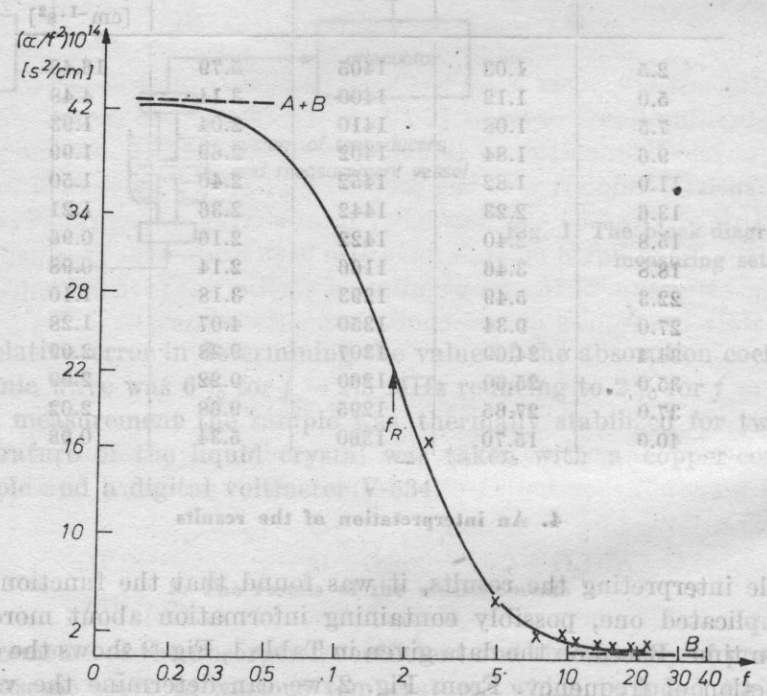

Fig. 3. The dependence of a/f^2 on the frequency of 4-*n*-octyloxyphenylene-4-*n*-pentyloxybenzoate at 58 °C

$t = 58.0$ °C, $A = 42.273 \cdot 10^{-14}$ s²/cm, $B = 0.409 \cdot 10^{-14}$ s²/cm, $f_R = 1.769$ MHz, $\tau = 9.011 \cdot 10^{-8}$ s, x – experimental points

Table 2. Measurements and calculations of the frequency and the time of relaxation for

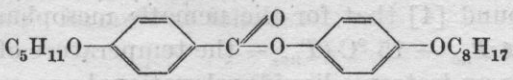

Acoustic			Dielectric*		
T [°C]	f_R [MHz]	$\tau_R \cdot 10^{-8}$[s]	T [°C]	f_R [MHz]	$\tau_R \cdot 10^{-8}$[s]
55.4	1.506 35.00	10.568 0.455	53.5	0.222	71.691
58.0	1.769 36.20	8.997 0.439	61.2	0.475	33.506
67.1	3.340 37.00	4.765 0.430	66.5	0.763	20.859
75.6	38.00	0.415	72.5	1.350	11.789
77.0	6.385	2.494	78.5	2.630	6.052
80.3	7.857	2.026			

* unpublished information received from Dr. H. KRESSE of the M. Luther University in Halle.

Table 3. Measurements and calculations of the frequency and the time of relaxation for

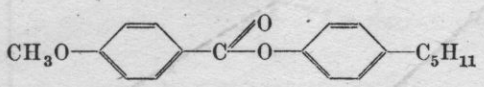

Acoustic			Dielectric*		
T [°C]	f_R [MHz]	$\tau_R \cdot 10^{-8}$ [s]	T [°C]	f_R [MHz]	$\tau_R \cdot 10^{-8}$ [s]
31.5	1.74 24.60	9.345 0.645	30.0	1.04	15.000
34.5	2.00 25.20	7.958 0.624	27.2	0.78	20.400
38.3	2.58 36.00	6.169 0.442	31.5	1.20	13.000
45.0	3.49 39.00	4.556 0.408	34.5	1.69	9.418
			38.3	2.40	6.634

* the measurements were carried out by the author in The M. Luther University in Halle.

It is possible to interpret the results of the ultrasonic absorption, if we assume that two relaxation regions exist in the frequency range under examination. It has been found [4] that for the nematic mesophase of liquid crystals at temperatures $T \ll T_{nc} - 15$ °C (T_{nc} — the temperature of the transition from the nematic phase to an isotropic liquid) relaxational processes occur with more than one relaxation time.

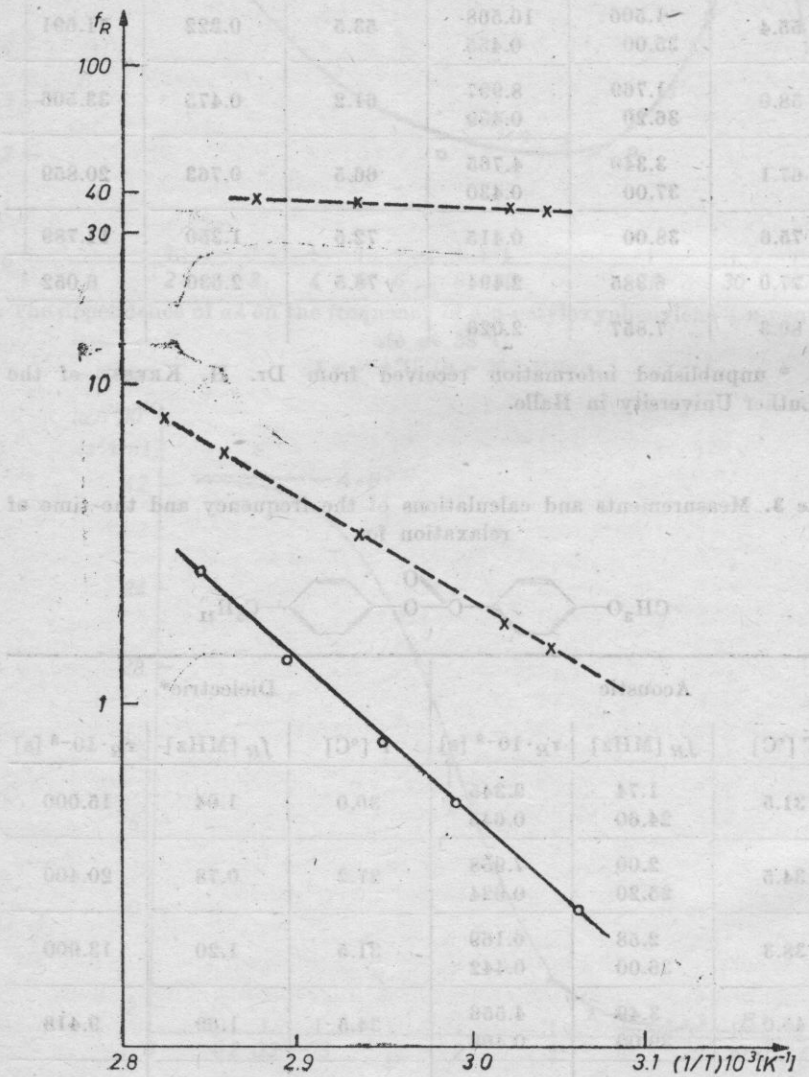

Fig. 4. The dependence of the natural logarithm f_R on $1/T$ of 4-*n*-octyloxyphenylene-4-*n*-pentyloxybenzoate
x — acoustic measurements, o — dielectric measurements

When we are dealing with only a single relaxation process then the expression for the absorption coefficient depends on the frequency and we can state it according to Lamb's formula as follows:

$$\frac{a}{f^2} = \frac{A}{1+\left(\frac{f}{f_R}\right)^2} + B, \tag{1}$$

where the constant A contains information on the contribution of the relaxation process to the absorption, whereas the constant B corresponds to the classical part of the absorption, and f_R denotes the frequency of relaxation. To determine the relaxation time for the lower frequencies, mathematical methods were employed together with the theoretical curve of relaxation given in Lamb's formula. Fig. 3 shows the results obtained for the sample in question over a frequency range of 0.1 to 20 MHz.

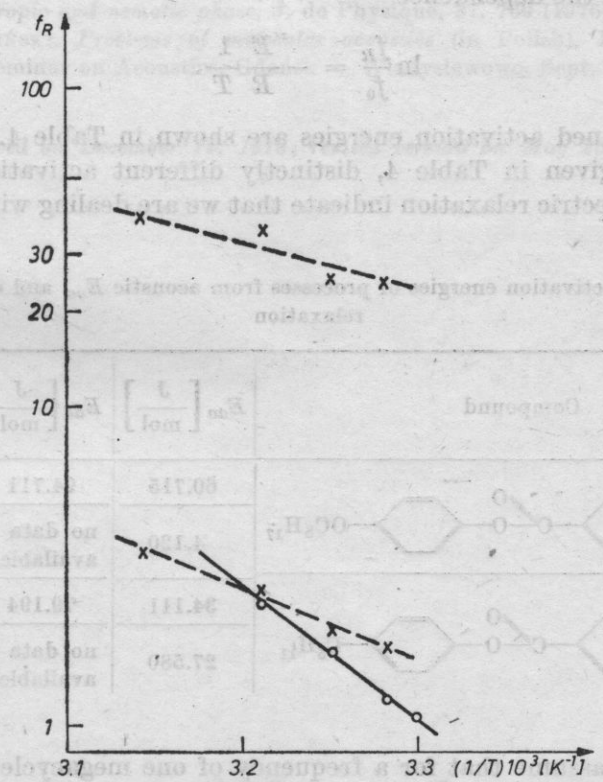

Fig. 5. The dependence of the natural logarithm f_R on $1/T$ of 4-*n*-methoxybenzoate-**4-*n*-pen**-tylphenylene
x – acoustic measurements, o – dielectric measurements

The results of measurements and calculations of the frequency of relaxation, and of the acoustic and dielectric relaxation times of the liquid crystals under consideration are given in Tables 2 and 3. The frequencies of relaxation determined in the investigations can be divided into two regions: the first one covers a frequency range up to about 20 MHz the second from 20-40 MHz. Figs. 4 and 5 show the dependence of the natural logarithm f_R on $1/T$ for the substances tested. The same figures show the dielectric relaxation data based on independently performed measurements. In both regions the relaxation frequencies increase as the temperature increases.

Making use of the fact that the relaxation frequency of the process is subject to the law of Arrhenius

$$f_R = f_0 \exp\left(-\frac{E}{RT}\right), \tag{2}$$

where E denotes the activation energy of the process, R is the gas constant, T is the absolute temperature, and f_0 is a constant, we can determine the activation energy from the dependence

$$\ln\frac{f_R}{f_0} = -\frac{E}{R}\frac{1}{T}. \tag{3}$$

The determined activation energies are shown in Table 4. As we can see from the data given in Table 4, distinctly different activation energies for acoustic and dielectric relaxation indicate that we are dealing with two different

Table 4. The activation energies of processes from acoustic E_{aa} and dielectric E_{ad} relaxation

Compound	$E_{aa}\left[\frac{\text{J}}{\text{mol}}\right]$	$E_{ad}\left[\frac{\text{J}}{\text{mol}}\right]$	Relaxation band [MHz]
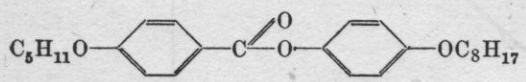	60.715	94.711	2.5-20
	4.120	no data available	20.0-60
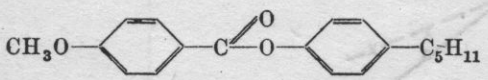	34.111	79.194	2.5-20
	27.580	no data available	20.0-60

processes. If we assume that for a frequency of one megacycle per second the relaxation is based on a mechanism of rotation of the end groups of the molecule, then the results obtained for both substances would testify that different fragments of the molecule are excited in dielectric and in acoustic relaxation.

References

[1] C. CASTRO, A. HIKATA, C. ELBAUM, *Ultrasonic attenuation anisotropy in a nematic liquid crystal*, Phys. Rev. A, 353 (1978).

[2] A. DRZYMAŁA, M. CIEŚLAK, K. KRUPA, A. SZYMAŃSKI, *On the mechanical relaxation in ultrafrequency range in 4-n-methoxybenzoešane-4-n-pentylphenylene*, III Liquid Crystal Conference, Budapest 1979.

[3] J. F. DYRO, P. D. EDMONDS, *Ultrasonic absorption and dispersion at phase transition in liquid crystalline systems: N-octylamine — water*, Molecular Crystals and Liquid Crystals, **8**, 141-155 (1996).

[4] A. P. KAPUSTIN, *Experimental investigations of liquid cristals*, Nauka, Moskwa 1978.

[5] F. KIRY, P. MARTINOTY, *Attenuation of sound in CBOOA near the nematic — smectic A transition*, European Conference on Physics and Applications of Smectic and Lyotropic Liquid Crystals, Madonna di Campiglio, 9-13 January 1978.

[6] H. KRESSE, D. DEMUS, K. SAUER, A. WIEGELEBEN, A. DRZYMAŁA, *Dielektrisches und elektrooptisches Verhaltén des nematischen 4n-methoxybenzoesaure 4n-pentylphenylesters*, Z. Chem., 19, Ig. 4 (1979).

[7] S. NAGAI, *A new interpretation of crystal ultrasonic absorption in the nematic phase of liquid crystals*, Japanese Journal of Applied Physics, **18**, 5 (1979).

[8] S. NAGAI, P. MARTINOTY, S. CANDAU, *Ultrasonic investigation of nematic liquid crystals in the isotropic and nematic phase*, J. de Physique, **37**, 769 (1976).

[9] A. ŚLIWIŃSKI, *Problems of molecular acoustics* (in Polish), Proceedings of the XXIV-th Open Seminar on Acoustics, Gdańsk — Władysławowo, Sept. 1977, vol. 3.

Received on December 14, 1978; revised version on May 26, 1980

ARCHIVES OF ACOUSTICS
6, 2, 173-178 (1981)

INFORMATION CONTENT AS A PARAMETER OF ACOUSTICAL HOLOGRAM RECONSTRUCTIBILITY

JÁN KALUŽNÝ

Department of Physics, Komenský University (Trnava, Czechoslovakia)

JERZY K. ZIENIUK

Institute of Fundamental Technological Research,
Polish Academy of Sciences (00-049 Warszawa, ul. Świętokrzyska 21)

The aim of this paper is to discuss the information content of an acoustical hologram and to determine its dependence on the determining parameters. It is also to look for the threshold of the information content which has to be reached in order to perform a successful reconstruction of the hologram.

Introduction

Information content is one of the parameters which characterises every information system. The holographic visualisation method may be considered as a method which permits the storage of a large amount of information. The rigorous determination of the information content of a hologram is a complicated problem which has not yet been fully solved. This paper presents a preliminary attempt to quantify the information content of acoustical holograms.

Theory

Let the coordinate plane x, y be identical with that of the hologram. Then the information content of the hologram, I_0 in the first approximation is determined as [1]

$$I_0 = \log_2(H_x H_y / l_x l_y) \quad [\text{bit}], \tag{1}$$

where l_x and l_y are the minimum resolvable distances along the x and y axes, respectively; H_x and H_y are the dimensions of the rectangular hologram. To

assess the information content of the acoustical hologram I_a we shall start from this formula.

During visualisation with acoustical holography the problem of sampling the hologram at discrete points often arises. It is necessary to determine the number of these points for which the amplitude has to be sampled in order to optimise the recording of the information on the subject coded in the interference pattern. The sampling theorem [2] determines the number of these sampling points. Under the theorem, an arbitrary wave front across the aperture S, containing spatial frequency variation up to a limit of B lines/cm is recorded fully if its amplitude is sampled at intervals of $1/2\ B$ cm. This means that for a rectangular aperture of area $S = H_x H_y$ cm^2 the wave front is fully determined by sampling at $4B^2S$ points. In this way the information about the subject coded in an acoustical hologram can be recorded most effectively. Further increase in the number of points recorded does not contribute to increasing the information content. This means that the points in which the information, for the determination of the information content of an acoustical hologram should be sampled, are spaced by $1/2\ B$ cm. Thus the information content of the hologram is

$$I_a = \log_2 4B^2S. \tag{2}$$

If the smallest spacing of lines d (d^{-1} is the spatial frequency of the interference pattern) is $d = \lambda/2\sin\theta\sin\Phi$ [2], where λ is ultrasonic wavelength, 2θ

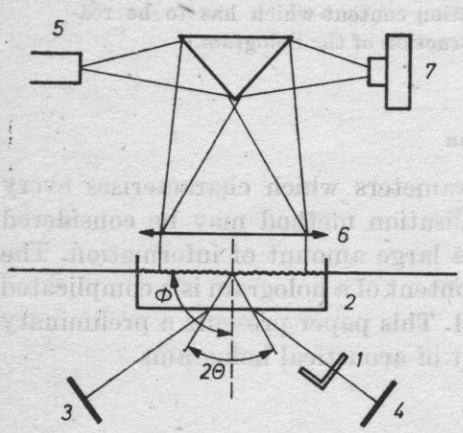

Fig. 1. Experimental set-up
1 – object, *2* – minitank, *3* and *4* – reference and object beams, respectively, *5* – He-Ne laser with optical system, *6* – lens, *7* – camera

is the angle between the reference and object beams, Φ is the angle between the line bisecting the angle 2θ and the hologram plane (see Fig. 1) then the information content of an acoustical hologram is given by

$$I_a = \log_2(16S\sin^2\theta\sin^2\Phi/\lambda^2) \tag{3}$$

or

$$I_a = \log_2(16Sf^2\sin^2\theta\sin^2\Phi/c^2) \quad [\text{bit}], \tag{4}$$

where c is the velocity of the ultrasonic wave and f its frequency. It is easy to see that I_a is a function of five independent parameters. Figs. 2-4 shows I_a as a function of some of these parameters. It can be seen from Fig. 2 that in order to increase the information content of the hologram, increasing the area is more effective than increasing the frequency. The influence of the value of the ultrasonic velocity on the information content of the hologram is shown in Fig. 3. It can be seen from this curve that it is necessary, when choosing the liquid in the minitank, to consider not only its surface tension and viscosity but also its

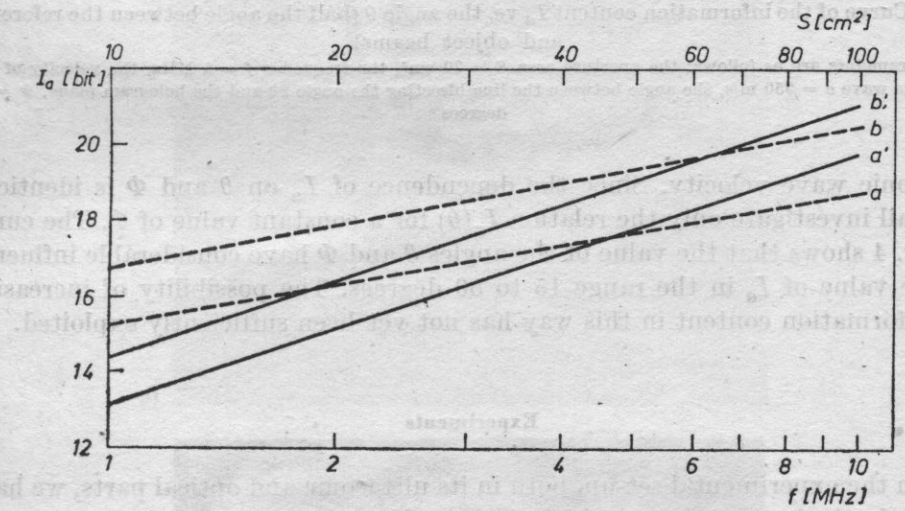

Fig. 2. Curves of the information content I_a vs. the aperture area S
a – for 3 MHz; b – for 5 MHz. Other parameters are as follows: the angle between the reference and object beams, $2\theta = 60$ degrees; the angle between the line bisecting the angle 2θ and the hologram plane, $\Phi = 90$ degrees; the velocity of the ultrasonic wave $c = 950$ m/s. Curves of I_a vs. the frequency f : a' – for S equal to 20 cm², b' – for S equal to 50 cm². Other parameters are as follows: $c = 950$ m/s, $2\theta = 60$ degrees, $\Phi = 90$ degrees

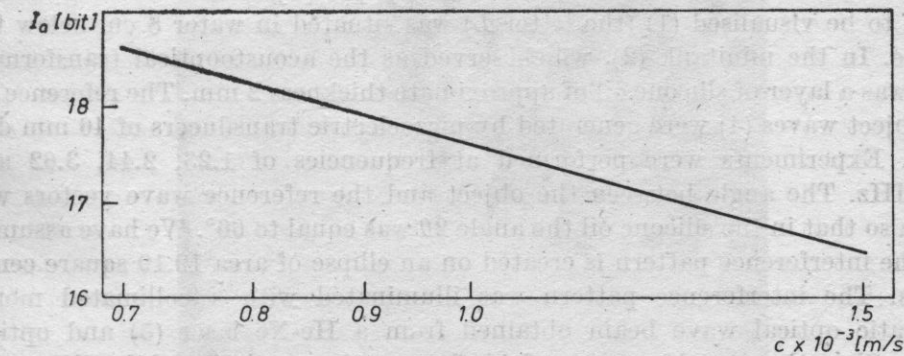

Fig. 3. Curve of the information content I_a vs. the velocity of the ultrasonic wave c
other parameters are as follows: the aperture area $S = 20$ cm², the frequency $f = 5$ MHz, the angle between the reference and object beams, $2\theta = 60$ degrees; the angle between the line bisecting the angle 2θ and the holograme plane $\Phi = 90$ degrees

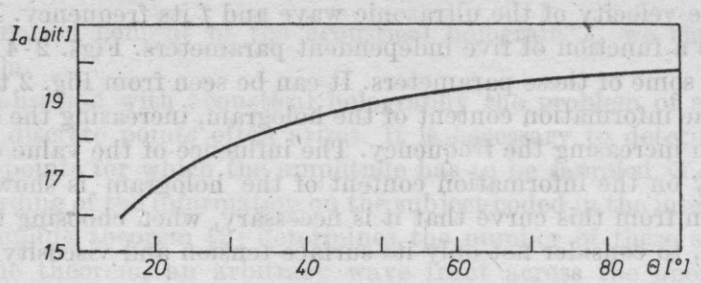

Fig. 4. Curve of the information content I_a vs. the angle θ (half the angle between the reference and object beams)
other parameters are as follows: the aperture area $S = 20$ cm², the frequency $f = 5$ MHz, the velocity of the ultrasonic wave $c = 950$ m/s, the angle between the line bisecting the angle 2θ and the hologram plane, $\Phi = 90$ degrees

ultrasonic wave velocity. Since the dependence of I_a on θ and Φ is identical, we shall investigate only the relation $I_a(\theta)$ for a constant value of Φ. The curve in Fig. 4 shows that the value of the angles θ and Φ have considerable influence on the value of I_a in the range 15 to 50 degrees. The possibility of increasing the information content in this way has not yet been sufficiently exploited.

Experiments

In the experimental set-up, both in its ultrasonic and optical parts, we have used only the basic elements which, from a theoretical point of view, are needed for holographic imaging. We have used no such elements or methods as acoustical lenses etc. which would decrease the intrinsic noise of the experimental apparatus and influence the amount of artifacts. The experimental acoustical holography set-up using free liquid surface deformation as the acoustooptical transformer, which is similar to that described in another paper [3], is shown in Fig. 1. The object to be visualised (1) (the letter L) was situated in water 8 cm below the surface. In the minitank (2), which served as the acoustooptical transformer, there was a layer of silicone oil of approximate thickness 2 mm. The reference (3) and object waves (4) were generated by piezoelectric transducers of 46 mm diameter. Experiments were performed at frequencies of 1.23, 2.44, 3.62 and 4.88 MHz. The angle between the object and the reference wave vectors was chosen so that in the silicone oil the angle 2θ was equal to 60°. We have assumed that the interference pattern is created on an ellipse of area 19.19 square centimeters. The interference pattern was illuminated with a collimated monochromatic optical wave beam obtained from a He-Ne laser (5) and optical system. Since the spatial frequency d^{-1} influences the separation of the diffraction orders [4], the record of the created interference pattern — the hologram — was reduced optically by a factor of aproximately four and recorded on a photographic plate (7). The reconstruction was thus not carried out in real time.

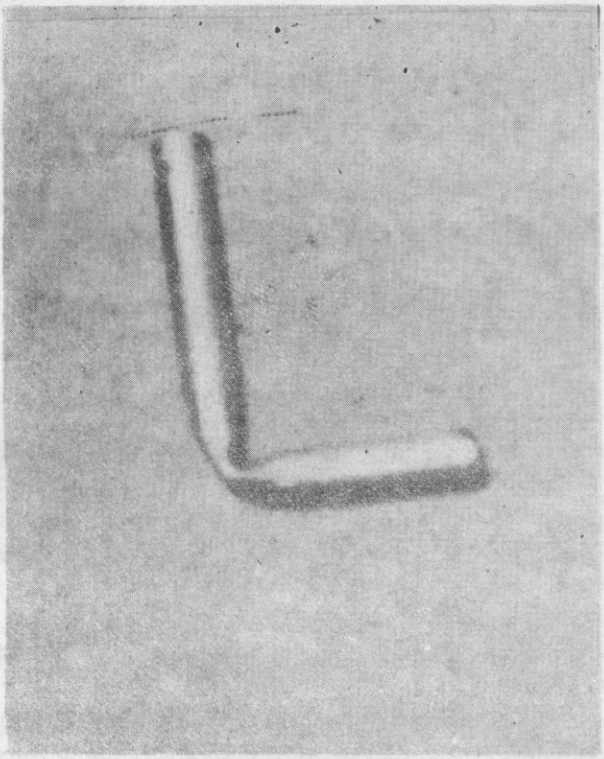

a)

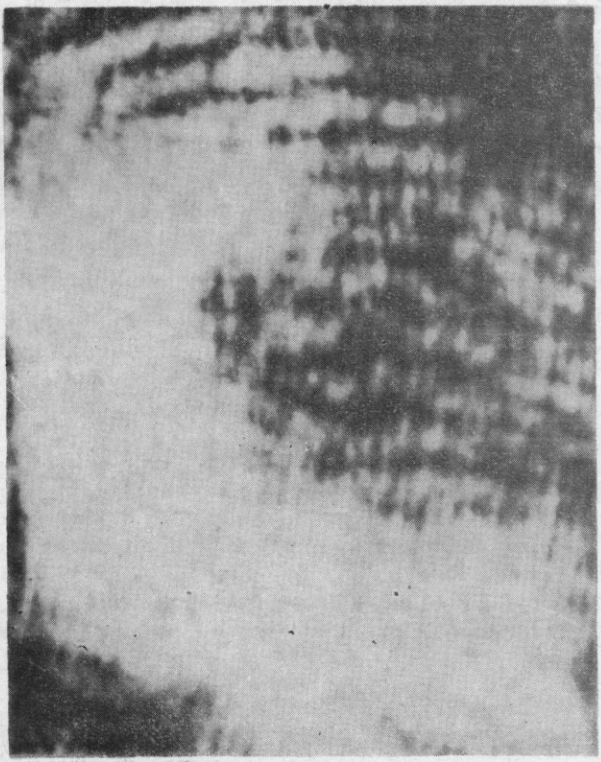

b)

c)

Fig. 5. a) photograph of the object. The diameter of the tube is 0.3 cm, the height is 2.0 cm; b) the reconstructed image at a frequency of 2.44 MHz; c) the image at a frequency of 4.88 MHz

Discussion

Values of the calculated information content of the acoustical holograms recorded on the elliptical area mentioned above for the described experimental conditions are presented in Table 1. The reconstruction of the object recorded

Table 1

f [MHz]	1.23	2.44	3.62	4.88
I_a [bit]	13.66	15.63	16.80	17.75

in the hologram at the lowest frequency of 1.23 MHz was not possible as a result of the strong influence of the noise of the experimental set-up and artifacts. The images of the same object obtained by reconstruction of the holograms recorded at frequencies of 2.44 and 4.88 MHz are shown in Fig. 5b and 5c along with the photo of the object itself (Fig. 5a). The improvement of the quality of the image of the object with the increasing I_a of the hologram is distinct. It is reasonable to assume that it should, in the near future, be possible to determine the quality of the reconstructed image by means of the parameter of the information content I_a, using some objective physical method.

On the basis of the preliminary results obtained we suppose that in order to obtain an image when reconstructing an acoustical hologram it is necessary to make a hologram having information content of about 15 bits. Since the quality of the image increases with increasing information content, it is necessary to reach as high a value of I_a as is possible. In acoustical holography visualization by means of a free liquid surface, it is necessary to take into account the aim of the visualization (nondestructive testing, medical diagnostics, etc.), and the dependencies plotted in Figs. 2-4. One should decide on the basis of an analysis of the purpose of the visualization process the physical parameters by means of which this goal could be achieved.

The results presented here are considered to be preliminary one. A more exact formula for I_a as well as objective criteria for the reconstructibility of acoustical holograms should be developed in the near future.

References

[1] F. T. S. Yu, *Introduction to diffraction, information processing and holography*, MIT Press, Cambridge 1973, p. 197.

[2] B. P. Hildebrand, B. B. Brenden, *Introduction to acoustical holography*, Plenum Press, New York 1972, p. 97.

[3] J. Kalužny, M. Konečný, *Slaboproudy obzor*, **40**, 1, 14-21 (1979).

[4] J. K. Zieniuk, *On some experiments with real time ultrasonics holography*, Proc. of 7th ICA, Budapest 1971, paper 20U9, pp. 465-468.

Received on December 1, 1979; revised version on December 12, 1980

ARCHIVES OF ACOUSTICS
6, 2, 179-204 (1981)

THE MOLECULAR CHARACTERISTICS OF OIL FRACTIONS DETERMINED FROM ULTRASONIC VELOCITY MEASUREMENTS

WIESŁAW SZACHNOWSKI, BOGDAN WIŚLICKI

Institute of Aviation, Warsaw

This paper presents the results of measurements of ultrasonic velocity in liquid hydrocarbon multi-fraction fuels and individual hydrocarbons, on the basis of which the Rao constants, the mean distances between the surfaces of the free molecules, the Langemann constants, and the acoustic diameters of the molecules were determined. The dependencies of the acoustic constants, the distances between the molecules and the acoustic diameters of the molecules on the density and on the molecular mass for different fractions of fuels and different individual hydrocarbons are presented. It was found that the quantities used in molecular acoustics can be used to characterize the properties of multi-component hydrocarbon mixtures and to identify their structure. The results of the investigations confirmed the usefulness of the concept presented in this paper – the concept of the inclusion of the intermolecular interaction forces by a change in the acoustically determined intermolecular distances in a hypothetical equivalent single – component liquid.

Notation

A, a, B, b – characteristic constants of a homologous series of hydrocarbons
C_A – content of aromatic carbon (in %)
C_N – content of naphthene carbon (in %)
C_P – content of paraffin carbon (in %)
c – ultrasonic propagation velocity
d_a – acoustic molecule diameter
d_{ref} – molecule diameter determined from refraction
J – mean distance between surfaces of free molecules
K – constant
K_A – number of aromatic rings
K_N – number of naphthene rings
K_0 – total number of rings
K_s – modulus of isentropic compressibility
L – Lagemann's constant

M — molecular weight
N — Avogadro's number
n — optical refractive index at the D line
R — Rao's constant
S — sulphur content
T — temperature
T_k — solidification temperature
T_z — ignition temperature
V — volume
V_M — molar volume
W — Rao's constant
β_s — coefficient of isentropic compressibility
ϱ — density
ϱ_0 — reference density
T — density at the temperature of the investigation
ν — kinematic viscosity

1. Introduction

The ultrasonic velocity and its relation to the density of a liquid permits information to be obtained on the chemical and physical structure of the liquid. The relation of these quantities to the molecular weight and the specific heat make it possible to determine the interaction forces, and the volumes and diameters of relevantly defined molecules, etc. The additivity of ultrasonic velocities in the case of liquid mixtures, which has been investigated by different workers [1, 8, 15], permits knowledge obtained about the physical structure, the solubility, and the accompanying dilatation effects to be evaluated. The use of the ultrasonic velocity for structural analysis and the determination of the physical and chemical properties of simple hydrocarbon mixtures, fractions, and products from crude oil has been limited to date. The investigations of CORNELISSON, WATERMAN, HARVE [2], for example, dealt with the relations between the viscosity, the optical refractive index, the surface tension, and the ultrasonic velocity (v-n-c and v-c-b), and the dependence of ultrasonic velocity on density for fractions of mineral oils. These papers had a fundamental character and were limited to saturated oil fractions. There is a lack, however, of detailed information on the relation of the ultrasonic velocity to the constitutional properties of fractions of crude oil: fuels, oils, etc. The investigations of the utilitarian properties of the products have been limited to the determination of the elastic constants — moduli and coefficients of adiabatic compressibility — and, more recently, of the density.

The present paper presents the results of measurements of the ultrasonic velocity and its relation to the molecular weight and density of multi-component hydrocarbon mixtures and fractions which are components of oil fuels.

The essential difficulty in the investigation of mixtures of this type, and in particular, the hydrocarbon fractions, is not only a lack of an equation of

state for the real liquid, but also of mixing principles. In the case of real liquids these principles exist only for two-component and sometimes three-component systems. Thus all the quantities, which are measured relatively, are determined by mean values. Of necessity the problem of mixtures is reduced to a hypothetical one-component liquid. Each molecular interpretation, both of the measurement data and of the material constants, including rheological models, also applies to this kind of liquid. How, therefore, should such quantities as the optical refractive index, the molecular weight, and particularly the molecular diameter, the intermolecular distance or the coefficient of compressibility be interpreted? Of necessity the only possibility is the use of the model of the mean liquid mentioned above. This involves, according to the present authors, the assumption of the unambiguous definition of a molecule of such a one-component mean liquid. From the point of view of molecular physical chemistry and mathematic correctness, the closest solution is the assumption of a molecule diameter which is defined on the basis of the statistical theory of liquids. This will be a space in which the probability of the existence of a molecule with a complex of interactions is equal to unity. Certainly for such a simple model, for the interpretation of phenomena related to wave propagation, it can be assumed that long-range interactions are represented by changes in the molecule diameter and the intermolecular distance. Accordingly a lack of intermolecular interaction can be assumed in a model of such a liquid. The model of ultrasonic wave propagation becomes simplified, and the velocity can be regarded as the sum of the wave propagation velocities in the intermolecular space, and inside the molecule.

The above gross approximations can, for the purposes of the understanding and description of multi-component mixtures, use the characteristic quantities defined by optical and dilatometric methods, and by the methods of molecular acoustics.

2. Relations and characteristic constants

The basic constitutional quantity of liquid organic compounds, which links the ultrasonic velocity and the density, is the coefficient or modulus of isentropic compressibility

$$\beta_s = \frac{1}{K_s} = \frac{1}{\varrho c^2}. \tag{1}$$

In liquids the quantities c and ϱ decrease as the temperature decreases, with the exception of water and some mixtures of strongly polarized compounds. This is described, for example, by the known Rao relation [11, 12]

$$R = \sqrt[3]{c\frac{M}{\varrho}} = \text{const}. \tag{2}$$

The significance of the quantity R, the so called molar sound velocity, results from its additive and constitutional properties. For most organic solutions, liquid chemical elements, and some mixtures, the constant R is usually independent of temperature. Over a moderate temperature range relation (2) is satisfied for some nonassociated liquids. There is, however, a group of organic compounds, e.g. paraffin or the aromatic hydrocarbons in crude oil, for which $R \neq \text{const}$.

In the case of oil hydrocarbons it is interesting to note the change of the quantity R in a homologous series and in mixtures of their components, and the dependence on P and T. The investigation of relation (2) as a function of molar mass has shown in many cases a linear character [12]:

$$R = aM + b. \tag{3}$$

For aliphatic hydrocarbons the values of a and b in equation (3) are respectively 13.97 and 155, while for aromatic hydrocarbons they are 14.02 and 120 [1]. The opinion has been voiced in the literature that the constant a is practically the same for different homologous series [11, 12].

For a number of liquids the expression $\varrho\sqrt[7]{\beta_s}$ takes constant values over a wide range of pressure and temperature [12]. This expression in the form of the relation

$$W = \frac{M}{\varrho\sqrt[7]{\beta_s}} \tag{4}$$

is known as the molar compressibility. From relations (1), (2) and (4) the following relation can be obtained

$$W = M^{1/7}R^{6/7}. \tag{5}$$

For nonassociated liquids the quantity W is also constant and should satisfy the condition of invariability better than does the constant R. This was confirmed in paper [10] for binary hydrocarbon mixtures of different concentrations. For most mixtures the following linear relation exists

$$W = AM + B. \tag{6}$$

For mixtures containing both "lighter" and "heavier" components, relation (6) is rectilinear, while relation (3) is not. The rectilinearity of relation (3) occurs with the introduction of equimolar volumes, while relation (6) is rectilinear in practically all cases.

In addition to the constants mentioned above another equation, proposed by Lagemann, may be used [1, 12]

$$L = \frac{\Delta c}{\Delta T}\sqrt{M} = \text{const}. \tag{7}$$

This is satisfied by many organic liquids and their mixtures. In the region of considerable change in the temperature coefficient of sound velocity, i.e.

near the critical and solidification temperatures, this relation is not satisfied [1, 12].

Knowing the temperature coefficient of the sound velocity and the coefficient of expansion, the density and the molecular weight, it is possible to define the acoustic diameter of the molecule [7]. This diameter may be interpreted as being close to the statistical molecular diameter. The acoustic molecular diameter can be defined, for example, using the following relation [7]

$$d_a = \frac{\frac{1}{c}\left(\frac{dc}{dT}\right)_P}{\frac{1}{c}\left(\frac{dc}{dT}\right)_P - \frac{1}{3}\frac{1}{V}\left(\frac{dV}{dT}\right)_P}\left(\frac{M}{\varrho N}\right)^{1/3}. \tag{8}$$

Assuming a spherical shape for the molecule JACOBSON gave a relation permitting the determination of the distance between the surfaces of the free molecules [5, 6]

$$J = \frac{K}{\varrho^{1/2} c}, \tag{9}$$

where $K = \text{const}$ for $T = \text{const}$.

By analogy with an ideal gas, the quantity J can thus be regarded as the free path. As for the molar sound velocity, this quantity, in view of its dimension, is interesting for interpretation only. The values of K for different temperatures are the following: 0 °C — 588; 10 °C — 604; 20 °C — 618; 30 °C — 631; 40 °C — 624; 50 °C — 652 [10].

3. Procedure

The hydrocarbon mixtures analyzed were separated in the form of fractions of the oil fuels: jet fuel (1) and Diesel fuel (2, 3, 4, Tables 1 and 2) [9].

Some of these fractions were represented by only one kind of structure, in other a specific kind of structure dominated [9]

I — n-isoparaffin and naphthene fractions,

II — n-paraffin fractions,

III — isoparaffin and naphthene fractions,

IV — isoparaffin and naphthene fractions with a majority of naphtene fractions,

V — isoparaffin and naphthene fraction swith a majority of isoparaffin fractions,

VI — aromatic unicyclic fractions, $n^{20} = 1.48 + 1.53$,

VII — aromatic polycyclic fractions, $n^{20} > 1.53$.

The method of separating the fractions is described in reference [19]. Using the methods of liquid and column chromatography, fractions I, VI and

Table 1. The standard properties of fuels

Properties	Sample 1	2	3	4
ϱ_4^{20}	0.8150	0.8371	0.8412	0.8484
distillation [°C]				
beginning	148	—	—	—
10%	158	—	—	250
50%	193	—	—	—
90%	242	—	—	—
98%	270	—	—	—
up to 300 °C	—	74%	50%	68%
up to 350 °C	—	95%	85%	92%
ν^{20} [cSt]	1.63	4.84	5.51	7.23
$T_k^{\blacksquare}$ [°C]	−60	−14.5	−13.0	−6.0
T_z^{i} [°C]	36 M.P.	80 M.C.	60 M.C.	36 M.P.
S [%]	0.029	0.271	0.650	0.372

Table 2. The physical and chemical properties and the structural composition of the fractions separated from the fuels

Fraction	T_k	ϱ_4^{20}	M	n^{20}	C_P	C_A	C_N	K_0	K_A	K_N
I −1	−60	0.7958	148.6	1.4395	51.2	1.5	47.3	0.87	0.04	0.83
I −3	−8	0.8088	225.9	1.4478	66.4	0.0	33.6	0.90	0.00	0.90
II −2	+11	0.8062	225.0	1.4351	93.7	0.0	6.3	0.17	0.00	0.17
II −3	+11	0.7742	218.4	1.4345	93.5	0.0	6.5	0.17	0.00	0.17
III −2	−70	0.8209	218.4	1.4530	58.6	0.0	41.4	1.12	0.00	1.12
III −4	−63	0.8286	228.0	1.4566	57.0	0.0	43.0	1.26	0.00	1.26
IV −1	−70	0.8101	152.0	1.4429	37.8	0.0	62.2	1.20	0.00	1.20
IV −3	−70	0.8065	229.0	1.4481	71.1	0.0	28.9	0.79	0.00	0.79
V −1	−70	0.7948	148.0	1.4400	48.9	0.0	51.1	0.89	0.01	0.88
V −2	−60	0.8266	222.0	1.4554	56.1	0.0	43.8	1.25	0.00	1.25
V −3	−70	0.8285	223.9	1.4561	56.5	0.0	43.5	1.25	0.00	1.25
V −4	−60	0.8331	228.5	1.5482	55.2	0.0	44.8	1.34	0.00	1.34
VI −1	−60	0.9008	150.9	1.5177	39.3	57.9	2.8	1.28	1.23	0.03
VI −3	−65	0.9093	216.9	1.5133	43.1	40.4	16.5	1.76	1.26	0.50
VI −4	−35	0.9137	231.5	1.5088	34.2	23.7	42.1	2.28	0.82	1.46
VII −2	−60	0.9689	176.5	1.5626	37.7	52.0	10.3	2.06	1.72	0.34
VII −3	−63	0.9632	182.5	1.5472	21.4	53.4	25.2	2.20	1.50	0.70
VII −4	−50	0.9856	199.4	1.5592	17.8	52.6	29.6	2.58	1.63	0.93

Table 3. The acoustic properties of individual hydrocarbons at 20 °C

No.	Product		$M \times 10^3$ [kg]	$\varrho \times 10^3$ [kgm^{-3}]	c [ms^{-1}]	$\beta_s \times 10^3$ [m^{2}kG^{-1}]	R [m$^{10/3}$s$^{-1/3}$]	W $\left[\frac{\text{kG}^{1/7}\text{m}^{20/7}}{\text{s}^{2/7}}\right]$	$J \times 10^{10}$ [m]	$d_a^* \times 10^{10}$ [m]	$d_{\text{ref}}^* \times 10^{10}$ [m]	References
1	*n*-hexane	C_6H_{14}	86.17	0.654	1083	1.322	1371.05	344.39	0.7105	5.39	4.56	[1]
2	*n*-heptane	C_7H_{16}	100.20	0.684	1162	1.083	1540.09	388.55	0.6431	5.60	4.79	[1]
3	*n*-octane	C_8H_{18}	114.22	0.704	1193	0.998	1720.74	435.37	0.6174	5.80	5.01	[2]
4	*n*-nonane	C_9H_{20}	128.25	0.738	1248	0.870	1870.99	475.57	0.5764	5.99	5.20	[1]
5	*n*-decane	$C_{10}H_{22}$	144.62	0.730	1253	0.873	2135.78	541.92	0.5777	6.16	5.73	[18]
6	*n*-dodecane	$C_{12}H_{26}$	170.15	0.749	1297	0.794	2477.40	629.88	0.5506	6.50	5.67	[18]
7	*n*-tridecane	$C_{13}H_{28}$	182.21	—	—	—	—	—	—	—	5.84	[18]
8	*n*-tetradecane	$C_{14}H_{30}$	198.24	0.763	—	—	—	—	—	6.82	6.00	[18]
9	*n*-hexadecane	$C_{16}H_{34}$	226.27	—	—	—	—	—	—	7.12	6.25	[18]
10	cyclohexane	C_6H_{12}	84.16	0.779	1276	0.788	1171.80	299.84	0.5487	5.08	4.46	[2]
11	methylcyclohexane	C_7H_{14}	98.18	0.764	1247	0.842	1383.20	353.34	0.5700	—	—	[1]
12	cis-decahydronaphthalene	$C_{10}H_{18}$	138.24	0.895	1451	0.531	1748.64	453.62	0.4500	—	—	[2]
13	trans-decahydronaphthalene	$C_{10}H_{18}$	138.24	0.873	1403	0.582	1772.71	458.97	0.4713	—	—	[2]
14	hydroindane	C_9H_{10}	118.17	0.910	1403	0.558	1453.73	378.62	0.4618	—	—	[1]
15	tetraline	$C_{10}H_{12}$	132.20	0.969	1484	0.469	1556.15	407.86	0.4231	—	—	[2]
16	benzene	C_6H_6	78.11	0.878	1326	0.648	977.37	253.91	0.4974	4.80	4.36	[2]
17	toluene	C_7H_8	92.13	0.866	1328	0.655	1169.36	303.20	0.5001	5.05	4.62	[2]
18	*m*-xylene	C_8H_{10}	106.16	0.863	1340	0.645	1356.18	351.31	0.4965	5.30	4.85	[1]
19	ethylbenzene	C_8H_{10}	106.16	0.868	1334	0.644	1347.70	349.43	0.4957	5.32	4.85	[2]
20	1,3,5-trimethylbenzene	C_9H_{12}	120.19	0.863	1362	0.625	1543.77	399.60	0.4884	5.66	5.08	[2]
21	1,3,5-trimethylbenzene	C_9H_{12}	120.19	0.894	1372	0.594	1493.88	388.50	0.4764	—	—	[18]
22	iso-propylbenzene	C_9H_{12}	120.19	0.862	1342	0.644	1537.96	398.31	0.4960	—	—	[1]
23	pseudobutyl-*m*-xylene	$C_{12}H_{18}$	162.28	0.868	1354	0.628	2068.97	535.97	0.4899	—	—	[1]
24	diphenylene methane	$C_{13}H_{12}$	168.22	1.007	1514	0.433	1918.18	505.03	0.4068	—	—	[2]

* d_a and d_{ref} [17]

VII were separated on silica gel. By complexing fraction I with urea fractions II and III were separated. By complexing fraction III with tiourea fractions IV and V were separated.

The density ϱ_4^{20} ($\pm 1 \times 10^{-4}$), the optical refractive index n_D^{20} ($\pm 1 \times 10^{-4}$), and the molecular weight M (1%) of the fractions were measured. The dependence of the density on temperature was calculated according to [14]. This other quantities were determined by standard methods according to the Polish Standards. The carbon content and the number of rings in specific types of structure were determined by the $n - \varrho - M$ and $G - L$ methods of structural analysis [3, 18]. The ultrasonic velocity (± 0.5%) as a function of temperature at normal pressure $c(T)$ was measured by the ultrasonic interferometric method developed at the Institute of Aviation (in cooperation with the Institute of the Fundamental Technological Research). The quantity $c(T)$ was measured over a temperature range from the solidification point of the fraction to $+80$ °C at a frequency of 10 MHz. Using the quantities c, ϱ, M, the respective values of the quantities defined by relations (1)-(9) were determined.

4. Results

The characteristic ranges of the values of the coefficient of isentropic compressibility at 20 °C for the paraffin and naphthene fractions (I-V), and for the aromatic fractions (VI, VII) were respectively $0.63\text{-}0.74 \cdot 10^{-3}$ m²·kG^{-1} and $0.45\text{-}0.57 \cdot 10^{-3}$ m²·kG^{-1} (see Table 4). It follows from these results that β_s can be used in structural identification. In the case of the aromatic hydrocarbon fractions, unicyclic structures can be distinguished from polycyclic ones.

The coefficients of correlation and regression (Table 7) showed a linear relation between c (n) and β_s (n) on a logarithmic scale, Figs. 1.2, particularly clearly for aromatic fractions.

The functions $R(M)$ and, particularly, $W(M)$ were also found to be linear (see Figs. 3, 4). As before this linearity was better for the aromatic hydrocarbon fractions. For the other fractions the maximum nonlinearity was ± 5 % (Table 4). This was confirmed by the coincidence of the value of the coefficients of regression (Table 7) and the behaviour of these functions for the individual hydrocarbons. No linear correlation was found for the relation $L(M)$.

The behaviour of the relation $J(T)$ (Fig. 5) and the temperature dependence of the other acoustic quantities (Tables 5, 6) confirmed the structurally varied character of the fractions. The same distinct differentiation of fractions occurs in the case of the relation $\beta_s(J)$ (Fig. 6). The results discussed so far can be used for the structural identification of multi-component hydrocarbon mixtures.

A separate group of results giving information about the molecular structure consists of the quantities describing such statistical parameters of the molecules as the diameters, defined acoustically or from refraction, and the Jacobson

Table 4. The acoustic properties of the fractions at 20 °C

No.	Product	c [m s^{-1}]	$\Delta c/\Delta T$ [m °C^{-1}s^{-1}]	$\beta_s \times 10^3$ [m^{2}kG^{-1}]	R [m$^{10/3}$s$^{-1/3}$]	$\frac{W}{[\mathrm{kG}^{1/7}\mathrm{m}^{20/7}/\mathrm{s}^{2/7}]}$	$J \times 10^{10}$ [m]	L [mkG$^{1/2}$s^{-1} °C^{-1}]	$d_a \times 10^{10}$ [m]	$d_{ref} \times 10^{10}$ [m]	V_M [mo]
1	I −2	1303.4	4.12^{-20}_{60}	0.740	2039.74	522.99	0.5315	50.22^{-20}_{50}	6.108	5.382	186.73
2	−3	1365.7	—	0.563	3098.80	794.61	0.5032	—	—	6.188	279.30
3	II −2	1354.1	3.63^{10}_{40}	0.676	3087.62	791.70	0.5083	54.40^{10}_{40}	6.920	6.136	279.09
4	−3	1363.5	—	0.695	3128.13	797.20	0.5151	—	—	6.155	282.10
5	III −2	1364.1	3.62^{-20}_{60}	0.655	2950.61	758.26	0.5000	53.42^{-20}	6.861	6.109	266.05
6	−4	1380.1	—	0.634	3063.56	787.90	0.4919	—	—	6.192	275.16
7	IV −1	1328.2	3.96^{-20}_{60}	0.699	2063.01	529.81	0.5166	48.86^{-20}	6.139	5.403	187.63
8	−3	1363.5	—	0.667	3148.59	807.11	0.5047	—	—	6.224	283.99
9	−1	1306.8	4.00^{-20}_{60}	0.737	2035.82	521.83	0.5305	48.68^{-20}_{60}	6.091	5.379	186.21
10	V −3	1367.5	3.78^{-20}_{60}	0.647	2981.03	766.74	0.4971	56.30^{-20}	6.865	6.138	268.57
11	−3	1371.9	—	0.641	3002.86	722.49	0.4949	—	—	6.153	270.25
12	−4	1384.4	—	0.626	3056.87	786.67	0.4891	—	—	6.142	279.28
13	−1	1399.4	3.86^{-20}_{60}	0.567	1873.73	487.36	0.4653	47.46^{-20}	5.998	5.439	167.52
14	VI −3	1439.8	—	0.531	2693.52	700.57	0.4501	—	—	6.104	238.53
15	−4	1438.7	—	0.529	2860.25	744.48	0.4494	—	—	6.213	253.36
16	−2	1482.5	3.55^{-20}_{60}	0.470	2077.13	544.42	0.4235	47.16^{-20}_{60}	6.225	5.723	182.16
17	VII −3	1473.0	—	0.478	2155.83	564.74	0.4275	—	—	5.755	189.77
18	−4	1488.0	—	0.458	2309.72	606.75	0.4183	—	—	5.917	202.31

Table 5. The dependence of the acoustic properties of the fractions of fuel 1 on temperature

No.	Product	T [°C]	$\varrho \times 10^3$ [kgm^{-3}]	c [ms^{-1}]	$\frac{\Delta c}{\Delta T}$ [m °C^{-1}s^{-1}]	$\beta_s \times 10^3$ [m^{2}kG^{-1}]	E [m$^{10/9}$s$^{-1/3}$]	$\left[\frac{W}{\frac{\text{kG}^{1/7}\text{m}^{20/7}}{\text{s}^{2/7}}}\right]$	$J \times 10^{10}$ [m]	L [mkG$^{1/2}$ s^{-1} °C^{-1}]	$d_a \times 10^{10}$ [m]
1		−20	0.8269	1471.6	—	0.558	2044.07	523.94	—	—	6.071
2		−10	0.8191	1425.2	4.64	0.601	2041.62	523.40	—	55.56	6.038
3		0	0.8114	1384.3	4.09	0.643	2041.08	523.29	0.4716	49.86	6.074
4	I — 1	10	0.8036	1342.5	4.18	0.690	2039.94	523.04	0.5019	50.95	6.066
5		20	0.7958	1303.4	3.91	0.740	2039.74	522.99	0.5315	47.66	6.108
6		30	0.7880	1263.6	3.98	0.795	2038.74	522.77	0.5625	48.52	6.130
7		40	0.7802	1224.5	3.91	0.855	2037.66	522.54	0.5936	47.66	—
8		−20	0.8402	1490.7	—	0.536	2066.61	530.60	—	—	6.080
9		−10	0.8327	1446.6	4.41	0.574	2064.45	530.13	—	54.37	6.041
10		0	0.8251	1496.9	3.97	0.612	2064.23	530.08	0.4601	48.95	6.054
11	IV — 1	10	0.8176	1368.8	3.81	0.653	2064.19	530.07	0.4880	46.97	6.107
12		20	0.8101	1329.2	3.96	0.699	2063.01	529.81	0.5165	48.82	6.139
13		30	0.8026	1289.5	3.97	0.749	2061.35	529.44	0.5462	48.96	6.122
14		40	0.7951	1252.9	3.66	0.801	2060.92	529.35	0.5747	45.12	—
15		−20	0.8259	1471.6	—	0.559	2038.28	522.37	—	—	6.001
16		−10	0.8181	1430.0	4.16	0.598	2038.14	522.34	—	50.61	6.007
17		0	0.8104	1390.6	3.94	0.638	2038.43	522.40	0.4697	47.93	6.090
18	V — 1	10	0.8026	1346.9	4.37	0.687	2036.45	521.97	0.5006	53.16	6.073
19		20	0.7948	1306.8	4.06	0.737	2035.82	521.83	0.5305	48.78	6.091
20		30	0.7870	1267.6	3.92	0.791	2035.23	521.70	0.5611	47.69	6.072
21		40	0.7792	1231.5	3.61	0.846	2035.91	521.85	0.5906	43.92	—
22		−20	0.9261	1555.7	—	0.446	1888.02	490.54	—	—	5.952
23		−10	0.9198	1514.7	4.10	0.474	1884.10	489.67	—	50.36	5.950
24		0	0.9135	1475.8	3.89	0.503	1880.72	488.91	0.4169	47.79	6.004
25	VI — 1	10	0.9071	1333.5	4.23	0.536	1875.71	487.80	0.4424	51.26	5.931
26		20	0.9008	1399.4	3.41	0.567	1873.73	487.36	0.4653	41.89	5.998
27		30	0.8945	1362.2	3.72	0.602	1870.06	486.54	0.4898	45.70	6.028
28		40	0.8881	1323.9	3.83	0.642	1865.72	485.57	0.5146	47.05	—

Table 6. The dependence of the acoustic properties of the fractions of fuel 2 on temperature

No.	Product	T [°C]	$\varrho \times 10^3$ [kg m^{-3}]	c [ms^{-1}]	$\Delta c/\Delta T$ [m °C^{-1}s^{-1}]	$\beta_s \times 10$ [m^{2}kG^{-1}]	R [m$^{10/3}$s$^{-1/3}$]	W $\left[\frac{\text{kG}^{1/7}\text{m}^{20/7}}{\text{s}^{2/7}}\right]$	$J \times 10^{10}$ [m]	L [mkG$^{1/2}$s^{-10}C]	$d_a \times 10^{10}$ [m]
1		10	0.8138	1390.3	—	0.636	3085.80	791.30	0.4857	—	6.883
2	II – 2	20	0.8062	1354.1	3.62	0.676	3087.62	791.70	0.5083	54.30	6.920
3		30	0.7985	1317.3	3.68	0.722	3088.89	791.90	0.5360	55.20	6.945
4		40	0.7909	1281.5	3.58	0.770	3090.06	792.24	0.5633	53.70	—
5		–20	0.8504	1508.0	—	0.517	2945.08	757.04	—	—	6.734
6		–10	0.8430	1470.5	3.75	0.549	2946.09	757.26	—	55.42	6.670
7		0	0.8357	1438.0	3.25	0.579	2949.77	758.07	0.4473	48.03	6.793
8	III – 2	10	0.8282	1400.1	3.79	0.616	2950.10	758.15	0.4740	56.01	6.808
9		20	0.8209	1364.1	3.60	0.655	2950.61	758.26	0.5000	53.20	6.861
10		30	0.8135	1326.5	3.76	0.699	2949.83	758.09	0.5274	55.57	6.853
11		40	0.8061	1291.1	3.54	0.744	2950.19	758.17	0.5538	52.32	—
12		–20	0.8561	1522.0	—	0.504	2982.86	767.15	—	—	6.750
13		–10	0.8487	1484.7	3.73	0.535	2984.09	767.42	—	55.58	6.840
14		0	0.8414	1444.6	4.01	0.570	2982.63	767.10	0.4437	59.75	6.838
15	V – 2	10	0.8340	1406.0	3.86	0.607	2982.05	767.00	0.4704	57.51	6.867
16		20	0.8266	1367.5	3.90	0.647	2980.67	766.66	0.4972	58.11	6.865
17		30	0.8192	1331.0	3.60	0.689	2980.96	766.73	0.5238	53.64	6.883
18		40	0.8118	1295.3	3.57	0.734	2980.99	766.74	0.5501	53.19	—
19		–20	0.9911	1624.0	—	0.383	2093.26	548.04	—	—	6.147
20		–10	0.9855	1587.3	3.67	0.403	2089.17	547.12	—	48.76	6.144
21		0	0.9800	1552.0	3.44	0.423	2085.61	546.32	0.3825	45.70	6.162
22	VII – 2	10	0.9744	1518.9	3.49	0.445	2105.35	551.64	0.4031	46.63	6.198
23		20	0.9689	1482.5	3.55	0.470	2100.67	550.59	0.4235	47.43	6.225
24		30	0.9634	1446.5	3.60	0.496	2095.42	549.41	0.4444	48.10	6.230
25		40	0.9578	1411.0	3.55	0.524	2090.29	548.25	0.4649	47.43	—

Table 7. The coefficients of correlation and regression for the dependencies analyzed

Dependence	Correlation coefficient	Coefficients of regression equations		
	r	a	b	c
	paraffin and naphthene fractions			
$\beta_s(n)$	−0.799	–	–	–
$\beta_s(n)$	0.808	9284.86	−11055.2	3715.04
$\log\beta_s(n)$	−0.795	4.9648	−2.1694	–
$\log\beta_s(\log n)$	−0.796	2.9801	−7.1954	–
$c\ (n)$	0.854	9223.64	−13306.7	5435.83
$R\ (M)$	0.989	230.47	12.546	–
$W\ (M)$	0.993	135.62	8.7459	–
	aromatic fractions*			
$\beta_s(n)$	−0.910	393.01	−222.62	–
$\beta_s(n)$	0.944	6486.69	−8210.97	2617.43
$\log\beta_s(\log n)$	−0.929	2.8772	−6.2770	–
$c\ (n)$	0.927	−38600.6	50688.0	−16023.6
$R\ (M)$	0.923	445.68	9.0799	–
$W\ (M)$	0.951	196.29	7.2590	–

* Data on the aromatic fractions of other fuels [16] were also used in the calculation of the coefficients.

constants, which are a measure of the intermolecular distances. They form a group of the same quantities at, for example, the density, the optical refractive index, the molecular weight, etc. which, in the case of mixtures, must be regarded as mean values. In the case of the dependence $d_{\mathrm{ref}}\,(M)$, a higher concentration of results occurs both for the fractions and for the individual hydrocarbons, than for $d_a(M)$ (Figs. 7, 8). It follows from this that the diameter determined from refraction is better related to the molecular mass. The larger interval of values of d_a corresponding to a given range of M indicates, in turn, the higher "precision" of the acoustic measurements. The relations between c, β_s, J and V_M are a complementary system (Figs. 2, 6, 9-11). The intermolecular distance decreases with increasing M, while the ultrasonic wave velocity and the coefficient of compressibility increase. Likevise, increasing J causes c to decrease and β_s to increase (Fig. 6).

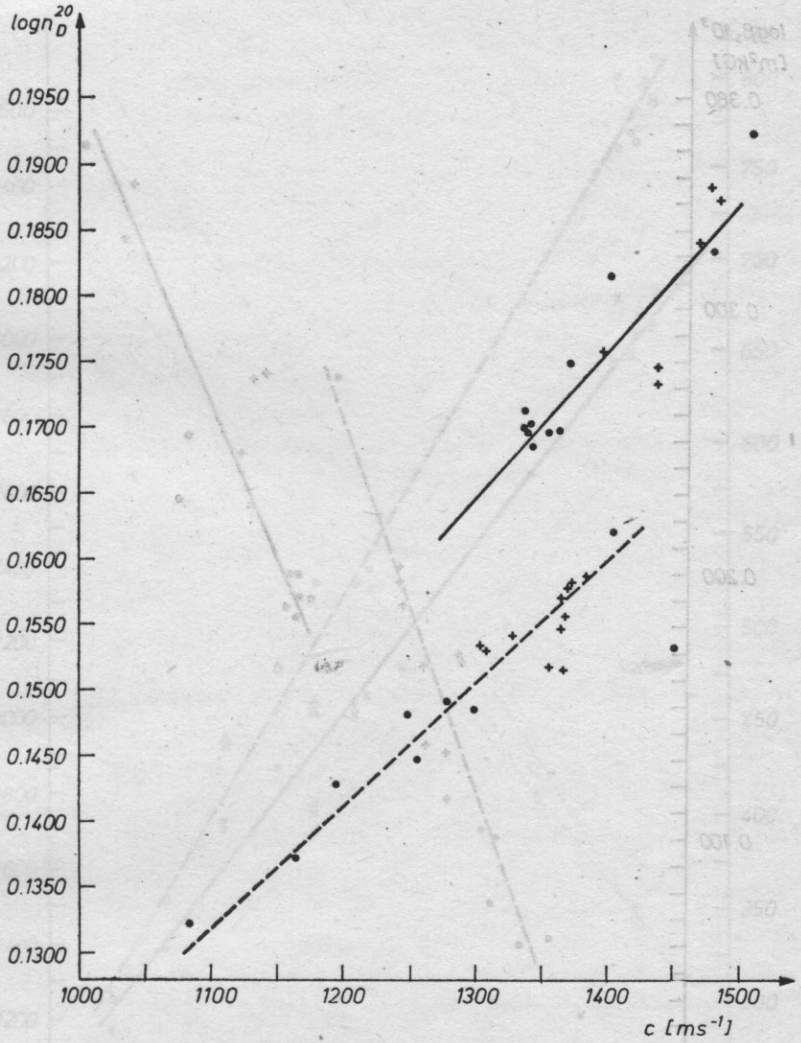

Fig. 1. The dependence of the optical refractive index on the ultrasonic velocity paraffin and naphthene hydrocarbons – – –, aromatic hydrocarbons ———, fractions x, individual. •

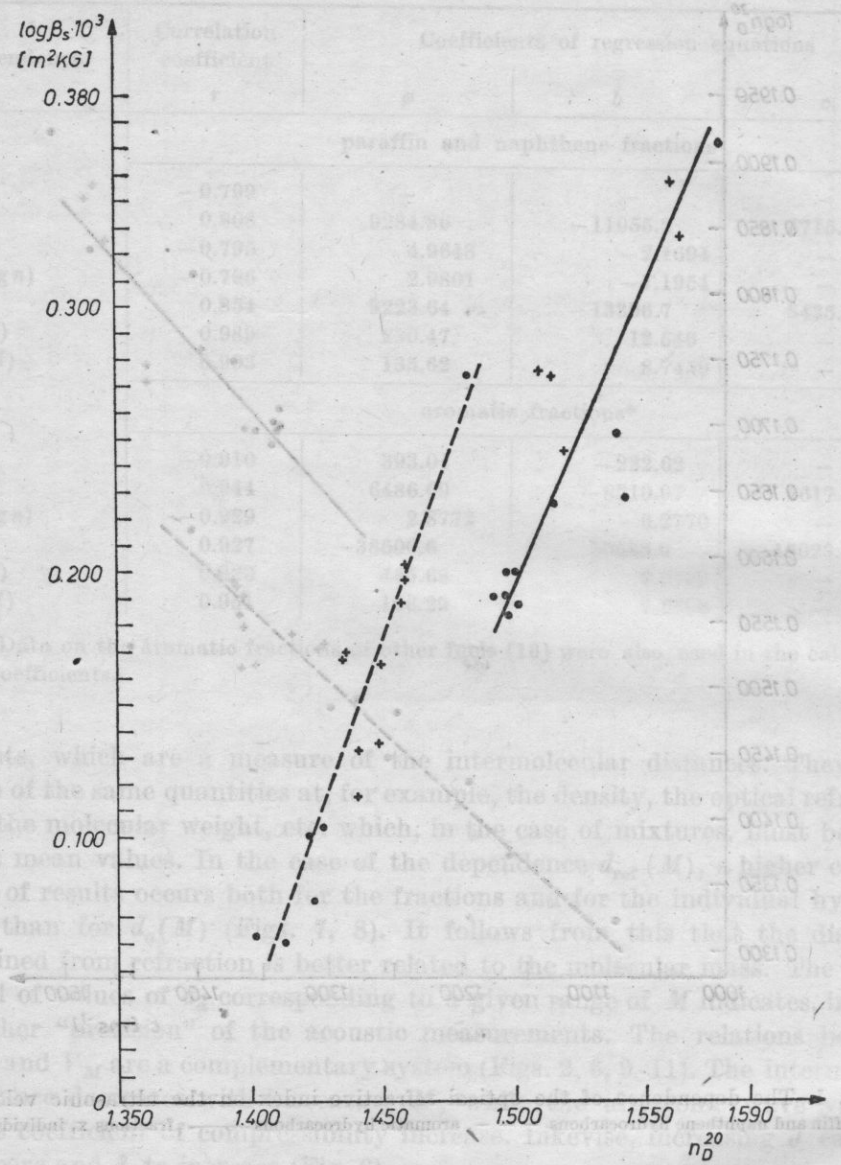

Fig. 2. The dependence of the coefficient of compressibility on the optical refractive index
symbols as in Fig. 1

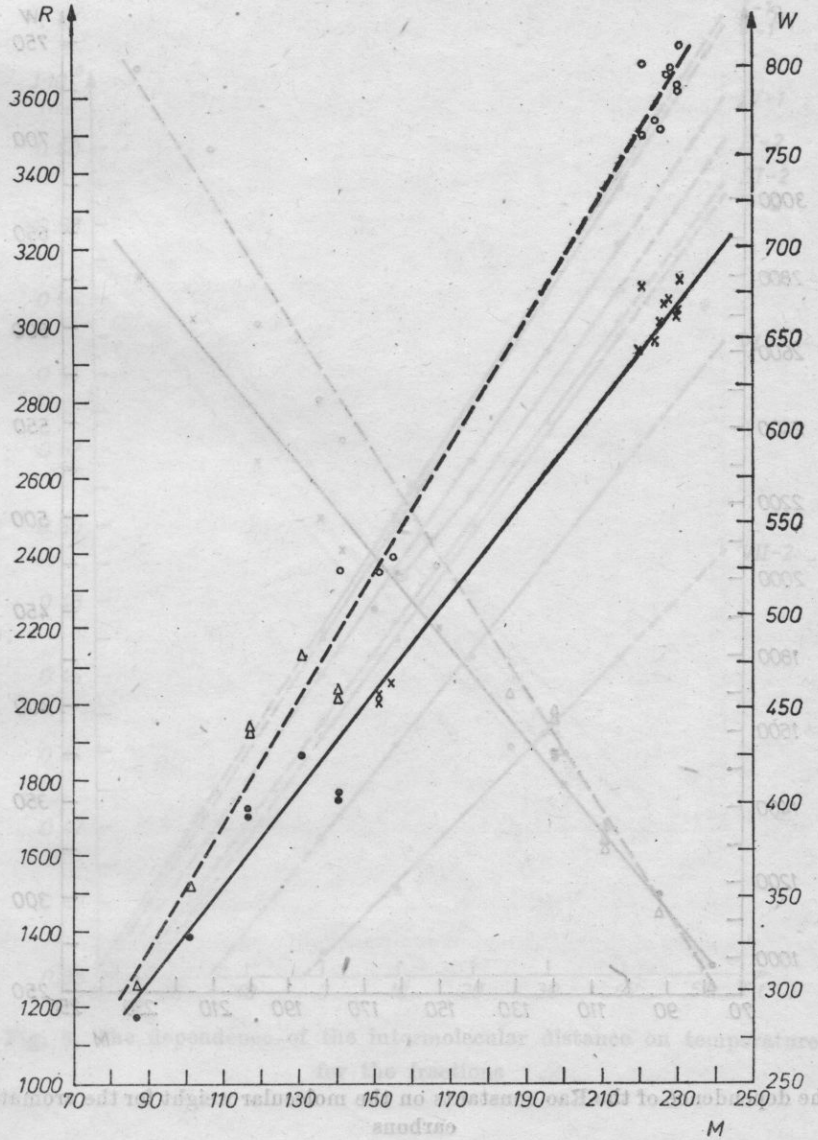

Fig. 3. The dependence of the Rao constants on the molecular weight for paraffin and naphthene hydrocarbons

$R(M)$ ———, fractions x, individual ● ; $W(M)$ – – –, fractions o, individual ●

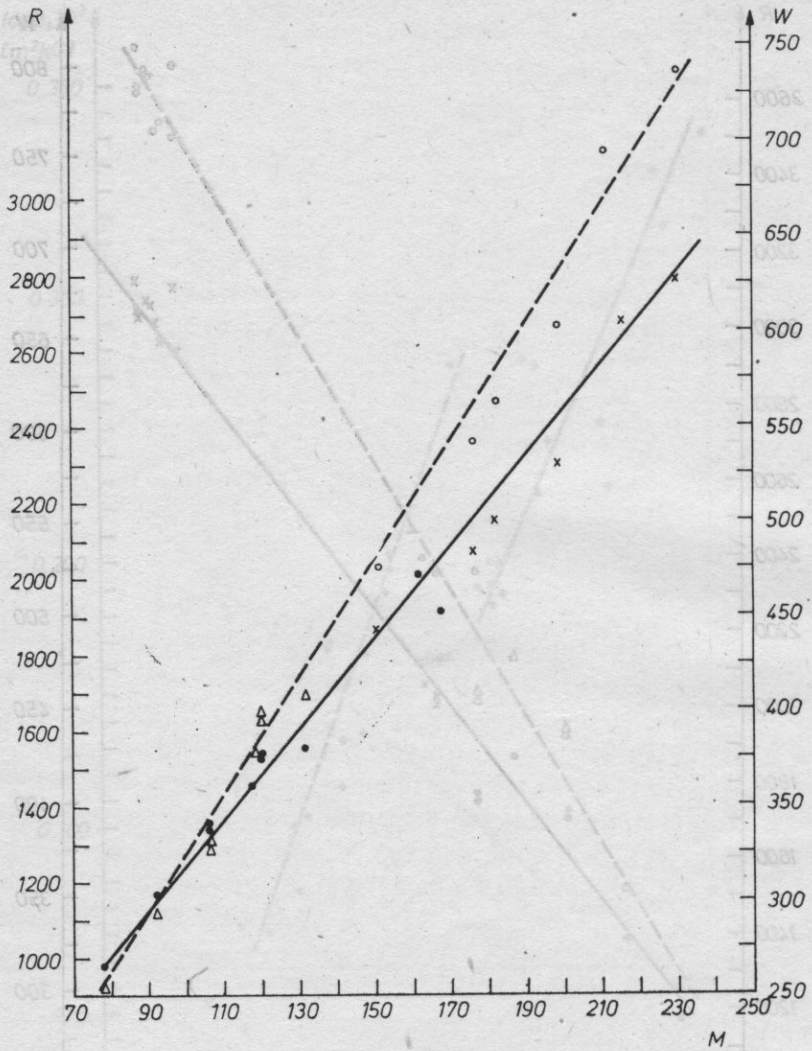

Fig. 4. The dependence of the Rao constants on the molecular weight for the aromatic hydrocarbons
symbols as in Fig. 3

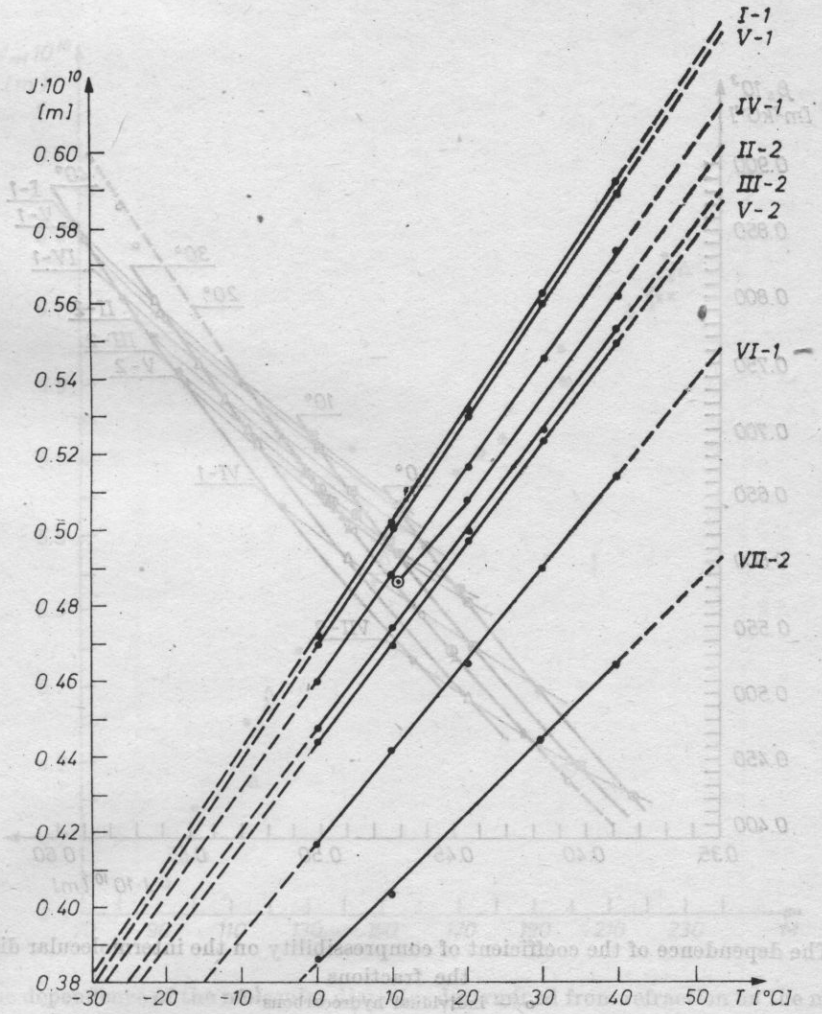

Fig. 5. The dependence of the intermolecular distance on temperature for the fractions

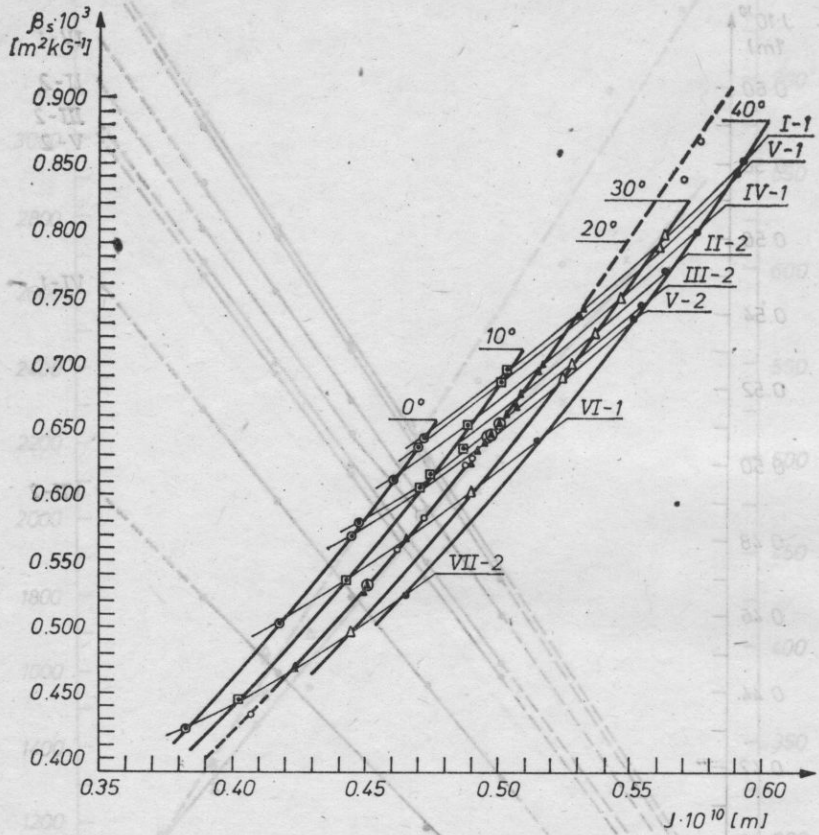

Fig. 6. The dependence of the coefficient of compressibility on the intermolecular distance for the fractions
o — individual hydrocarbons

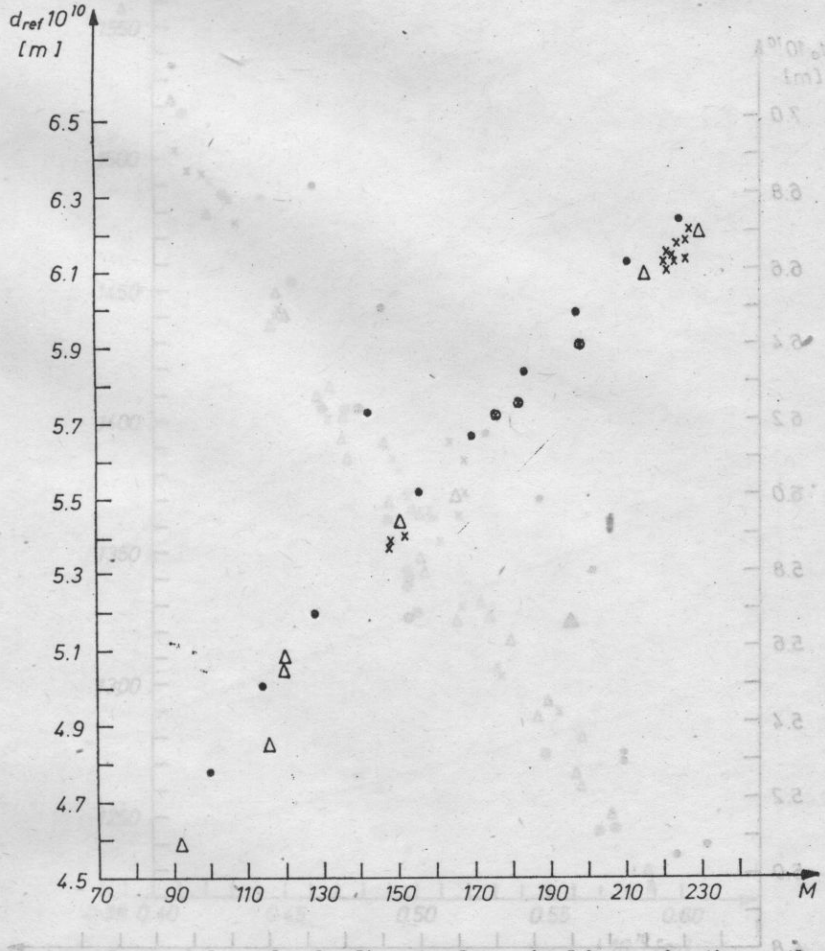

Fig. 7. The dependence of the molecular diameter determined from refraction on the molecular weight

paraffin and naphthene fractions x; fractions of aromatic hydrocarbons: unicyclic △, polycyclic x, individual hydrocarbons ●

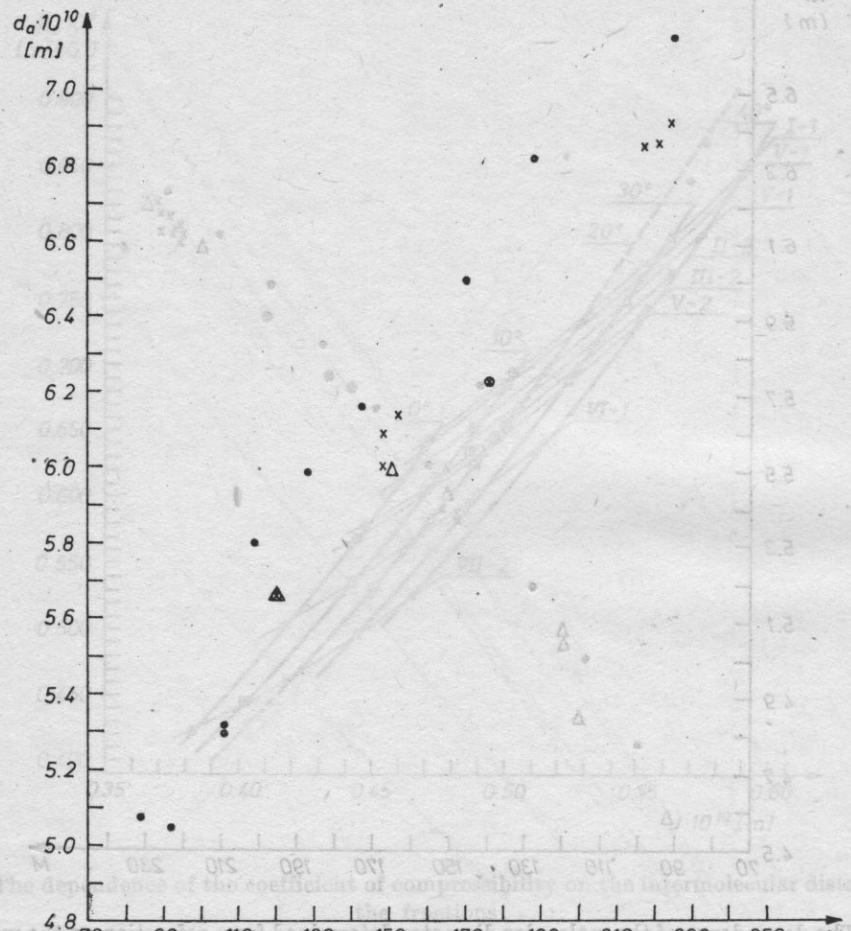

Fig. 8. The dependence of the molecular diameter determined acoustically on the molecular weight

symbols as in Fig. 7

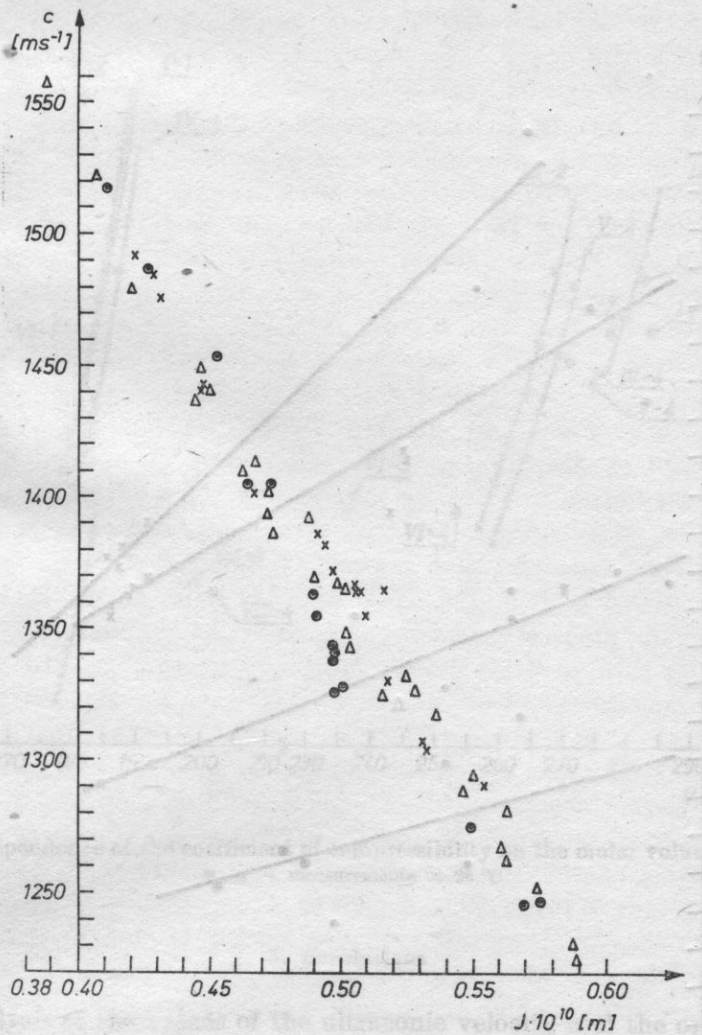

Fig. 9. The dependence of the ultrasonic velocity on the intermolecular distance for fractions and individual hydrocarbons at 20 °C, x and ⊙, and for fractions at other temperatures △

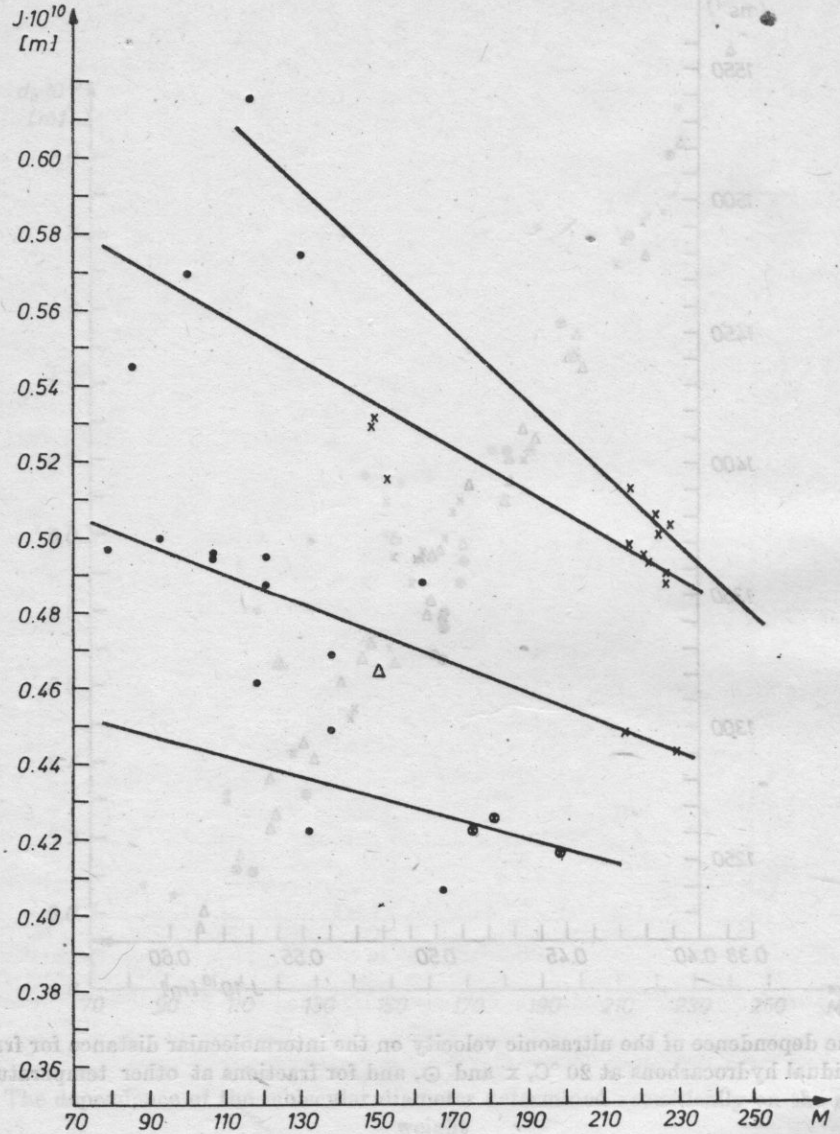

Fig. 10. The dependence of the intermolecular distances at 20 °C on the molecular weight
symbols as in Fig. 7

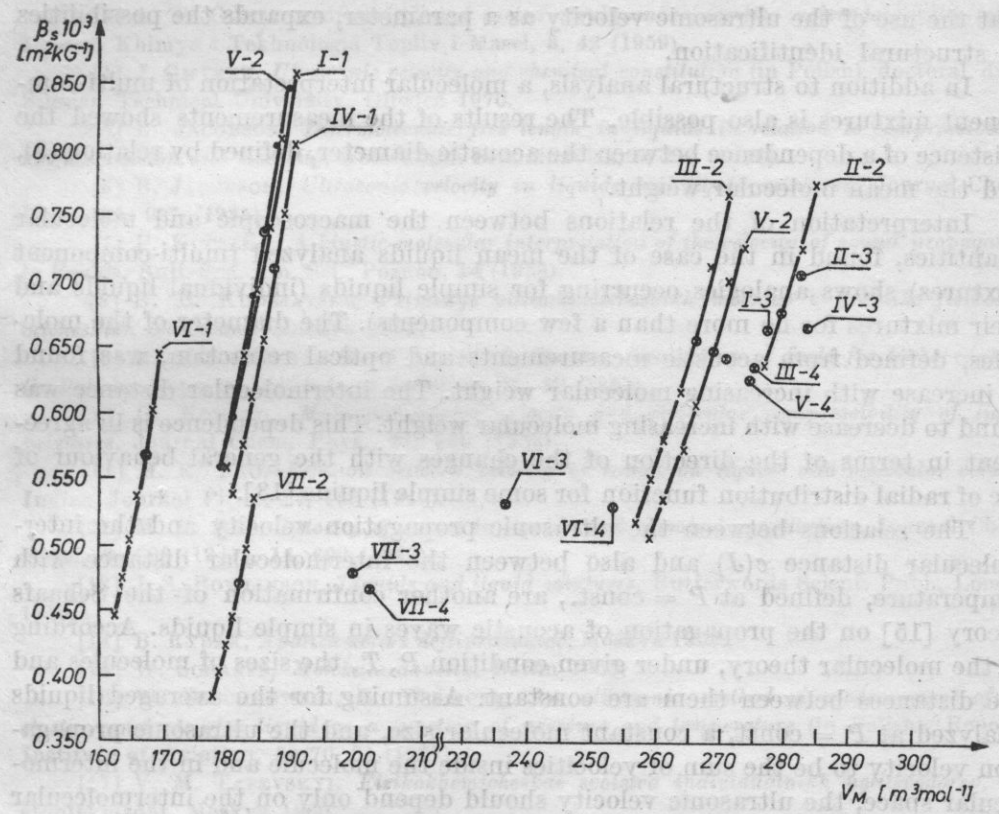

Fig. 11. The dependence of the coefficient of compressibility on the molar volume of fractions
●, x – measurements at 20 °C

5. Conclusions

The analysis of the values of the ultrasonic velocity and the optical refractive index for saturated individual hydrocarbons and their complex mixtures permits the following analogies to be stated; a distinct change in the value of c and n can be observed with an increase in the number of carbons in the molecules and with the density, and in the transition from paraffin or naphthene structures to aromatic structures, unicyclic and polycyclic, in condensed systems, particularly in the latter case.

The results of the investigations of the fractions showed the validity of the Rao rules to extend to complex multi-component mixtures. Extrapolation permits the use of these quantities for identifying the type of the basic structure of mixtures of unknown content. This applies both to hydrocarbon mixtures of different structural types, and to the introduction into molecules of a given structural type of other structures, e.g. paraffin chains into a benzene ring. Changes in the value of R and W should be expected in both cases. It follows

that the use of the ultrasonic velocity as a parameter, expands the possibilities of structural identification.

In addition to structural analysis, a molecular interpretation of multi-component mixtures is also possible. The results of the measurements showed the existence of a dependence between the acoustic diameter, defined by relation (8), and the mean molecular weight.

Interpretation of the relations between the macroscopic and molecular quantities, found in the case of the mean liquids analyzed (multi-component mixtures) shows analogies occurring for simple liquids (individual liquids and their mixtures for no more than a few components). The diameter of the molecules, defined from acoustic measurements and optical refraction, was found to increase with increasing molecular weight. The intermolecular distance was found to decrease with increasing molecular weight. This dependence is in agreement in terms of the direction of the changes with the general behaviour of the of radial distribution function for some simple liquids [13].

The relations between the ultrasonic propagation velocity and the intermolecular distance $c(J)$ and also between the intermolecular distance with temperature, defined at $P = \text{const.}$, are another confirmation of the Schaafs theory [15] on the propagation of acoustic waves in simple liquids. According to the molecular theory, under given condition P, T, the sizes of molecules and the distances between them are constant. Assuming for the averaged liquids analyzed at $P = \text{const}$, a constant molecular size, and the ultrasonic propagation velocity to be the sum of velocities inside the molecule and in the intermolecular space, the ultrasonic velocity should depend only on the intermolecular distances. This has been confirmed by the results of the investigations.

The analysis of the relations between the macroscopic and molecular quantities also leads to the conclusion that they have distinctly different characters depending on the structural type dominating in the fractions analyzed. This applies to the dependences of the intermolecular distances and the coefficients of compressibility, which are in some manner a measure of these distances, on the temperature, the molecular mass and the molar volume.

It should be noted that in all the cases where the presence of a factor strongly dependent on the interaction of the long-range forces can be expected, the model of a mean liquid can fail, e.g. $\beta_s(M)$. These forces are not sufficiently well accounted for by intermolecular distances, and even less by molecular sizes. The use of a larger variety of narrower and more monostructural fractions would probably be more relevant to these qualifications.

References

[1] L. Bergman, *Der Ultraschall u. seine Anwendung in Wissenschaft u. Technik*, Zurich 1964.

[2] J. Cornelisson, O. Harva, H. I. Waterman, *Correlation between physical constants and chemical structure*, ed. H. I. Waterman (in Polish), PWN, Warszawa 1964, p. 65.

[3] L. P. GILIATSETDINOV, *Novyi metod strukturnovo analiza uglevodorodnikh topliv i masel*, Khimya i Tekhnologia Topliv i Masel, **8**, 42 (1959).

[4] J. GMYREK, *Ultrasonic velocity and chemical constitution* (in Polish), doctoral diss., Silesian Technical University, Gliwice 1970.

[5] B. JACOBSON, *Intermolecular free length in liquids in relation to compressibility, surface tension and viscosity*, Acta Chim. Scandinavica, **5**, 214 (1951).

[6] B. JACOBSON, *Ultrasonic velocity in liquids and liquid mixtures*, Journal Chem. Phys., **20**, 927 (1952).

[7] F. KUCZERA, *A kinetic-molecular interpretation of the velocity of sound propagation in liquids*, Bull. Soc. Am. Sci., Poznań, **14** (1958).

[8] B. B. KUDRIATSEV, *Primenye ultraakusticheskikh metodov v praktike fizikokhimicheskikh isledovani*, Moskva 1952.

[9] B. MIELNIKOWA. B. WIŚLICKI. S. KLEIN, *Evaluation of fuels for turbo engines*, (in Polish), Reports, Institute of Aviation, 18, 19 (1963).

[10] O. NOMOTO, *Molecular sound velocity and molecular compressibility of liquid mixtures*, Journal Chem. Phys., **21**, 950 (1953).

[11] M. R. RAO, *Relation between velocity of sound on liquids and molecular volume*, Indian Journal Phys., **14**, 109 (1940).

[12] M. R. RAO, *Velocity of sound in liquids and chemical constitution*, Journal Chem. Phys., **9**, 628 (1941); **14**, 699 (1946).

[13] J. S. ROWLINSON, *Liquids and liquid mixtures*, Butterwords Scient. Publ., London 1959.

[14] B. RYBAK, *Analiza nefti i neftiproduktov*, Moskva 1962.

[15] W. SCHAAFS, *Molekularakustik*, Berlin 1963.

[16] W. SZACHNOWSKI, B. WIŚLICKI, *An ultrasonic method of measurement of the elastic constants of a liquid as a function of pressure and temperature* (in Polish), Reports, Institute of Aviation, 69/70, 31 (1977).

[17] V. M. TATEVSKYI, *Fizikokhemicheskae svoistva individualnikh uglitsvodorov*, Gostoptekhizdat, Moskva 1960.

[18] K. VAN NES, H.A. VAN WESTEN, *Sostav maslyanikh fraktsi nefti i ikh analiz*, Moskva 1954.

Received on June 4, 1979; revised version on November 21, 1980

C H R O N I C L E

XXVII OPEN SEMINAR ON ACOUSTICS

Puławy, 15-19 October, 1980

The XXVII Seminar on Acoustics (OSA 80) was held in Puławy on 15-19 October, 1980. It was organized by the Warsaw Division of the Polish Acoustical Society and the Institute of the Fundamental Technological Research of the Polish Academy of Sciences, and the Experimental Department Techpan. The chairman of the Scientific Committee was Prof. Ignacy MALECKI, and the chairman of the Organizing Committee was Dr. Jerzy ETIENNE.

More than 300 persons expressed their wish to participate in the Seminar, out of which 240 from Poland and 13 from abroad (from GDR, West Germany, Czechoslovakia, Greece, Iran and Holland) took part. 155 papers, including four general papers, were delivered. 13 papers were presented in poster sessions. Discussions were held in four parallel sessions in the mornings and afternoons and embraced a main theme, divided into thematic sections:

I – ultrasound in medicine (section *M*), underwater acoustics (section *H*), piezoelectric and piezomagnetic transducers (section *P*),

II – physical acoustics (section *B*), acousto-optics, crystals (section *F*), sonochemistry (section *S*), non-destructive testing (section *U*),

III – architectural acoustics, vibration, noise (section *A*),

IV – electroacoustics, acoustics of speech and hearing, acoustics of music (section *E*).

The papers accepted for delivery by the divisions of the Polish Acoustical Society and submitted to the Organizing Committee were published by the Publishing Section of the Institute of the Fundamental Technological Research of the Polish Academy of Sciences in two volumes (printed by the Wrocław Scientific Printing-House in 270 copies), and a supplement (printed by the Warsaw Scientific Printing-House in 350 copies). 190 papers, including 2 general ones, were published.

The Marek Kwiek competition was traditionally organized, for which only 9 papers were entered, of which 8 were delivered and evaluated. On behalf of the absent Dr. Z. WĄSOWICZ, Dr. R. GUBRYNOWICZ was responsible for the smooth running of the Seminar, both scientifically and organizationally. Dr. W. STRASZEWICZ and Z. PUSŁOWSKI, M. Sc., were in charge of the implementation of the scientific programme of the Seminar. Z. PUSŁOWSKI was responsible for the poster sessions and the round table sessions. The Secretaries of the Seminar who were responsible for administration and catering were G. ŁYPACEWICZ, J. ABŁAMOWICZ-POTAPOWICZ, I. ŻUCHOWICZ, B. WOYCZYŃSKA, K. TULICKA, B. SOSNOWSKA, M. BORKOWSKA. J. DODACKI was responsible for the technical organization.

An exhibition by the company Brüel and Kjaer was open during the Seminar showing the latest developments in electroacustic measurement techniques. The Experimental Department Techpan also held an exhibition showing their products: ultrasonic apparatus for applications in medicine (diagnostic apparatus) and industry.

Three organizational meetings were held on the first day of the Seminar: a meeting of the Executive Board of the Polish Acoustical Society, the General Congress of the Delegates of the Polish Acoustical Society, and a meeting of the Committee on Acoustics of the Polish

Academy of Sciences. The Seminar was officially opened in the afternoon of the same day. The guests and participants were addressed by the chairman of the Organizing Committee, Dr. J. ETIENNE on behalf of the Organizing Committee, by Z. CZAJKOWSKI, Mayor of Puławy, Prof. Dr. Z. JAGODZIŃSKI on behalf of the Executive Board of the Polish Acoustical Society, Prof. Dr. L. FILIPCZYŃSKI on behalf of the Committee on Acoustics of the Polish Academy of Sciences and Mr. J. SZERSZEŃ, director, on behalf of the director of the Institute of Fundamental Technological Research and Techpan. The unaugurative general paper: The use of analogy in electroacoustics — in memory of the tragically deceased acoustician J. WEHR, was delivered by the chairman of the Scientific Committee of the Seminar, Prof. Dr. I. MALECKI.

General papers

L. FILIPCZYŃSKI, *Methods of ultrasonic visualization in medicine.*
C. PUZYNA, *The psychoacoustic aspects of the orientation in space.*
A. RAKOWSKI, *Categorial perception of sound phenomena.*

Papers in sections

Section M (chairmen: A. WAGNER, J. KRETOWICZ)

A. CHROŚCICKI, L. FILIPCZYŃSKI, W. SECOMSKI, *Measurements of blood velocity in the tricuspid valve in children and youths by Doppler methods.*
L. HIRNLOWA et al., *Doppler ultrasound examination in the diagnosis of the carotid occlusive disease.*
L. HIRNLOWA et al., *Curve of blood flow velocity in the jugular vein in the diagnosis of intracardiac shunt.*
L. HIRNLOWA et al., *Estimation of the left ventricular performance in patients with previous myocardial infarction on the basis of the aortic blood flow velocity tracings by the ultrasound Doppler method.*
A. WAGNER, *Analysis of the blood velocity changes following extrasystole.*
A. WAGNER, *Influence of respiration on blood flow velocity in man.*
K. IWASZKIEWICZ, I. GIŻYCKA, A. CHROŚCICKI, A. HEŁCZYŃSKA, T. POWAŁOWSKI, *Quantitative examinations of the blood flow velocity in the femoral artery in children with warctation of aorta.*
K. IWASZKIEWICZ, T. POWAŁOWSKI, *Quantitative measurements of the blood flow velocity in the peripleral arteries of children with patent ductus artery.*
J. CZAJKOWSKI, *Doppler ophthalmosonographic evaluation of the blood flow velocity in stenosis and thrombosis of the carotid artery.*
J. ETIENNE, T. POWAŁOWSKI, M. WOJTKOWIAK, *Application of the ultrasonic Doppler method to the evaluation of the human condition during acceleration.*
L. FILIPCZYŃSKI, *Attempt to evaluate the detectability of blood vessels by ultrasonic echo method.*
J. WESOŁOWSKI, G. ŁYPACEWICZ, *Ultrasonography in aneurism diagnosis.*
J. GRONIOWSKI, J. KRETOWICZ, I. RUSZKOWSKI, *Ultrasonographic diagnosis of fetal abnormalities.*
D.K. NASSIRI, C. R. HILL, *Absolute measurement of volume scattering cross-section for human tissues.*
H. GAWDA, J. BEDNARA, *Propagation of ultrasonic waves in a wheat stalk and its anatomy.*

Section H (chairmen: A. STEPNOWSKI, R. SALAMON)

D. RUSER, *Signal analysis in hydrolocation.*
L. KILIAN, *Model of reverberation in the hydroacoustic channel.*
L. KILIAN, *Reverberation background level setting in sonar receivers.*
L. KILIAN, *On some problems of the reception of sonar signals in the presence of reverberation and noise.*
R. BOBER, A. DYKA, *Filter bandwith analysis for the sonar pulse interfered by reverberation.*
H. CHODKIEWICZ, E. KOZACZKA, *Influence of the flexible connection of the ship engine with its foundation on the level of underwater acoustic disturbances.*
A. DYKA, J. MARSZAL, *Deconvolution filter for resolution improvement of rectangular sonar pulses.*
A. DYKA, Cz. GUT, *Optimization of coherent coded words for sonar pulse compression.*
A. CHMIELARZ, *Digital filter for the sonar beamformer.*
Z. CZARNECKI, A. KOWALSKI, W. LIS, *System for ultrasound transponder localization — I — range.*
Z. CZARNECKI, A. KOWALSKI, W. LIS, *System for ultrasound transponder localization-II-depth.*
Z. CZARNECKI, A. KOWALSKI. W. LIS, *System for ultrasound transponder localization-III-direction.*
S. KUBICA, T. KRUSZEWSKA, *Acoustic properties of diver masks.*
D. Hamann, *Normal modes in a cylindrical system.*
A. STEPNOWSKI, *Equivalent beam width and its relations to moments and distribution of the beam pattern.*
A. STEPNOWSKI, Z. CZARNECKI, *Design of the beam pattern of the transducer array of a side scanning sonar.*
J. MARSZAL, H. LASOTA, *Hydrophone array.*
J. MARSZAL, H. LASOTA, *Apparatus for hydrophone array beam synthesis.*

Section P (chairmen: Z. KACZKOWSKI, Z. JAGODZIŃSKI)

H. LASOTA, R. SALAMON, *Method for the analysis of the broadband wave acoustic field.*
W. LIS, R. SALAMON, *Application of the impulse response in determination of the dynamic parameters of ultrasonic transducers.*
W. PAJEWSKI, *Acoustic lines with active elements.*
T. WASZCZUK, J. SOMER, *Development of phase annular array system for mechanical contact scanning.*
B. PIWAKOWSKI, H. LASOTA, *Simple matrix model of an acoustic imaging system.*
J. GOLANOWSKI, T. GUDRA, Z. IANNELLI, *Analysis of a disk type piezoelectric transducer by the finite element method.*
Z. KACZKOWSKI, *Dependence of the mechanical quality factor on the magnetic field in a 33 kHz ultrasonic alcofer transducer.*
Z. SIWKIEWICZ, W. FILIPOWICZ, *Influence of ultrasonic vibration of the matrix on the intensification of the production of thin-walled metal powder cylinders.*
J. LEMANOWICZ, A. SKRZYNECKI, Z. RODOWALD, *Ring shaped transducers in wire cleaning.*
J. LEMANOWICZ, A. SKRZYNECKI, Z. RODOWALD, *Influence od the liquid level on the acoustic load of an ultrasonic transducer and cavitation erosion.*

Section B (chairman: E. SOCZKIEWICZ)

W. BANDERA, *Useful frequency range in the mechanical impedance method for the determination of the dynamic properties of viscoelastic materials.*
L. LIPIŃSKI, *Ultrasonic relaxation of strains.*

W. Ziółkowski, *Role of the mass impedance of the measuring head in the complex elastic modulus by the driving–point impedance method.*

T. Zamorski, R. Wyrzykowski, *Extension of the theoretical model of dynamic flow generators for higher feeding pressures.*

T. Gudra, E. Talarczyk, *Method for increasing the efficiency of a high-energy liquid jet by ultrasound.*

J. Lewandowski, *Relations between the acoustic field and the structure of a solid random medium.*

C. Roszkowski, *Propagation of nonlinear spherical acoustic waves.*

Section F (chairmen: W. PAJEWSKI, J. NARKIEWICZ-JODKO)

A. Klimasek, A. Opilski, J. Zabawa, *Effect of doping with elements of groups III and V on the elastic constants of the Si crystals.*

Z. Kleszczewski, A. Kwaśniewska, *Acoustic properties of GaP crystals.*

M. Krzesińska, A. Krzesiński, A. Opilski, T. Łukasiewicz, *Three-phonon processes in* $Bi_{12}\ GeO_{20}$.

O. Delekta, A. Opilski, *Acoustic investigations of single crystals* $K(H_{1-x}D_x)_2\ PO_4$ *in the frequency range 10 MHz – 750 MHz.*

E. Drescher, *Dislocative attenuation in deformed Cu single crystals.*

Z. Tylczyński, *Temperature changes of a quasi-longitudinal ultrasonic wave propagating in the (010) plane of TGS crystals.*

A. Pilarski *Propagation of surface waves in thin layers on a half space for different boundary conditions.*

Z. Jakubczyk, A. Krzesiński, E. Gruszka, *Surface waves in a ZnO-glass layer system.*

M. Szalewski, *Thin film waveguides of surface waves.*

E. Danicki, *Simple equivalent circuit of interdigital transducers.*

R. Tajchert, P. Kaczmarski, A. Leszczyński, J. Narkiewicz-Jodko, *Propagation of bulk acoustic waves generated by an interdigital transducer.*

J. Berdowski, M. Strozik, *Investigations of elastic waves generated by an interdigital transducer using acousto-optic methods.*

Z. Kleszczewski, *Elastic and photoelastic anisotropy of selected acousto-optic crystals.*

Z. Kubik, *Effect of the humidity of air on the value of an acoustoelectric effect.*

I. Wojciechowska, A. Śliwiński, *Optical holography with a modulated reference beam used for examination of the vibration of ultrasonic transducers.*

P. Kwiek, A. Markiewicz, A. Śliwiński, *Optical holograms of an ultrasonic wave with a modulated reference beam.*

P. Loranc, *Ultrasonic binding of volumetric acoustical transducers to an acousto-optical medium.*

Section S (chairman E. TALARCZYK)

E. Soczkiewicz, *Correlations between thermodynamic fluctuations in liquids and the ultrasound velocity.*

J. Bednarek, J. Golanowski, E. Talarczyk, *Ultrasonic measurement of the solid phase content in water suspension.*

R. Hnatków, *Absorption of sound waves in* $CaCO_3$ *aerosols.*

W. Kasprzyk, J. Berdowski, J. Gmyrek, H. Król, *Aproximation of the atomization of fuel by an ultrasonic micropulser using the splines functions.*

Section U (chairmen: E. DRESCHER, J. DEPUTAT)

S. HARUMI, *Computer simulation of propagation of ultrasonic waves in solid media (film).*
J. DEPUTAT, *Application of ultrasonic tensometry.*
A. BROKOWSKI, *Reflection of ultrasonic beams at critical incidence angles.*
B. KUŚMIDER, E. KANIA, A. PILARSKI, *Bond quality evaluation in the valve of the marine engine.*
R. RYLL-NARDZEWSKA, W. MIKIEL, M. ZDANOWICZ, *Method of acoustic emission in the investigation of mechanical strength of ceramic – metal seals.*
S. PILECKI, J. RANACHOWSKI, F. REJMUND, *Acoustic emission generated by moving dislocations.*
W. KOŁTOŃSKI, *Application of acoustic echo method in non-destructive testing in mining and hydrotechnic building.*
P. PAWŁOWSKI, L. KILIAN, *Ultrasonic level meter for energetic gas in steel bottles.*
I. AUERBACH, W. SZACHNOWSKI, *Ultrasonic inspection of a plastic – metal joint of an aircraft ski.*
B. PEŃSKO, E. DURIASZ, *Optimization of the shape of fatigue samples used in ultrasonic investigations.*
A. PILARSKI, *Reflection of incident normal ultrasonic waves from interface with finite rigidity.*
A. PILARSKI, J. SZELĄŻEK, *Remarks on the ultrasonic pulse velocity measurement in bounded medium.*
J. NARKIEWICZ-JODKO, A. LESZCZYŃSKI, P. RAJCHERT, *Ultrasonic velocity measurements of bulk and surface waves by the sing-around method.*

Section A (chairmen: W. STRASZEWICZ, J. SADOWSKI, S. CZARNECKI, A. LIPOWCZAN, R. PANUSZKA)

A. KULOWSKI, *Statistical parameters of a numerical model of the acoustic field in the enclosure*
E. BROMBERG-ZIĘBA, J. ZALEWSKI, *Computer simulated model of the reverberation process for experimental investigations of the acoustic properties of auditoria.*
T. LIPIŃSKI, K. MUZALEWSKI, *Reverberation time of recessed rooms.*
H. IDCZAK, A. JAROCH, *Analysis of the amplitude of scattering sound wave on the rigid surface with irregularities.*
K. ŚRODECKI, B. NIENAŁTOWSKI, *Application of correlation analysis for identification of periodic reflections (flutter echo) in rooms.*
J. DYŻEWSKI, *Measurements of listening conditions in the Open Air Opera in Sopot.*
A. WITKOWSKI, *Sound diffusivity evaluation by optical model measurements.*
H. KUSEK, *Optical technique for the determination of isophonic lines.*
F. SUJKOWSKI, *Principles of selection of prefabricated sheet metal elements for given noise conditions.*
I. ŻUCHOWICZ, *Resonant frequency of slit resonators.*
S. WEYNA, *Vibro-acoustic parameters of ship floors.*
A. IŻEWSKA, *Nelson's method and its application in the statistical analysis of traffic noise on the model scale.*
E. TZEKAKIS, G. PAPANIKOLAU, *Prediction and measurements of noise in an urban area.*
J. SUŁOCKI, L. LIPIŃSKI, B. NIENAŁTOWSKI, K. ŚRODECKI, J. KONOPACKI, L. TARGOŃSKI, *Investigation of city noises in the case of Gdynia.*
E. TZEKAKIS, S. KONIDARIS, *Measurements of the noise field of balconies.*
R. MAKAREWICZ, *Green belt as an acoustic barrier.*
J. MIAZGA, J. BAK, K. JANICKA, *Effect of noise on the performance of truck drivers.*

B. Rudno-Rudzińska, B. Demel, M. Rabiega, J. Zalewski, *Noise from a single vehicle in flowing traffic.*
D. Augustyńska, *Infra-sonic noise generated by piston compressors. Methods of measurement, evaluation and control.*
R. Michalski, D. Trynkowska, *Speech intelligibility in noise when using ear protectors.*
Z. Jagodziński, *Ultrasonic measurements of vibrations.*
W. Cholewa, *Model of objects for diagnostic investigations.*
A. Lipowczan, *Analysis of the acoustic wave generation in the linear coal-cutting process.*
W. Moczulski, *Analysis of the shape of vibration time series emitted by a gearbox.*
D. Nitecki, J. Motylewski, *Vibroacoustic diagnostics of slide bearings in the process of quality control in the production of motor-car engines.*
R. Panuszka, Z. Engel, *Application of loose materials for the reduction of vibroakustical power in foundry machines.*
K. Dyszlewska, *Quarter-wave silencers for power plant fans.*
C. Rybicki, *The factor of "easiness of play" in mouth harmonicas.*
S. Czarnecki, A. Lipowczan, Z. Nieczyporuk, *Problem of the determination of the aeroacoustical parameters for microphone windscreens.*

Poster form session of Section A

Z. Pusłowski, M. Stawiarski, *Absorbing and insulating industrial partitions.*
J. Abłamowicz-Potapowicz, G. Brzęcka, T. Mindak, S. Podraza, *Acoustic design of a protective area for ZWCH "Chemitex-Celwiskoza" at Jelenia Góra.*
J. Dodacki, *Incombustible slit and plate resonators.*
W. Mrukwa, W. Beblo, *Experimental results of the dependence of noise attenuation on some plastic materials used for construction of the ear protectors.*
Z. Engel, E. Zalewska, J. Zalewski, *Geometrical method to estimate the acoustic energy transmitted through a hole.*
F. Sujkowski, *Principles of selection of prefabricated sheet-metal elements for given noise conditions.*

Section E (chairmen: J. ZALEWSKI, S. CZARNECKI, A. RAKOWSKI, H. HARAJDA, R. GUBRYNOWICZ, J. KACPROWSKI)

B. Rogala, R. Zmonarski, *Problem of optimizing the method of measuring nonlinear distortions in the electroacoustical channel radio receivers.*
S. Nuckowski, J. Szymbor, *Spectral verification of a nonlinear model of an electroacoustical system.*
W. Rdzanek, *Acoustic impedance of a circular membrane for the excitation vibration.*
P. Perz, P. Jabłoński, *Holographic investigations of the vibration patterns of electroacoustic transducers.*
K. Rudno-Rudziński, *Lay-out of loudspeakers versus stereophonic listening area.*
R. Makowski, *Influence of acoustic conditions of the recording room on some parameters of stereophonic signals.*
B. Bogusz, A. Jaroch, *Investigations of the gradient method of sound power determination in an acoustic tube.*
S. Czarnecki, *Transfer function method for the evaluation of the effect of the conditions of the surroundings on the effectiveness of obstacles.*
S. Czarnecki, R. Janczur, E. Kotarbińska, E. Walerian, *Influence of external conditions on the effectiveness of barriers and mufflers.*

B. Rudno-Rudzińska, K. Rudno-Rudziński, *Selection of a tweefer for a multi-way loudspeaker system in terms of power.*

A. Rakowski, A. Miśkiewicz, *Tuning of musical intervals with sinewave, triangle-wave and square-wave tones.*

M. Gryczyński, *Discrimination of slight changes in the sound frequency by patients of different ages.*

M. Gryczyński, *Discrimination of slight changes in the sound frequency with pathology of the hearing organ.*

M. Gryczyński, *Influence of musical education on the discrimination of slight changes in the sound frequency.*

J. Fik, *Sensitivity of musical hearing to pitch changes.*

H. Harajda, *Intonation of melodic intervals by children of average musical ability.*

S. Prus, *Does the psychometric function behaviour confirm the neural quantum theory?*

A. Hajdukiewicz, *Investigation of audio-visual analogies.*

D. Gryczyńska, B. Latkowski, *Studies of the effect of the sound phase change on hearing localization.*

J. Florkowski, *Influence of the rise time of a pulse on the accuracy of the localization of a sound source in a horizontal plane.*

H. Sieńkowska, W. Mikiel, P. Żarnecki, B. Wierzchowska, *Rhythmic and melodic organization of speech in children with hearing impairment.*

K. Mlicka, *Momentary pitch of a signal of frequency transitions.*

W. Nowakowska, P. Żarnecki, *Computer model for the determination of acoustic parameters of the vocal tract analogue.*

B. Adamczyk, W. Kuniszyk-Jóźwiak, Z. Skorzyński, J. Czarnota, *Analogue digital echo-reverberation speech corrector.*

W. Majewski, J. Jurkiewicz, *Speaker identification over telephone lines.*

R. Siwanowicz, J. Sobkowski, J. Szubert, *Application of linear prediction to spectral coding of a speech signal using the Walsh function.*

H. Kubzdela, *Visualization of a speech signal using binary spectograms.*

R. Gubrynowicz, *System for a detailed analysis of acoustic signals, and particularly speech signals.*

W. Jassem, *Computer — assisted recognition of English vowels.*

W. Wieźlak, R. Gubrynowicz, *Preliminary segmentation of speech in the recognition of isolated words.*

J. Kamiński, *Segmentation of a certain class of signals by means of sample similarity measures.*

J. Kaźmierczak, *Utilization of pattern homology measures in the analysis of acoustic signals.*

J. Zalewski, H. Jurkiewicz, *System for the vocal-pitch estimation by homomorphic analysis.*

The seminar included a Round Table Conference on 18-19 October on the subject of "Acoustic fields in industrial halls". 35 persons from the following institutions took part in the Conference: Warsaw Technical University; Institute of the Fundamental Technological Research of the Polish Academy of Sciences, Warsaw; MBP Warcent, Warsaw; COBR PJB, Katowice; BP Bistyp, Institute of Wood Technology, Warszawa; PPB Bistyp, Legionowo; Agromet-Projekt, Poznań; ZFDWSO, Zielona Góra; SPBiKS, Gorzów Wielkopolski; Department of Acoustics, Poznań University; Institute of Aviation, Warsaw; ZUK UNIPROT, Warsaw; PKNMiJ, Warsaw; ITA, Wrocław Technical University; Polish Radio and Television, Szczecin; OBiKS, Poznań; Szczecin Technical University.

The sessions were chaired by Prof. Stefan Czarnecki. The secretaries of the sessions were Dr. J. Abłamowicz-Potapowicz (BP Warcent) and Z. Pusłowski, M. Sc. (Bistyp). The participants in the Conference draw attention to the imperfect methods currently used in design, which are based on classical relations resulting from a statistical method of acoustic field analysis. When the properties of the field resulting from the configuration of the indus-

trial hall are distinctly different from the assumptions of the method, considerable disagreement can be observed between the values resulting from a design of acoustic adaptation and the values measured after its execution. In particular, attention was drawn to the necessity of explaining the use of the values of absorption coefficients shown in catalogues for spatial absorbers that are larger than unity and the necessity of developing standard methods for the acoustical design of industrial halls where the properties of the acoustic field deviate distinctly from the assumptions of the statistical theory.

The discussion touched upon the problem of using digital methods when computers are used. A separate issue was the necessity of deriving principles of economic analysis of the effectiveness of using technical methods for noise reduction.

The participants in the Conference proposed:

(a) expansion of the range and acceleration of scientific research connected with the acoustic properties of industrial halls, which should lead to the development of better design methods that can be easily used by designers,

(b) the development of methods of economic analysis of the effectiveness of using technical methods for acoustic energy reduction in industrial halls,

(c) the development of ways for the better utilization of sound absorbing and sound insulating materials and elements made in Poland,

(d) the standardization of measurement methods used to determine the properties of the acoustic field in industrial halls in order to achieve better agreement between design calculations and measured results.

The director of the Metal-Sheet Processing Company (Bistyp, Legionowo) offered an unused hall owned by the company for experimental research. This may be an essential part in the implementation of proposal *a*.

In addition to the above specialist Round Table Conference, there were unofficial discussions which doubtless contributed to the free exchange of scientific thought and closer relations in the acoustical community.

The next, XXVIII Seminar on Acoustics will be organized by the High Silesian Division of the Polish Acoustical Society.

Jerzy Etienne, Witold Straszewicz
(Warsaw)

ACOUSTICAL EVENTS IN 1982

Winter School on Machinery Diagnostics
Wisla, January 1982

Organizer	Institute of Transport, Silesian Technical University
Organizing committee:	Prof. L. Müller

8th Colloquium on Acoustics
Budapest, Spring 1982 (Hungary)

Organizing committee: OPAKFI, Anker koz. 1, 1061 Budapest (Hungary)

VI Latin American Meeting on Acoustics
Mexico, Spring 1982

Meeting of the Acoustical Society of America
Chicago, 26–30 April 1982 (USA)

Organizing committee: Mahlon D. Burkhard,
Industrial Research Products. Inc, 321 North Bond St,
Elk Grove Village, Illinois 60007 (USA)

INTER—NOISE 82
San Francisco, 16—19 May 1982 (USA)

Sponsor: I/INCE
Organizing committee: Dr W.W. Lang
Language: English

3rd FASE CONGRESS
Göttingen, 13–17 September 1982 (RFN)

Sponsor: FASE and DAGA
Range: Aeroacoustics, psychological acoustics, construction acoustics, structure-borne sound, underwater acoustics, nonlinear acoustics
Organizing committee: FASE 82, c/o

Physikalisch-Technische Bundesanstalt,
Post Box 33 45,
D-3300 Braunschweig (RFN)

Noise Control Conference 82
Kraków, 20—22 September 1982

Sponsor: Committee on Acoustics of Polish Academy of Sciences, Polish Acoustical Society
Organizer: Institute of Mechanics and Vibroacoustics, Academy of Metallurgy and Mining
Organizing committee: Prof. dr Zbigniew Engel,
Institute of Mechanics and Vibroacoustics,
Academy of Metallurgy and Mining,
Kraków, Mickiewicza 30

21st Acoustical Conference on Noise and Environment
Vysoké Tatry, October 1982 (CSRS)

Organizing committee: Ing. L. Goralikova
House of Technology, Skultétyho Street,
881 30 Bratislava (CSRS)

Meeting of Acoustical Society of America
Orlando, 8—12 November 1982 (USA)

Sponsor: ASA
Organizing committee: Joseph R. Blue
Naval Research Laboratory, P.O. Box 8337,
Orlando, Florida 32856 (USA)

The Journal of the Acoustical Society of Japan (E)

With real satisfaction we welcome the English version of periodical of the Acoustical Society of Japan, *The Journal of the Acoustical Society of Japan (E)*.

Many of the papers in this periodical, which has appeared essentially in the Japanese language for many years, have been published in English. In addition the Editors have done much to bring the other papers closer to the international scientific community by publishing their abstracts, figure and table legends etc. in English. All these efforts have contributed to establishing a very good opinion of the investigations of Japanese acousticians and their Journal in the scientific world.

Nevertheless, in many cases, the language barrier has caused the periodical to contribute only partially to the international exchange of scientific information. This incomplete share of Japanese acousticians in this exchange was also felt by the Acoustical Society of Japan which, after analysis of the situation, decided to publish an English version of the journal of the Society each quarter of the year and to invite scientists in other countries to submit their papers to it, which will doubtless give the periodical a more international character.

Archives of Acoustics wishes every success to the Editorial Committee of the Journal of the Acoustical Society of Japan.

R. GUBRYNOWICZ